

# The discovery and exploration of a universal targeting mechanism in eukaryotic cells

Priyanka Sivadas  
*Marquette University*

---

## Recommended Citation

Sivadas, Priyanka, "The discovery and exploration of a universal targeting mechanism in eukaryotic cells" (2011). *Dissertations (2009 - )*. Paper 168.  
[http://epublications.marquette.edu/dissertations\\_mu/168](http://epublications.marquette.edu/dissertations_mu/168)

THE DISCOVERY AND EXPLORATION OF A UNIVERSAL TARGETING  
MECHANISM IN EUKARYOTIC CELLS

by

Priyanka Sivadas, B.Tech

A Dissertation submitted to the Faculty of the Graduate School,  
Marquette University,  
in Partial Fulfillment of the Requirements for  
the Degree of Doctor of Philosophy

Milwaukee, Wisconsin

December 2011

ABSTRACT  
THE DISCOVERY AND EXPLORATION OF A UNIVERSAL TARGETING  
MECHANISM IN EUKARYOTIC CELLS

Priyanka Sivadas, B.Tech

Marquette University, 2011

A wide range of eukaryotic organisms generate motile cilia and flagella. These slender organelles beat rhythmically to move the surrounding fluid or to propel cells in aqueous environment. Organisms use these powerful yet nimble organelles to forage, evade, adapt and mate. The machinery that drives this tightly controlled movement is the sophisticated microtubule-based axoneme. As it is critical for the survival of individual species, this machinery has largely been preserved to the molecular level throughout evolution. Proteomic studies have shown that most proteins in this biological machine consist of molecular modules commonly used in the cell body. But the usage of these modules is clearly diverged in many cases. This defined machinery with diverged applications provides an opportunity to understand the true capacity of the conserved modules. One example is the radial spoke (RS) that controls the oscillatory beating. This macromolecular complex contains complementary molecular modules that are responsible for localizing cAMP-dependent protein kinase (PKA) in the cell body. However, the RS does not have the features that account for the effector mechanisms of PKA and thus the mechanism discovered for localizing PKA has a broader role that has previously not been recognized. The work described in this dissertation discovered that the core of the RS utilizes two similar sets of PKA anchoring modules for four distinct effector mechanisms that underlie the assembly and function of this regulatory complex. These results elucidate the function of this complex and are applicable to more than 600 diverged proteins that also share the docking module of PKA. Some of them have been shown to play vital roles in myriads of cellular reactions ranging from flagellar beating to trans-Golgi trafficking to chromosome modifications. Founded on this discovery, new reagents and assays were engineered. These tools could be used for the exploration of proteins with similar docking and anchoring modules. Together, these findings will accelerate the advancements in the field of anchoring and docking of proteins in the cell.

## ACKNOWLEDGEMENTS

Priyanka Sivadas, B.Tech

I would like to express my deepest gratitude and appreciation to my advisor Dr. Pinfen Yang for her valuable insight, guidance and support over the past five years. Her patience, motivation and encouragement have helped me develop as a critical thinker. Our invigorating discussions whether it is the lab meetings or the one on one talks, have tremendously impacted my understanding of science and research. I would also like to thank her for her incredible **patience** and for being a wonderful teacher and for instilling in me some of her amazing work ethic.

I would also like to thank all my committee members, Dr. Kathleen Karrer, Dr. Dale Noel, Dr. Rosemary Stuart, Dr. Martin St.Maurice and Dr. David Wagner for their invaluable suggestions, feedback and guidance.

I would like to thank my lab members, Dr. Chun Yang, Dr. Radhika Gopal, Dr. Mei Wei, Anjali Gupta and Stephanie Davis for all the camaraderie, support, intellectual discussions and fun times. You guys made the five years a little easier.

And most importantly, my biggest thanks go to my family and loved ones. I express the deepest gratitude to my mother and father for their constant encouragement, support and for always believing in my abilities. And also my brother for being my 3AM friend, for setting the bar really high and pushing me to do better. I also want to thank my husband, Tushar Dharampal, for being there during the most stressful times and for all his patience, love and understanding in the past few years.

## TABLE OF CONTENTS

ACKNOWLEDGEMENTS.....	i
LIST OF TABLES.....	vii
LIST OF FIGURES.....	viii
LIST OF ABBREVIATIONS.....	x
 CHAPTER	
1: INTRODUCTION	
1.1 Cilia and Flagella.....	1
1.1.1 The Function and Significance.....	1
1.1.2 The 9+2 Axoneme.....	4
1.2 9+2 Machinery.....	4
1.3 Proposed Roles of RS and CP.....	6
1.4 The Radial Spoke.....	8
1.4.1 Radial Spoke: The Mechanochemical.....	8
Signal Transducer	
1.4.2 Radial Spoke Composition.....	10
1.4.3 RSP3.....	12
1.4.3.1 RSP3: Sequence and Homology.....	12
1.4.3.2 RSP3 Docks the RS to the Axoneme.....	12
1.4.3.3 RSP3: A Homodimer.....	15
1.4.3.4 RSP3: The Spoke AKAP.....	15
1.5 The RIIa Clan.....	19
1.5.1 The RIIa Clan Domains.....	20
1.5.1.1 RIIa Domain.....	20

1.5.1.2 Dpy-30 Domain.....	21
1.5.1.3 RIIa Clan Domain Containing RSPs.....	24
1.6 Objectives of Research.....	26
<b>2: MATERIALS AND METHODS</b>	
2.1 Materials.....	29
2.1.1 Chemical Reagents.....	29
2.1.2 Oligonucleotides.....	29
2.1.3 Antibodies.....	29
2.2 Cell Strains and Culture Conditions.....	35
2.3 Molecular Biology.....	35
2.3.1 Polymerase Chain Reaction-based DNA Fusion.....	35
2.3.2 Engineering Genomic DNA Constructs.....	35
2.3.3 Engineering cDNA Constructs.....	41
2.3.4 Transformation of <i>Chlamydomonas</i> .....	43
2.4 Cell Biology.....	44
2.4.1 Microscopic Screening of Transformants.....	44
2.4.2 Electron Microscopy.....	44
2.5 Biochemistry.....	45
2.5.1 Screening of Transformants: Flagella Miniprep.....	45
2.5.2 Extraction of Axonemal Proteins.....	46
2.5.3 Fractionation of Axonemal Proteins.....	46
2.5.4 SDS-PAGE.....	47
2.5.5 Native-PAGE.....	47

2.5.6 Western Blot.....	48
2.5.7 Ni-NTA Affinity Purification.....	49
2.5.8 Overlay.....	50
2.5.9 Chemical Blocker Screening with..... Native Gel Electrophoresis	50
2.5.10 Chemical Blocker Screening with..... Ni-NTA Pull- Down	51
2.6 Sequence Analysis.....	51
<b>3: RSP3 FORMS THE RS SCAFFOLD WITH TWO DISTINCT SITES THAT ANCHORS RIIA CLAN DOMAINS</b>	
3.1 Introduction.....	52
Section I: In vivo Approach.....	55
3.2 Results.....	55
3.2.1 Sequence Analysis of RSP3.....	55
3.2.2 RSP3 Truncation Mutagenesis Clarifies the Binding..... Region for the RIIa Domain and its Tethered Moieties	57
3.2.3 A Downstream Helical Region Associates with..... Dpy-30 Domain Containing Proteins	62
3.2.4 Truncations in RSP3 Lead to Smaller Spoke Particles.....	65
3.2.5 Electron Microscopy Reveals Distinct Dwarf RSs..... in RSP3 Mutant Axonemes	67
Section II: In vitro Approach.....	71
3.3 Results.....	73
3.3.1 RSP3 Directly Interacts with RIIa Domain..... of RSP7 and Dpy-30 Domain	73
3.3.2 Defining the Dpy-30 Domain Binding Site.....	76

3.3.3 Dpy-30 Protein Interacts with RSP3 through the.....	78
Dpy-30 Domain	
3.3.4 Construction of a Dpy-30/RSP2 Hybrid Molecule.....	80
3.3.5 Comparing the RIIa Clan Domains.....	82
3.3.6 Comparing the RIIa Clan Binding Sites.....	86
3.4 Discussion.....	88
3.4.1 RSP3 Contains Two Binding Sites for the RIIa and.....	89
Dpy-30 Domain	
3.4.2 The Topography of the RS.....	90
3.4.3 The In vitro System Identified the RIIa and.....	91
Dpy-30 Binding Sequence	
3.4.4 The Comparison of the RIIa and Dpy-30.....	92
Binding Sequences	
<b>4: DEVELOPMENT OF TOOLS FOR THE STUDY OF DPY-30 ANCHORING</b>	
<b>MECHANISM</b>	
4.1 Introduction.....	93
4.2 Results.....	95
4.2.1 Strategies to Identify Dpy-30 Interacting Polypeptides.....	95
4.2.1.1 Affinity Co-Purification.....	95
4.2.1.2 Native Gel Electrophoresis.....	97
4.2.1.3 Overlay.....	101
4.2.2 Development of Quantitative Assays.....	105
4.2.2.1 GFP as a Reporter for a 96-Well Plate Assay.....	105
4.2.3 Screening of Non-peptide Blockers for Dpy-30.....	108
4.2.3.1 Screening Chemical Blockers.....	108
with Native PAGE	



4.2.3.2 Screening Chemical Blockers with.....	111
Co-Purification	
4.3 Discussion.....	114
5: DISCUSSION	
5.1 A New RS Model.....	116
5.2 Versatility of the AH-D/D Localization System.....	119
5.3 The AH Molecular Scaffolds.....	120
5.4 The Conservation and Divergence of the AH-D/D System.....	122
5.5 Selective Cross-Reactivity of the AH and D/D Domain.....	123
5.6 Tools for the DAPs.....	124
BIBLIOGRAPHY.....	127

**LIST OF TABLES**

Table 1-1. *Chlamydomonas* radial spoke mutants that are relevant to this dissertation.

Table 1-2. The RIIa-clan members.

Table 2-1. Chemicals used in this study.

Table 2-2. Oligonucleotides used in this study.

Table 2-3. Antibodies used in this study.

Table 3-1. Screening of RSP3 truncation mutants.

Table 3-2. Screening of RSP3 truncation mutants.

Table 3-3. The incidence of lateral-shifted central pair (CP) apparatus in axonemes and the extent of deviation.

Table 4-1. List of chemical compounds.

## LIST OF FIGURES

- Figure 1-1. Cross sectional view of the 9+2 axoneme.
- Figure 1-2. Radial spoke proteins and their predicted functional domains.
- Figure 1-3. The tetrameric holoenzyme of cAMP-dependent protein kinase.
- Figure 1-4. AKAPs: The signaling scaffolds and their interaction with the RIIa domain.
- Figure 1-5. Crystal structure of the RIIa clan domains.
- Figure 2-1. The PCR strategy to fuse the coding sequences for a large tag and a small amphipathic helix.
- Figure 2-2. Cloning Strategy for the generation of pRSP3-3HA-12His.
- Figure 2-3. Strategy for the generation of RSP3 truncation constructs.
- Figure 3-1. Sequence Analysis and the model of RS.
- Figure 3-2. Truncation around the Coil 1 region results in deficiencies in RIIa-domain-dependent assembly.
- Figure 3-3. Truncation between the first two coils results in deficiencies in Dpy-30-domain-dependent assembly.
- Figure 3-4. Radial spokes extracted from mutants largely sedimented as smaller particles.
- Figure 3-5. Distinct stubby spoke in the axonemes from the  $\Delta 1$  and 1-178 mutants.
- Figure 3-6. Two regions in RSP3 bind to the RIIa and the Dpy-30 domain in vitro.
- Figure 3-7. The Dpy-30 protein binds to a.a.# 280-308 in RSP3.
- Figure 3-8. The Dpy-30 domain binds to a.a.# 280-308 in RSP3.
- Figure 3-9. The Dpy-30 binding domain (RSP3<sub>280-308</sub>) binds to the hybrid molecule albeit with low affinity.
- Figure 3-10. Sequence Alignment of the RIIa clan domains.
- Figure 3-11. Comparison of crystallographic structures of the Dpy-30 domain

and the RIIa domains from PKA.

Figure 3-12. Similarities of the RIIa- and Dpy-30-domain binding sequences.

Figure 4-1. The Dpy-30 domain cross-reacts with the AH<sub>R</sub>.

Figure 4-2. Native gel electrophoresis for identifying Dpy-30-binding peptides.

Figure 4-3. Schematic depicting the Dpy-30 overlay procedure.

Figure 4-4. The Dpy-30 overlays.

Figure 4-5. Developing quantitative assays to test the affinity of Dpy-30 binding peptides.

Figure 4-6. Screening a library of compounds using the native gel assay.

Figure 4-7. Pull-down assay for screening organic compounds.

Figure 5-1. The new RS model.

## LIST OF ABBREVIATIONS

AH	Amphipathic Helix
AH <sub>D</sub>	Dpy-30 binding Amphipathic Helix
AH <sub>R</sub>	RIIa binding Amphipathic Helix
AKAP	A Kinase Anchoring Protein
AKAP-Lbc	AKAP- Lymphoid Blast Crisis oncogene
ARM	ARMadillo
ATP	Adenosine TriPhosphate
BIG1	Brefeldin A-Inhibited Guanine nucleotide-exchange protein 1
BIG2	Brefeldin A-Inhibited Guanine nucleotide-exchange protein 2
cAMP	Cyclic Adenosine MonoPhosphate
cNMP	Cyclic Nucleotide MonoPhosphate
CP	Central Pair
CSF	CerebroSpinal Fluid
D/D	Docking and Dimerization
D-AKAP	Dual AKAP
DAP	D/D Anchoring Proteins
DMSO	Di-Methyl SulfOxide
DRC	Dynein Regulatory Complex
ELISA	Enzyme Linked ImmunoSorbent Assay
EM	Electron Microscopy
GFP	Green Fluorescent Protein
GST	Glutathione-S-Transferase
GTP	Guanine TriPhosphate
GTPase	Guanine TriPhosphatase
HA	HemAgglutinin
HSP40	Heat Shock Protein 40
IC140	Intermediate Chain 140
IDA	Inner Dynein Arms
IPTG	Iso-Propyl Thio Galactosidase
KI	Potassium Iodide
LC8	Light Chain 8
NDK	Nucleoside Diphosphate Kinase
NDP	Nucleoside DiPhosphate
Ni-NTA	Nickel-NitriloTriAcetic acid
NTP	Nucleoside TriPhosphate
ODA	Outer Dynein Arms
PCD	Primary Ciliary Dyskinesia
PCR	Polymerase Chain Reaction
<i>pf</i>	paralyzed flagella
PKA	Protein Kinase A
PKD	Polycystic Kidney Disease
PMM	Paromomycin
PP1	Protein Phosphatase 1

PP2A	Protein Phosphatase 2A
RS	Radial Spoke
RSP	Radial Spoke Protein
SDS	Sodium Dodecyl Sulfate
WT	Wild Type

## **Chapter 1: Introduction**

### ***1.1 Cilia and Flagella***

Cilia and flagella are hair-like organelles adopted by unicellular and multicellular organisms alike. Albeit differing in length and number, the fundamental structure and mechanism of these organelles are identical. Discoveries over the past decade have revealed their broad significance for a wide range of cell types and tissues. Yet the mechanisms related to the generation, function and maintenance of cilia and flagella are just emerging. Recent genomic and proteomic tools have hastened the identification of new proteins and molecular domains within these organelles. While some of these molecular domains appear to be cilia-specific, most are utilized in other cellular compartments as well. The proteins with these widely utilized molecular domains have become new targets for focused investigation. Elucidation of these key proteins and molecular domains will shed critical insight on these important organelles and will provide a solid foundation to understand and treat congenital disorders and diseases related to these organelles.

#### **1.1.1 The Function and Significance**

Cilia and flagella are analogous to cellular antennae, sensing environmental conditions for cells. Some cilia and flagella are also motile with tightly controlled rhythmic movement (Ishikawa and Marshall, 2011). These two main functions seem unrelated to each other, yet in many instances they are tightly coupled, providing cells the means to sense the environment and then respond accordingly.

The importance of these dual functional organelles has been recognized for three decades (Pederson and Rebbe, 1975; Afzelius, 1979 and 1981). However, the broad impact of the sensory function in mammals did not emerge until about 10 years ago (Pazour et al., 2000). As sensory organelles, the compartmentalized ciliary membrane is enriched with various channels (Singla and Reiter, 2006; Rohatgi et al., 2007; Hildebrandt et al., 2011) and vital receptors, like those for hedgehog, Patched, growth factors, hormones and those coupled to G proteins. For instance, in kidney, the primary cilium of the tubular epithelium senses the fluid flowing through the tubules using mechano-sensitive calcium channels. The fluid flow deforms the cilia which lead to opening of the channels. The calcium influx induces a cascade of signal transduction pathways which maintain the polarity and the homeostasis of the epithelium (Nauli et al., 2003; Dalagiorgou et al., 2010). Defects in these cilia, whether they are ciliogenesis, sensing or signal transduction defects, result in dedifferentiation and unchecked mitosis of the tubular epithelial cells (Praetorius and Spring, 2003; Liu et al., 2005; Deane and Ricardo, 2007; Belibi et al., 2010). Clinically, these responses are manifested as a rather common disorder, polycystic kidney disease (PKD) (Pazour et al., 2000). By the same token, sensory cilia are pertinent to the development and maintenance of homeostasis of most organs (Hirokawa et al., 2009; Snell et al., 2004). Thus defects in the sensory function are also manifested as situs inversus, polydactyly, blindness, deafness, diabetes, obesity and hypertension (Lee, 2011).

Motile cilia are important as well, albeit for different purposes. Most eukaryotic organisms generate motile cilia at a certain phase of their life cycle. Their distribution in multicellular organisms is mostly restricted to the respiratory system, ventricle of the



brain and reproductive organs (Baker and Beales, 2009). In the respiratory tract, motile cilia constantly propel mucus overlying the epithelium, along with trapped microorganisms, harmful compounds and irritating particulates. Ineffective mucociliary clearance from the respiratory tract leads to chronic respiratory infection and ultimately bronchiectasis and the need for a lung transplant (Lee, 2011). Motile cilia of the ependymal cells surrounding the ventricle of the brain circulate the cerebrospinal fluid (CSF). The purpose of the flow of CSF is not entirely clear. However, defects in ependymal cilia lead to stagnant CSF, increased ventricular pressure, hydrocephaly and loss of cortical neurons (Lee, 2011). During development, the cilia in the node play a critical role in the polarized distribution of morphogens that determine the development of left right asymmetry (Nonaka et al., 2002). Defects in nodal cilia result in situs inversus -- the internal organs are distributed in a mirror image of the normal pattern. Lastly, in the reproductive system motile cilia are crucial for fertility. In the female reproductive system, the cilia lining the fallopian tube help in the transport of the egg from the ovary to the uterus (Lyons et al., 2006). In the male reproductive system, a single flagellum propels the sperm towards the oocytes (Kaupp et al., 2008). Defective motility in these cilia impairs male and female fertility. Together these symptoms due to defective motility are referred to as primary ciliary dyskinesia (PCD) or Kartagener syndrome (Kartagener, 1933; Afzelius, 1976 and 1981).

As the motility machinery is comprised of hundreds of distinct polypeptides, PCD is a polygenic congenital disorder. At least 1 in 16,000 people are afflicted with PCD (Lee, 2011), yet the true incidence is likely to be higher since the symptoms, albeit diminishing the quality of life, are not life threatening. Understanding the molecular

mechanism of the motility machinery will provide a solid foundation for the diagnosis and treatment of PCD patients.

### **1.1.2 The 9+2 Axoneme**

Regardless of the variety, all motile cilia and flagella contain a microtubule-based scaffold, the axoneme. Barring a few exceptions, a majority of them employ the 9+2 format (Li et al., 2004; Hoops and Witman, 1983; Schrevel and Besse, 1975). It consists of nine outer microtubule doublets encircling two singlet microtubules. In contrast, the axoneme in immotile sensory cilia appears more primitive. Most still have 9 outer doublets but the central pair of singlet microtubules is absent. Hence they are referred to as the 9+0 format. Exceptions are found in some cell types. For example, some motile cilia that beat with less sophisticated motion adopt 9+0 axonemes (Okada et al., 1999).

In the 9+2 axoneme, the microtubule scaffold is associated with several distinctive molecular complexes. It is the axonemal complexes that enable these machines to beat with extraordinary capacity. It is not conducive to study this motility machinery using higher organisms because of its complicated composition and mechanism. Most of our current understanding of this complex machinery is derived from investigation of the 9+2 axoneme in the biflagellate model organism, *Chlamydomonas reinhardtii*.

### **1.2 9+2 Machinery**

The 9+2 axoneme is highly conserved (Figure 1-1). It consists of 9 outer microtubule

doublets surrounding 2 microtubule singlets. Each doublet is comprised of a complete A tubule and a partial B tubule (Satir, 1980). The 9+2 axoneme contains all of the machinery and regulatory elements necessary for the controlled movement. Isolated axonemes, without the plasma membrane and cytoplasm, can be reactivated to beat rhythmically when ATP is provided (Summers and Gibbons, 1971). In addition, this movement is sensitive to calcium and cAMP (Kamiya and Witman, 1984). The controlled movement relies on the many molecular complexes associated with the 9+2 microtubule platform. The complexes that are easily visible in electron micrographs are best characterized.

The two microtubule singlets in the center of the axoneme associate with multiple projections. Together these structures in the center of the axoneme are referred to as the central pair (CP) apparatus. Outer dynein arms (ODAs) and inner dynein arms (IDAs) dock to the A tubule on the outer doublet and project towards the B tubule of the neighboring outer doublet. Also attached to the outer doublet is the T-shaped radial spoke (RS). It docks to the outer doublet with a thin stalk and projects a bulbous head toward the CP. These axonemal structures of the 9+2 machinery appear at precise locations relative to each other and at exact periodicities along the length of the axoneme. When viewed longitudinally, four ODAs, three IDAs and two RSs are present in each 96-nm register (Warner and Satir, 1974; Mastronarde et al., 1992, Nicastro et al., 2005, 2006). Each projection has a distinct role but they operate in concert to generate oscillatory beating.

It is well established that oscillatory beating of motile cilia and flagella is founded on the inter-doublet sliding driven by dynein motors (Summer and Gibbons, 1971). ATP

hydrolysis in the motor head induces conformational changes, leading to a power stroke. The motor walks against the neighboring outer doublet towards the minus end, i.e. the tip of the flagella. This conversion of chemical energy into physical force by the dynein motor triggers the sliding between adjacent outer doublets (Lindemann and Lesich, 2010). The static linkers like nexin between outer doublets convert this sliding into bend formation. In theory, alternate sliding of opposing outer doublets is the foundation of oscillatory beating (Smith and Yang, 2004).

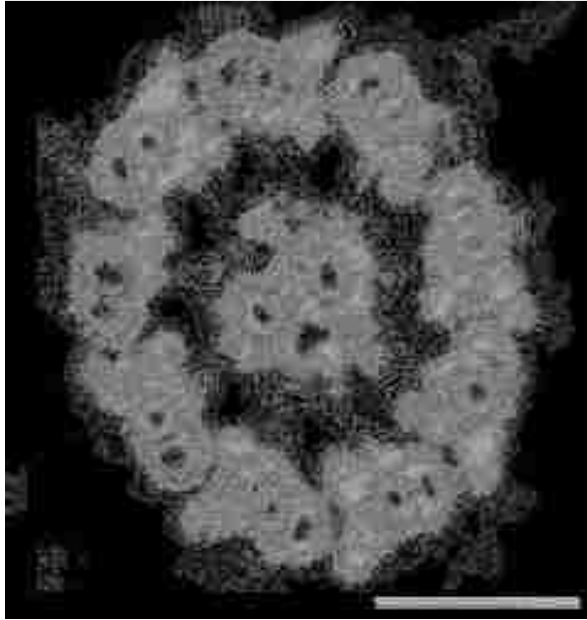
In contrast to the well characterized dynein motors and the dynein-driven sliding, the control of this sliding is not well understood.

### ***1.3 Proposed Roles of RS and CP***

It is apparent that the thousands of dynein motors distributed in each of the 9 outer doublets and along the length of the axoneme must take turns undergoing the power stroke in order to alternate inter-doublet sliding, generate bends and thus oscillatory beating. If all of the motors became activated simultaneously, there would be no net movement and the flagella would become paralyzed. Such paralysis has been observed in *Chlamydomonas* mutants as well as human patients, due to deficiencies in the RS or the CP (Witman et al., 1978; Zariwala et al., 2007; Castleman et al., 2009). Independent lines of evidence suggest that the RS and the CP constitute a system that determines which subsets of motors become activated and which sets of outer doublets undergo sliding.

Studies of suppressor mutations of the paralyzed RS and CP mutants have found that mutations in dynein motors and a group of 6 proteins adjacent to the motors can partially rescue the paralysis of RS and CP mutants without restoring either structure.

A



B

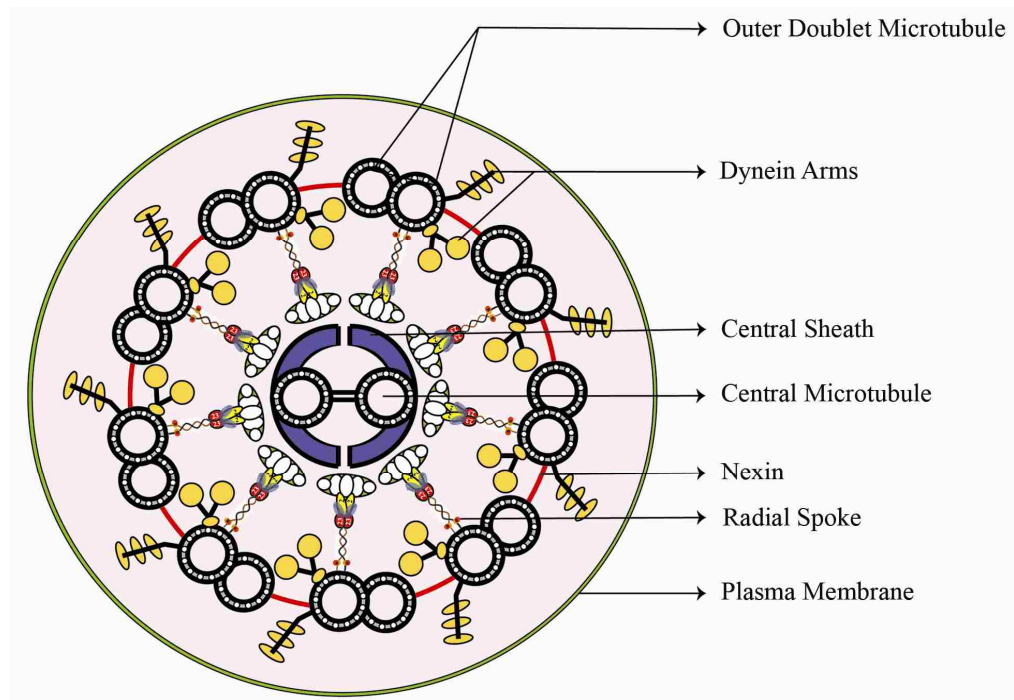


**Figure 1-1. Cross sectional view of 9+2 axoneme.**

(A) Electron microscopy of *Chlamydomonas* axoneme and (B) the schematic representation. The scale bar represents 100 nm.

Therefore, these 6 proteins were referred to as the dynein regulatory complex (DRC) (Huang et al., 1982; Porter et al., 1994; Piperno et al., 1992, 1994). These results led to a well-accepted model that the RS and the CP constitute a system to control dyneins through the DRC. In theory, without the RS or the CP, dyneins are inhibited and suppressor mutations in the dynein motors and DRC bypass this inhibition and restore the motility.

Despite the paralysis of the RS and CP mutants, these two prominent features in the 9+2 axonemes are not required for motility. Certain cilia, like nodal cilia are motile in spite of their 9+0 axonemal arrangement (Nonaka et al., 1998). These cilia beat with a very shallow waveform and at a low frequency, contrary to the planar waveform and high frequency beating characteristic of 9+2 axonemes (Okada et al., 1999). Similarly, the suppressor mutants exhibit a symmetric flagellar waveform unlike the asymmetric waveform of wild-type cells (Omoto et al., 1996; Brokaw et al., 1982). Thus it was postulated that the RS/CP control system overrides the rudimentary machinery, primarily composed of 9+0 outer doublets and motors (Kamiya, 2002) and confers the high frequency, asymmetric waveform characteristic of most cilia and flagella. This dissertation investigates molecular interactions that underlie the assembly and the mechanism of the RS.

## ***1.4 The Radial Spoke***

### **1.4.1 Radial spoke: The Mechanochemical Signal Transducer**

The radial spoke is in position to directly activate dynein motors. The base of the RS is near IDAs. Furthermore, electron microscopy of cilia that were instantaneously fixed

while beating showed that the radial spoke is a mobile element similar to dynein motors and the CP. It undergoes cycles of attachment and detachment with the CP. This conclusion was founded on the observation that the RSs at the bend of the flagella tilt and lengthen slightly (Warner and Satir, 1974; Goodenough and Heuser, 1985; Curry and Rosenbaum, 1993). Also, in most motile cilia, during oscillatory beating the central pair apparatus rotates once per beat (Tamm and Tamm, 1981; Omoto et al., 1999). It was postulated that the tension or force experienced by the RS from the rotating central pair and sliding outer doublets activates subsets of dynein motors (Omoto et al., 1999).

The radial spoke is also implicated in the modulation of oscillatory beating. The beating of all cilia and flagella is sensitive to common second messengers like calcium and cNMP (Smith and Yang, 2004). These second messengers induce changes in the beating partly through phosphorylation (Tash et al., 1989). For instance, calcium concentrations affect the flagellar waveform. At  $10^{-8}$  M calcium, the reactivated axonemes beat with a highly asymmetric waveform which allows the cells to swim forward. When the concentration increases to  $10^{-4}$  M, the movement switches from asymmetric to symmetric waveform, enabling cells to swim backward (Bessen et al., 1980; Kamiya and Witman, 1984). As the suppressor of RS mutant exhibits symmetric flagellar waveform, it was proposed that the RS is required for the generation of asymmetric waveform at low calcium concentrations (Brokaw et al., 1982). A study using microtubule-sliding of axonemes from the RS mutants also implicates the RS in calcium-induced changes in motility (Smith, 2002).

In addition, it was proposed that dynein activity is inhibited by kinases and the RS in the WT axoneme operates to inhibit the kinases. While the flagella lacking the RS are

paralyzed, the axonemes can still undergo sliding. However, the sliding velocity is reduced to half that of the WT flagella. The sliding velocity was restored to WT levels if inhibitors for cAMP-dependent protein kinases and casein kinases were present (Howard et al., 1994; Yang and Sale, 2000). On the other hand, inhibitors for phosphatases, PP1 and PP2A reversed the effects of the kinase inhibitors (Habermacher et al., 1996; King and Dutcher, 1997; Yang and Sale, 2000). Thus it was proposed that the kinases inhibit dynein motors and the RS operates to eliminate this inhibition.

Together, the evidence from genetic and functional studies supports a model that the radial spoke regulates flagellar beating as a mechanochemical signal transducer.

#### **1.4.2 Radial Spoke Composition**

The composition of the RS was first revealed indirectly by the studies of *Chlamydomonas* mutants. Electron microscopy shows that the flagella of *pf14* mutants lack the entire RS complex (Witman et al., 1978). The compositional analysis demonstrated that the morphological phenotype correlated with the absence of 17 proteins. Thus it was concluded that the T-shaped complex is composed of at least these 17 polypeptides, referred to as radial spoke proteins (RSPs) (Piperno et al., 1977, 1981) (Figure 1-2). Using dikaryon cytoplasmic complementation and revertant mutagenesis, it was found that the phenotype is caused by a mutation in the RSP3 gene. Comparison of RSPs in the axonemes from the spoke-less mutants and the mutants lacking only part of the RS predicts that the bulbous spoke head consists of five proteins (RSP1, 4, 6, 9 and 10). The rest of the proteins are proposed to be located in the spoke stalk (Piperno et al., 1977; Huang et al., 1981). Based on the RSP2 mutant *pf24*, the stalk proteins, RSP2, RSP16



and RSP23 are predicted to be located underneath the spoke head in a subcomplex referred to as the spoke neck complex. In the *pf24* axoneme, RSP2, RSP16, RSP23 and spoke head proteins are less abundant, while the remaining spoke stalk proteins appear normal (Huang et al., 1981; Patel-King et al., 2004; Curry and Rosenbaum, 1993). These predictions are further supported by selected loss of RSPs by low salt dialysis (Piperno et al., 1981) and by chemical crosslinking (Kohno et al., 2011). This arrangement is related to the questions addressed in this dissertation.

Consistent with the genetic evidence, the 17 RSPs are present in an isolated radial spoke that sediments as a 20S particle in a sucrose gradient. The 20S RS also contains 5 more molecules. Among the five, three molecules, IP2,3 and 4, form a complex that associates with the RS and may be involved in anchoring the RS to the outer doublets (Dymek et al., 2007; 2011). The other two are LC8 and calmodulin, the calcium sensor (Yang et al., 2001; Patel-King et al., 2004). This finding supports the notion that the radial spoke is involved in calcium induced motility changes. As these two molecules are present in multiple axonemal complexes, they were not absent from the spoke mutants, they were only recognized as RSPs following purifications of the RS.

Through multiple independent approaches, the genes encoding most molecules were identified. Their amino acid sequences and predicted molecular domains were determined (Williams et al., 1989; Curry et al., 1992; Patel-King et al., 2004; Yang et al., 2004; Yang and Yang, 2006; Yang et al., 2006; Dymek et al., 2007). Interestingly, molecular modules related to signal transduction are located exclusively in the spokestalk, while the spokehead primarily consists of structural proteins. In particular, two stalk proteins, RSP7 and RSP11 contain a RIIa domain that is also present in PKA.

Curiously, two molecules, RSP2 and RSP23 contain a Dpy-30 domain that resembles the RIIa domain. In addition, these four molecules also contain calcium-binding motifs and calmodulin-binding domains (Yang et al., 2006). This dissertation study reports the discovery that RSP3 is the key molecule that integrates these RSPs with distinctive molecular modules.

### **1.4.3 RSP3**

#### 1.4.3.1 RSP3: Sequence and Homology

Independent lines of evidence have shown that RSP3 plays multiple roles in the RS. One striking feature of RSP3 is its sequence homology. RSP3 orthologues from various organisms, ranging from *Chlamydomonas* to humans, share a higher homology than most components unique to axonemes (Gaillard et al., 2001). All RSP3 orthologues contain the highly conserved N terminal 320-a.a. (amino acid) region. *Chlamydomonas* RSP3 has an additional ~200 a.a. at the C-terminus, while a mammalian alternative-spliced isoform has a ~100 a.a. extension at the N-terminus (Jivan et al., 2009). This high sequence homology of the 320 a.a. residues implies a strong evolutionary pressure to maintain a key function.

#### 1.4.3.2 RSP3 Docks the RS to the Axoneme

RSP3 is essential for the assembly of the RS (Luck et al., 1977; Piperno et al., 1981). The RSP3 gene in the *pf14* mutant has a premature stop codon near the translation initiation site. Translation initiated from a downstream ATG produces diminished amounts of truncated RSP3 polypeptides that fail to assemble into the axoneme (Williams et al.,

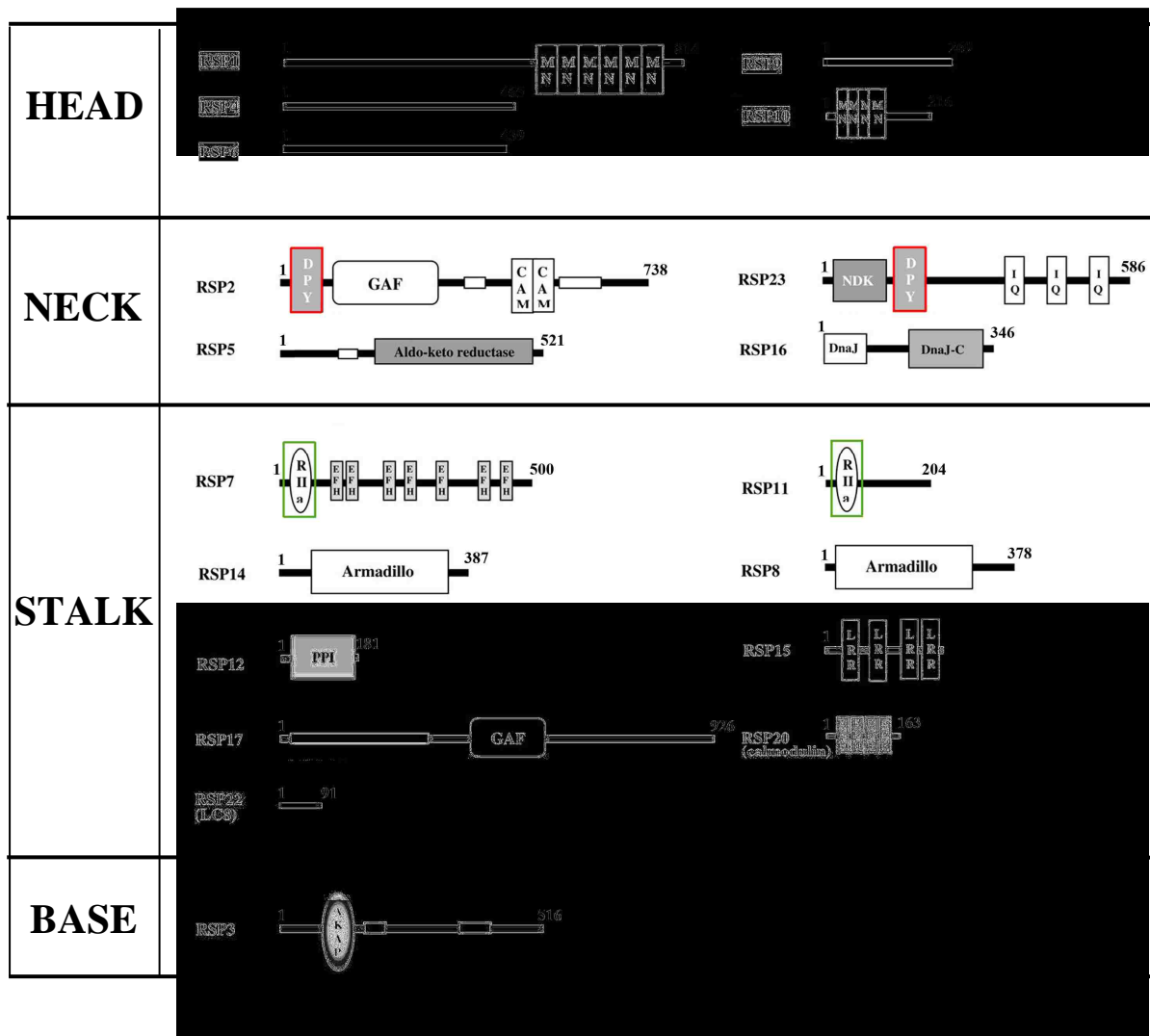


**Figure 1-2. Radial spoke proteins and their predicted functional domains.**

The radial spoke proteins are arranged based on their predicted locations. The Dpy-30 domain and RIIa domains are highlighted in red and green boxes respectively. MN, MORN domain; DPY, Dpy-30 domain; GAF, cyclic GMP Adenyl cyclase FhlA domain; CAM, calmodulin binding motif; AKAP, A-Kinase Anchoring Protein; IQ, calmodulin binding motif; NDK, Nucleoside Diphosphate Kinase domain; DnaJ and DnaJ-C, molecular chaperone homology domains; RIIa, RII alpha domain; EFH, EF-hand domain; PPI, Peptidyl Prolyl Isomerase domain; LRR, Leucline Rich Repeat domain. Coiled coil regions are depicted by open bars. This figure was modified from Yang et al., 2006.

**Table 1-1. *Chlamydomonas* radial spoke mutants that are relevant to this dissertation**

<b>Mutants</b>	<b>Motility phenotype</b>	<b>Morphological Defect</b>	<b>Gene product</b>	<b>Protein missing</b>	<b>RSPs in reduced amount</b>	<b>Predicted location</b>
<i>pf14</i>	Paralyzed	Spokeless	RSP3	All spoke proteins	NA	Base
<i>pf24</i>	Paralyzed	Less spokeheads and stalks	RSP2	None	1,4,6,9,10,2,16,23	Neck
<i>pf25</i>	Swimming/Paralyzed	None	RSP11	11	8	Base

1989), leading to spoke-less axonemes in *pf14*. The importance of the N-terminus is clarified by a reconstitution experiment. Reconstitution of axonemes and recombinant RSP3 synthesized in rabbit reticulocyte lysate showed that RSP3 binds to the axoneme. The binding site is confined to the N-terminal 85 a.a.. In parallel, expression of truncated RSP3 from a cDNA minigene construct also showed that the N-terminus of RSP3 is required for rescuing the motility of *pf14* while the C-terminus is dispensable (Diener et al., 1993). Based on these results from in vitro and in vivo experiments, it was proposed that RSP3 is located at the base of the RS for anchoring the entire RS to outer doublets. The function of the rest of the conserved region is unknown.

#### 1.4.3.3 RSP3: A Homodimer

Chemical crosslinking of isolated axonemes showed that RSP3 exists as a homodimer in the RS. The axoneme-binding region is capable of dimerization (Wirschell et al., 2008). It is speculated that this stable homodimer forms the scaffold at the base of the RS onto which other RSPs assemble. The results from this dissertation show that the dimeric RSP3 is a scaffold extending throughout the RS, not just at the base, which directly interacts with key RSPs.

#### 1.4.3.4 RSP3: The Spoke AKAP

RSP3 is currently referred to as an A-kinase anchoring protein (AKAP). From a historic perspective, the key role of AKAPs is to anchor the cAMP dependent protein kinase (PKA) (Pidoux and Tasken, 2010). PKA is a tetrameric holoenzyme with two catalytic subunits and two regulatory subunits, RI or RII (Figure 1-3). It is the primary effector for

the cAMP signal transduction pathways (Logue and Scott, 2010). Like the ubiquitous second messenger, cAMP, many AKAPs have been identified in various intracellular compartments. They differ drastically in their size and sequence. Yet they all have several common properties (Welch et al., 2010) (Figure 1-3). First of all, they all contain a ~14-18 a.a. amphipathic helix (AH) that interacts with the 40-a.a. dimerization and docking domain (D/D), RIIa, in the regulatory subunit, either RI or RII isotypes of PKA (Carr et al., 1991) (Figure 1-3 and 1-4). It is this very interaction that localizes PKA. In addition, all AKAPs contain a site that binds to a particular intracellular compartment, such as the cytoskeleton, mitochondria or Golgi (Wong and Scott, 2004). Lastly, they also contain additional motifs for binding to various molecules critical for different signal transduction pathways such as phosphatases and other kinases (Klauck et al., 1996; Welch et al., 2010). Thus it was proposed that AKAPs localize this enzyme of broad substrate specificity near its intended target proteins. The binding of cAMP to the regulatory subunit leads to the release and activation of the catalytic subunits which in turn phosphorylate the adjacent substrate (Figure 1-3). Presumably the anchoring of PKA through AKAPs improves the precision and efficiency of cAMP mediated signal transduction (Scott and Pawson, 2009). Furthermore, by anchoring PKA along with other molecular switches which may be synergistic or antagonistic, the different signal transduction pathways can be integrated (Figure 1-4 A).

Initially, anchoring proteins of PKA were identified based on their co-purification with PKA (Lohmann et al., 1984; Vallee et al., 1981). The interaction was mapped to the RIIa domain in the regulatory subunit (Scott et al., 1990) and an AH in AKAPs (Carr et al.,

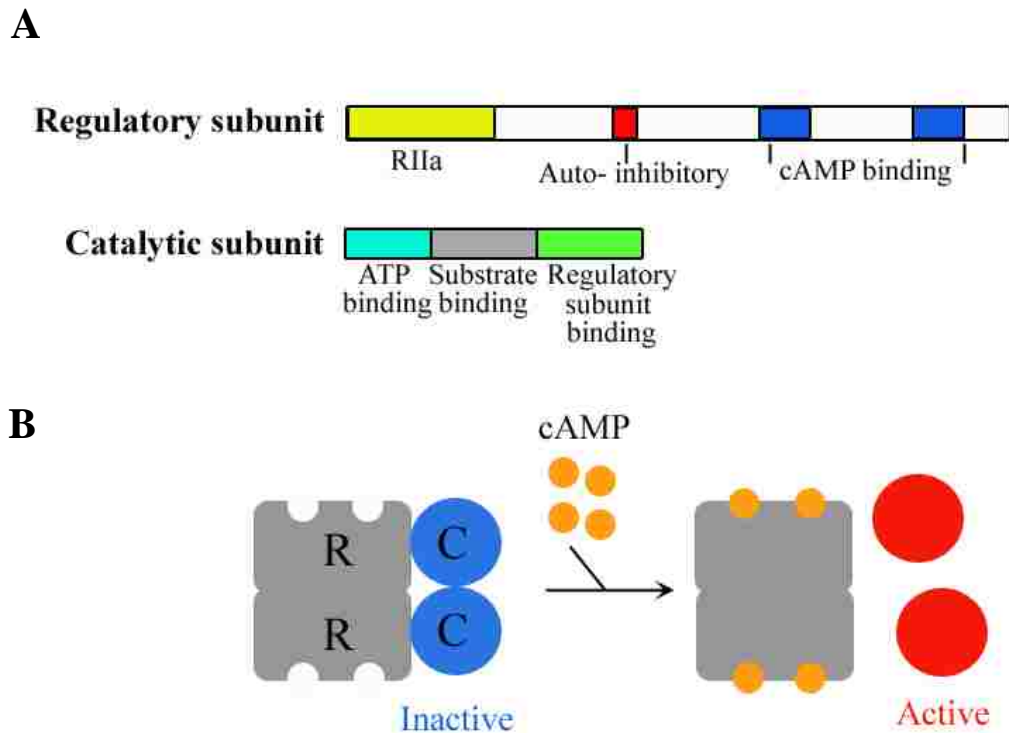
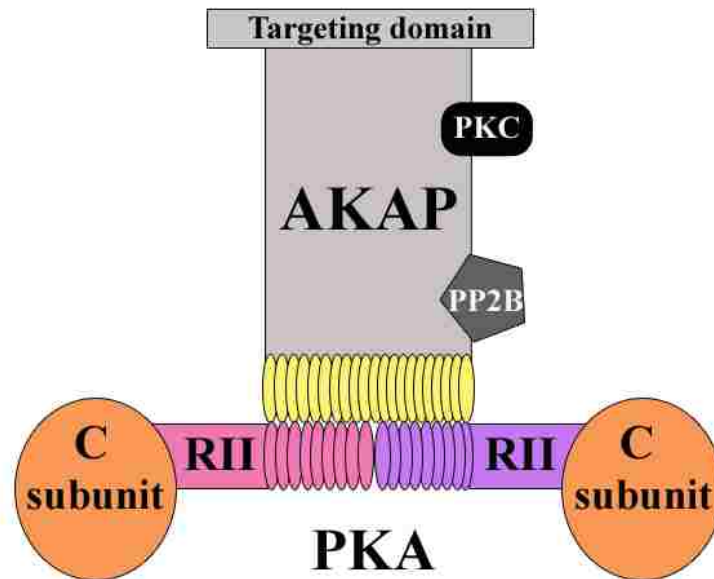


**Figure 1-3. The tetrameric holoenzyme of cAMP-dependent protein kinase.**

(A) The functional domains in the regulatory and catalytic subunits of PKA. The regulatory subunit contains an N terminal docking and dimerization domain known as the RIIa domain; two cAMP-binding sites and an auto-inhibitory site that binds the catalytic subunit and blocks catalysis. The catalytic subunit contains an ATP binding site, a substrate binding site and a regulatory subunit binding site. (B) The mechanism of PKA. The PKA tetramer contains two regulatory subunits (grey boxes) and two catalytic subunits (blue circles). The holoenzyme is inactive until cAMP (orange circles) occupies the cAMP binding sites in the regulatory subunit. This releases the active catalytic subunits (red circles) which phosphorylate the substrates.

A



B

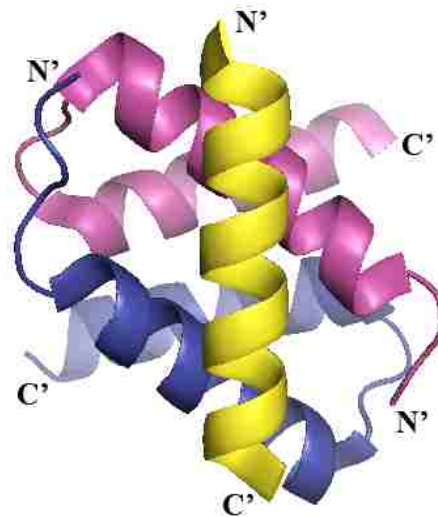


**Figure 1-4. AKAPs: The signaling scaffolds and their interaction with the RIIa domain.**

(A) Schematic showing three main features of an AKAP: a targeting domain that anchors an AKAP to a specific subcellular location; an amphipathic helix (yellow) that binds to the RIIa domain of PKA (pink and purple) and additional sites that binds other signaling molecules. RII, regulatory subunit; C, catalytic subunit. (B) Crystal structure of RIIa domain (blue and pink helices in complex with AKAP (yellow)). This structure is modified from PDB ID: 2IZY (Gold et al., 2006).



1991). Most AKAPs were identified using an overlay using radioactive RII as a ligand (Lohmann et al., 1984). This assay was used to screen expression libraries or protein blots. The binding is blocked by AHs with high affinities for the dimeric RIIa (Carr et al., 1992; Alto et al., 2003; Burns-Hamuro et al., 2003). Many proteins were found to bind RII in vitro, and thus they were referred to as AKAPs and presumed to anchor PKA in vivo. The micro-compartments that they are located in are presumed to be regulated by PKA. Similarly, the RI regulatory subunit of PKA is also used in overlays. Based on the affinity and specificity of AKAPs for RI or RII, AKAPs are classified into three categories, RI-AKAP that interacts with RI alone; RII-AKAP that interacts with RII alone; and dual AKAP (D-AKAP) that interacts with both RI and RII.

### ***1.5 The RIIa Clan***

While the AH-RIIa interaction was exploited to identify the PKA anchoring proteins, AKAPs, the RIIa domain has been found in many proteins that are irrelevant to PKA. In fact, this domain is present in more than 200 molecules with diverged molecular architectures in various eukaryotic genomes. Most of them are poorly characterized. Two such molecules are in the radial spoke complex of *Chlamydomonas* flagella, RSP7 and RSP11 (Yang and Yang, 2006; Yang et al., 2006). Furthermore, a RIIa-like domain, Dpy-30, was found in equally numerous poorly characterized molecules, including two proteins in the radial spoke complex, RSP2 and RSP23 (Yang et al., 2006). These proteins with either a RIIa or Dpy-30 domain are classified into two subfamilies within the RIIa clan in the protein family database Pfam (Table 1-2).

### **1.5.1 RIIa Clan Domains**

RIIa and Dpy-30 domains share considerable similarities in sequence, secondary structure and tertiary structure. However, they also have significant distinctions that define the two domains.

#### 1.5.1.1 RIIa Domain













The RIIa domain is usually 40-a.a. long. RIIa domains share extensive sequence homology, except the N-terminal region. The core is comprised of a helix-loop-helix secondary structure (Newlon et al., 1999 and 2001). Structural studies have primarily focused on RII's RIIa domain. The structures showed that two helix-loop-helix monomers fold into a X-type four helix bundle (Gold et al., 2006; Kinderman et al., 2006) (Figure 1-4). The dimerization forms a shallow groove that binds to the AH in various AKAPs. The lateral boundary was defined by a  $\beta$ -strand from the N-terminus (Kinderman et al., 2006).

The interaction of the dimeric RIIa and the AH is primarily hydrophobic in nature. The hydrophobic residues in the groove of the RIIa dimer, including the  $\beta$ -strand, associate with the hydrophobic residues clustered on one side of the amphipathic helix. More recent structures of RI's RIIa domain in complex with an AH also revealed a similar X-type four-helix bundle (Banky et al., 2003; Sarma et al., 2010). However, the N-terminus unique to RI's RIIa is helical, contrary to the  $\beta$ -strand in RII's RIIa. The additional helix folds inwards, resulting in a much deeper hydrophobic, AH-binding cavity (Banky et al., 2003; Sarma et al., 2010).

### 1.5.1.2 Dpy-30 Domain

In contrast to the RIIa domain, the study of the Dpy-30 domain is relatively nascent. Dpy-30 in *C.elegans* was the first Dpy-30-domain containing protein discovered. The name was derived from the dumpy phenotype of the mutant nematode defective in the encoded gene. Genetic analyses revealed that the protein is part of the chromosome modification complex. It not only affects the body shape but is also involved in X-chromosome dosage compensation (Hsu et al., 1994). Studies in other organisms revealed that the Dpy-30 protein is also a small yet critical subunit in various Set1- like histone methyltransferase complexes that mediate epigenetic regulation in most eukaryotic cells (Roguev et al., 2001; Cho et al., 2007; Patel et al., 2009). In embryonic stem cells, depletion of Dpy-30 blocks the neuronal differentiation (Jiang et al., 2011). A 40-a.a region in this ~100-a.a. Dpy-30 ortholog shares limited sequence homology with the RIIa domain in PKA (Roguev et al., 2001). As more genome sequencing projects were completed, sequences with homology to this region were found in many divergent proteins. The sequences associated with this conserved domain vary drastically. Thus this conserved motif was named the Dpy-30 domain.

Analogous to the RIIa domain, this new domain is also composed of a helix-loop-helix secondary structure. However, this common unit in all Dpy-30 domains is preceded by a short helical sequence that is absent in RII's RIIa domain (Wang et al., 2009) (Figure 1-4). The recently solved X-ray crystal structure of this domain from the human Dpy-30 protein also forms an X-type four-helix bundle. The N-terminal helix occupies the position of the  $\beta$ -strand in RII's RIIa domain. The cavity in the dimer is deeper and less hydrophobic than RII's RIIa domain (Wang et al., 2009). Numerous AHs that bind the

	RIIa domain  containing proteins	Dpy-30 domain  containing proteins
Nucleotide phosphotransferase	Guanylate Kinase 	ADK 7  ADK 5  RSP 23 
2nd Messenger	RSP 7  PKA 	RSP 23  RSP 2 
Uncharacterized	RSP 11 	DPY-30 

**Table 1-2. The RIIa-clan members**

The RIIa clan consists of two subfamilies, RIIa and Dpy-30. The RIIa clan domain containing proteins listed above are classified based on the functional modules associated with the RIIa clan domain. RIIa, RII alpha domain; GK, Guanylate Kinase domain; ADK, Adenosine Diphosphate Kinase domain; NDK, Nucleoside Diphosphate Kinase domain; Dpy-30, Dpy-30 domain; IQ, calmodulin binding motifs; EF, calcium binding EF hands; cNMP, catalytic subunit of proteins kinase A; CaMB, calmodulin binding motif.

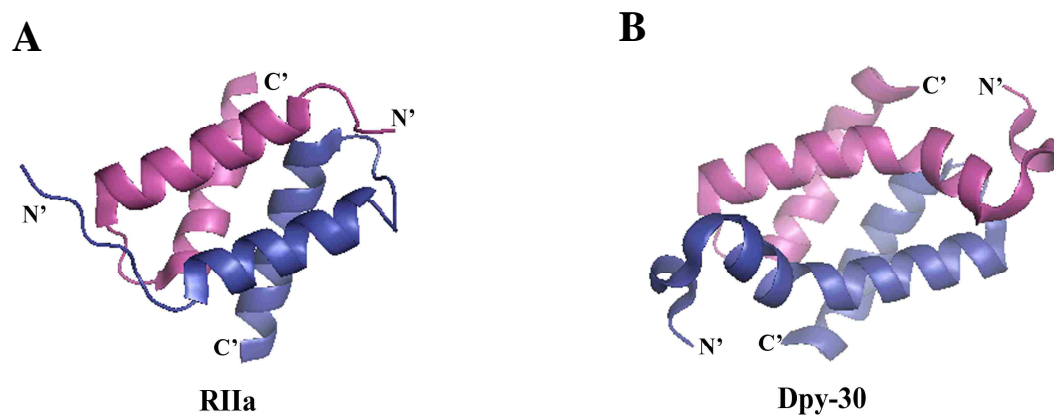


**Figure 1-5. Crystal structures of the RIIa clan domains.**

(A) The RIIa domain from RII (PDB ID: 2HWN, Gold et al., 2006) and (B) the Dpy-30 domain from the human Dpy-30 protein (PDB ID: 3G36, Wang et al., 2009).

RIIa domain have been discovered and two sequences in Ash2 of the histone methyltransferase complex and BIG1 GTPase exchange factor in the Golgi apparatus were found to bind Dpy-30 protein during the period of this thesis (South et al., 2010; Xia et al., 2010). The common feature among Dpy-30 binding sequences remains uncertain.

The similarity of these D/D domains and the numerous proteins with these domains begs an important question about the specificity. How do these similar domains dock these important proteins to the appropriate locations: PKA to the cAMP-signaling sites, Dpy-30 to the histone methyltransferase complex and BIG1 GTPase exchange factor to the Golgi? What are the other functions that these similar D/D domains may dock?

#### 1.5.1.3 RII- Clan-Domain Containing RSPs

These questions can be elucidated by investigating the RS. The RS contains an AKAP that binds PKA's RII in vitro (Gaillard et al., 2001). Instead of PKA, the RS also harbors four non-PKA RIIa clan members. RSP7 and RSP11 have RIIa domains; and RSP2 and RSP23 have Dpy-30 domains (Yang et al., 2006). All four proteins are in the stalk.

Consistent with the docking function of the domains, genetic evidence suggests that the paired RIIa-containing RSPs and Dpy-30-containing RSPs are located at opposite ends of the stalk. It is unclear how these four molecules with a similar D/D domain dock onto the different parts of the small RS complex and contribute to its role in mechanochemical regulation.

The RSP2 mutant, *pf24*, generates paralyzed flagella due to an initiation codon mutation in the gene encoding RSP2 (Huang et al., 1981; Yang et al., 2004). The

axoneme has diminished amounts of RSP2 protein, the spoke HSP40 and Dpy-30-containing RSP—RSP23, while the spokehead components are reduced, albeit less drastically (Huang et al, 1981; Patel-King et al., 2004). Thus it was predicted that Dpy-30 domain containing RSP2 and RSP23 are co-assembled along with RSP16 near the neck. Note that the deficiency of the spoke head is less severe than that of RSP2, indicating that RSP2 is only one of the molecules linking the spoke head to the spoke stalk.

It was recently shown that the assembly of RSP2 to the RS is mediated by the Dpy-30 domain and the trailing coiled coil. The calmodulin binding motifs within the C terminal region of RSP2 also suggest that RSP2 is involved in regulating flagellar beating (Gopal et al., unpublished). The additional sequence in RSP23 contains a NDK domain that converts NDP to NTP. Consistent with this, the RS contributes to a fraction of the NDK activity in the axoneme. The role of this NDK domain remains to be determined.

The two RIIa-containing RSPs appear normal in the *pf24* axoneme and thus they are predicted to be located away from the neck region. The sequences tethered to the RIIa domain are equally intriguing. A series of calcium-binding EF hands trail the RIIa domain in RSP7. The additional sequence in RSP11 is devoid of any molecular domains. RSP11 is not essential for the assembly of the RS or for motility (Yang and Yang, 2006). Mutants lacking RSP11 generates motile flagella only when the media is fresh and enriched. The flagella become paralyzed when the media is exhausted of nutrients in the stationary phase. The mutant also displays reduced levels of RSP8, another RS subunit with armadillo (ARM) repeats known for protein-protein interactions (Yang et al., 2006). This suggests that RSP8 and RSP11 interact. However, the nature of the association of

these two proteins and why deficiencies in these two proteins result in reversible paralysis is unclear.

Although RII, RSP7 and RSP11 all have the RIIa domain, mutations of the AH in RSP3 abolished only the interaction of RSP3 with RII in the overlay assay (Gaillard et al., 2006). The same mutation when introduced into *Chlamydomonas*, caused a mixed population of swimmers and immotile cells (Gaillard et al., 2006) but the amount of the RIIa-domain containing proteins, RSP7 and RSP11, was not reduced (Gaillard et al., 2006). These inconsistencies raise several questions. Does the amphipathic helix serve to anchor PKA to the RS; or the non-PKA RIIa-containing RSP7 and RSP11? If it does anchor these two RSPs, why are they still assembled when the amphipathic helix is perturbed? What molecules do the Dpy-30 domain in RSP2 and RSP23 interact with and what are their sequences? The answers to these questions will reveal the topology of the RS and help to understand how RS regulates flagellar beating mechanically and chemically. Importantly, the answers could elucidate the mechanisms that distinguish the specificity of these two similar RIIa clan domains and the effector mechanisms that tether to these putative D/D domains.

### ***1.6 Objectives of the Research***

**Objective 1: Test the hypothesis that the spoke AKAP, RSP3, forms the backbone of the radial spoke stalk.**

We reason that the arrangement of the four RSPs with the RIIa clan domains must provide the predicted rigidity necessary for RS to couple the mobile CP and the outer doublets at high frequency (Warner and Satir, 1974). The simplest model is that all four



molecules anchor to the dimeric RSP3. As RSP2 and RSP23 are located near the spokehead and the RSP3 N-terminus binds to the axoneme, this prediction implies that RSP3 forms the spoke scaffold, extending throughout the RS complex. Chapter 3 is focused on testing this hypothesis. To test this hypothesis, truncations were made within RSP3. The flagella of the mutant strains were analyzed for their composition and morphology. We predict that deleting the binding sites for the RIIa domain or for the Dpy-30 domain shall result in deficiencies in the four RSPs, either in their composition or their stability. Electron microscopy studies on some of these mutants showed that truncating RSP3 results in a dwarfed radial spoke stalk which is consistent with RSP3 forming the RS scaffold. This work is described in Section I of Chapter 3.

**Objective 2: Identify the binding sites for the RIIa domain and the Dpy-30 domain in the RS**

Once the binding proteins and the binding regions were identified in vivo, an in vitro approach was taken to define the binding sequence. The binding sequence and the D/D domains were co-expressed in bacteria for testing their interaction by co-purification. Once the binding sequence for the Dpy-30 domain was identified, sequence analyses were conducted to determine the similarity and distinction of the binding sequences for the RIIa and the Dpy-30 domains. This work is described in Section II of Chapter 3.

**Objective 3: Develop tools to study the RIIa domains and Dpy-30 domains.**

The study of Dpy-30 domains is still emerging. Many Dpy-30 domain containing proteins and their anchoring proteins are poorly characterized. Even the Dpy-30 domain in the Dpy-30 protein, is known to anchor at least two molecules, Ash2 in the histone methyltransferase complex and BIG1 in the Golgi apparatus (South et al, 2010; Xia et al.,

2010). It is likely that more Dpy-30-anchoring proteins remain to be discovered. In addition, the similarity of the anchoring sequences discovered in this dissertation raises question about the distinction in the specificity, affinity and kinetics of the two types of D/D domains. This dissertation developed alternative reagents and assays to address these questions. This project is described in Chapter 4.

## **Chapter 2: Materials and Methods**

The chemicals, biological reagents, molecular biology, cell biology and protein biochemistry methods used in this study are outlined in this chapter.

### ***2.1 Materials***

#### **2.1.1 Chemical Reagents**

Chemical reagents used in this study are summarized in Table 2-1.

#### **2.1.2 Oligonucleotides**

Oligonucleotides used in this study for polymerase chain reactions (PCR) to engineer plasmids and truncation mutants are listed in Table 2-2.

#### **2.1.3 Antibodies**

The antibodies used in this study are listed in Table 2-3.

**Table 2-1. Chemicals used in this study**

Vendor	Name
Amresco	Yeast Extract Dithiothreitol (DTT) Isopropyl- $\beta$ -D-thio-galactoside (IPTG)
Bio-Rad	Acrylamide
Biolab Inc.	dNTPs
Calbiochem	Nonidet-P40
Celliance	Aprotinin
EM Sciences	Osmium Tetroxide Propylene oxide 2,4,6-(Tri(Dimethylaminoethyl)phenol) (DMP30) Dodecanyl succinic anhydride (DDSA) Nadic methyl anhydride (NMA) EMBed-812 Uranyl Acetate
Invitrogen	Urea
JT Baker	Methanol Potassium hydrogen phosphate ( $K_2HPO_4$ ) Potassium dihydrogen phosphate ( $KH_2PO_4$ ) Tris Base
Fisher Scientific	Potassium iodide
Mallinckrodt	Sucrose
Midwest Sci.	Agarose Tryptone
MP Biomedicals	Paromomycin
Polysci Inc.	Sodium Cacodylic acid
Shelton Scientific	Bromophenol blue
Spectrum Chemical	Dibucaine
Stratagene	Pfu DNA polymerase
TCI America	Luminol

---

Sigma	Acetic acid
	Agar
	Ammonium chloride ( $\text{NH}_4\text{Cl}$ )
	Ammonium persulfate
	Ammonium nitrate ( $\text{NH}_4\text{NO}_3$ )
	Boric acid ( $\text{H}_3\text{BO}_3$ )
	Bovine Serum Albumin (BSA)
	Calcium Chloride dehydrate ( $\text{CaCl}_2 \cdot 2\text{H}_2\text{O}$ )
	Cobalt Chloride hexahydrate ( $\text{CoCl}_2 \cdot 6\text{H}_2\text{O}$ )
	Coumaric acid
	Cupric sulfate pentahydrate ( $\text{CuSO}_4 \cdot 5\text{H}_2\text{O}$ )
	L-Cysteine
	Ammonium heptamolybdate ( $(\text{NH}_4)_6\text{Mo}_7\text{O}_{24}$ )
	Dimethyl Sulfoxide (DMSO)
	Ethidium Bromide
	Ethylenediaminetetraacetic acid (EDTA)
	Ethylene glycol tetraacetic acid (EGTA)
	Ferrous sulfate ( $\text{FeSO}_4 \cdot 7\text{H}_2\text{O}$ )
	Glycerol
	Glycine
	Glutaraldehyde
	4-(2-hydroxyethyl)-1-piperazineethanesulfonic acid (Hepes)
	Hydrogen peroxide ( $\text{H}_2\text{O}_2$ )
	Imidazole
	Kanamycin
	$\beta$ -mercaptoethanol
	Manganese sulfate ( $\text{MnSO}_4$ )
	Manganese chloride ( $\text{MnCl}_2$ )
	Magnesium sulfate heptahydrate ( $\text{MgSO}_4 \cdot 7\text{H}_2\text{O}$ )
	Phenylmethanesulfonyl fluoride (PMSF)
	Polyethylene glycol (PEG 8000)
	Ponceau S
	Potassium Acetate ( $\text{KCH}_3\text{COO}$ )
	Potassium chloride
	Ribonuclease
	Sodium Dodecyl Sulfate
	Sodium chloride ( $\text{NaCl}$ )
	Sodium Hydroxide ( $\text{NaOH}$ )
	Sodium Acetate ( $\text{NaCH}_3\text{COO}$ )
	Sodium Carbonate ( $\text{Na}_2\text{CO}_3$ )
	Sodium phosphate ( $\text{NaH}_2\text{PO}_4$ )
	Sulfosalicylic Acid
	Tannic acid
	Tetramethylethylenediamine (TEMED)
	Zinc sulfate heptahydrate ( $\text{ZnSO}_4 \cdot 7\text{H}_2\text{O}$ )

---

**Table 2-2. Oligonucleotides used in this study**

Name	Sequence
XbaS	AGCTCTAGACTACTCTCAGCTTGAGCCACATTTATGC
XhoAS	TCTCCATCAGGCCCTGCTCGAGCACCTTGCCCAC
XhoS	TCTCGAGCTGTCTGGCATTGTCAACACGGTG
AS	TCTTGTCCGCCTCCCCTTGGCGTTG
SpeS	CCGCAAGCTCACTCGTTCACCATAAAC
NotAS	AGCGGCCGCGCGATTGGCTGCCAGCGCCGCCGC
EcoRIS	GGAATTCCCGCTCTGCTCTCCAGTCCGACTAGGG
XbaAS1	GCTCTAGACGCCAGGGTGCTGCGATTGGCTGCC
XbaAS2	GCTCTAGAGCCGCGCGCAAAGGCGCTGGCCGCC
XbaAS3	GCTCTAGACTCCTCCTCCTCCAGCACCTCCATCAGG
XbaS(tag)	GCTCTAGACAGGCGCTGGCGGTGCACGCGCTGGG
EcoRIAS	GGAATTCTGTTGCCTGAGAGCTCCGCCTCGGCC
XhoS	ACCTCGAGCACCACCACCACCACCTAAGCTAGAGGG
ICAS	ACCTCGAGGGGGTACGTAGATGTAGCCGCT
96BamS	GCGGATCCCGGCACATCGACATCCAAACGGAC
180RIAS	CGGAATTCTTACTCCTCCAGCACCTCCATCAGGC
245BamS	GCGGATCCGCCTTTGCGCGCGGCTACCTGTCTGGC
316RIAS	GCGAATTCGGTGCTGCGATTGGCTGCCAGCGCCGC
269BamS	GCGGATCCCCCGTCATGCGCGAGGTGGAGACGG
NdeS	CCCATATGGAGCCAGAGCAGATGCTGGAG
DpyHindAS	GCAAGCTTCTGGAGATCTACCTTCTGCTTTGATGAC
RSP2HindS	GCAAGCTTCCCGACACAGCCTACCTCAAAGAGAC
RSP2XhoAS	GCCTCGAGTCATTCTACTTCAGCATTTTTTCACGTATTTGAGC
PstIS	GCTGCAGAAGGTAGATCTCCAGTCTTTGCCAAC
NheIAS	GGCTAGCTCAGTTTCGATCTTCAAACCTGTGCC
NcoS	GCCCATGGAGTCCCCTATACTAGGTTATTGG
GSTAS	GGGGGATCCACGCGGAACCAGATCCG
280BamS	GCGGATCCCCCTGGCTCAAGGAGCAGG
306RIAS	GCGAATTCGTCTCCACCAGCTTGTCCACC
298RIAS	GCGAATTCGCGCCGCGCCACCAC
308RIAS	GCGAATTCGCGCGTCTCCACCAGCTTGTCC
HybridS	GATCTGGTTCCGCGTGGATCCCCCTGGCTCAAGGAGC
V*PS	GTGGCGCGGCGGTGCCGACAAGCTGGTGGAG

V*PAS	CTCCACCAGCTTGTCCGGCACGCGCCGCGCCAC
H301BamS	GCGGATCCGAAAAACCATGGAATATAGCATGG
H325RIAS	GCGAATTCCTCTTTTCAACCACCTCACG
HHybS	GATCTGGTTCCGCGTGGATCCGAAAAACCATGGAATATAGC
AatIIS	GGACGTCGACGGCGGGGAGCTCGCTG
AatIIAS	GGACGTCGGTACCCGCTTCAAATACGCC

S: Sense primer; AS: Antisense primer

**Table 2-3: Antibodies used in this study**

<b>Antigen</b>	<b>Host</b>	<b>Reference</b>
RSP1	Rabbit	Yang et al., 2008
RSP2	Rabbit	Yang et al., 2001
RSP3	Rabbit	Yang et al., 2001
RSP6	Rabbit	Yang et al., 2008
RSP7	Rabbit	Yang et al., 2006
RSP8	Rabbit	Yang et al., 2006
RSP11	Rabbit	Yang et al., 2006
RSP16	Rabbit	Yang et al., 2005
RSP23	Rabbit	Yang et al., 2008
IC140	Rabbit	Yang and Sale, 1998
HA	Rabbit	Covance Inc.,
GST	Mouse	Genscript
Radial spoke	Chicken	Yang et al., 2005
<b>Secondary Antibodies</b>		
Anti-chicken IgY-peroxidase	Rabbit	Sigma
Anti-rabbit IgG-peroxidase	Goat	Sigma
Anti-mouse Ig –peroxidase	Goat	Sigma



## ***2.2 Cell Strains and Culture Conditions***

*The Chlamydomonas reinhardtii* strains used in this study were wild-type strain *cc124(-)*, and paralyzed RSP3 mutant strain, *pf14*. They were obtained from the Chlamydomonas Resource Center (Duke University, Durham, NC).

The cells were grown on Tris-Acetate-Phosphate (TAP) plates for 6-7 days. Subsequently a loop of cells were inoculated into ~350 ml TAP liquid medium and cultured under aeration in a 14/10 light/dark cycle (Harris, 2009).

## ***2.3 Molecular Biology***

### **2.3.1 Polymerase Chain Reaction-based DNA Fusion**

To generate small (< 100 bp) truncation constructs a mixed PCR strategy was adopted. For instance, to create a vector that expresses GST-RSP3<sub>280-308</sub>, GST and RSP3<sub>280-308</sub> were amplified. The PCR fragments, 5 ng each, were used as the templates for the fusion PCR reaction. They were amplified using three primers: GST forward primer; RSP3<sub>308</sub> reverse primer and a hybrid forward primer that contains the 3' end sequence of GST and 5' end sequence of RSP3<sub>280-308</sub>. The resulting PCR product with both coding sequences could be cloned into an expression vector using conventional cloning techniques. The conditions used for the mixed PCR took into the consideration the annealing temperature of all the three primers and DMSO was omitted from the PCR reaction. Other parameters were not varied.

### **2.3.2 Engineering Genomic DNA Constructs**

A NcoI fragment containing the RSP3 genomic DNA was released from a BAC clone

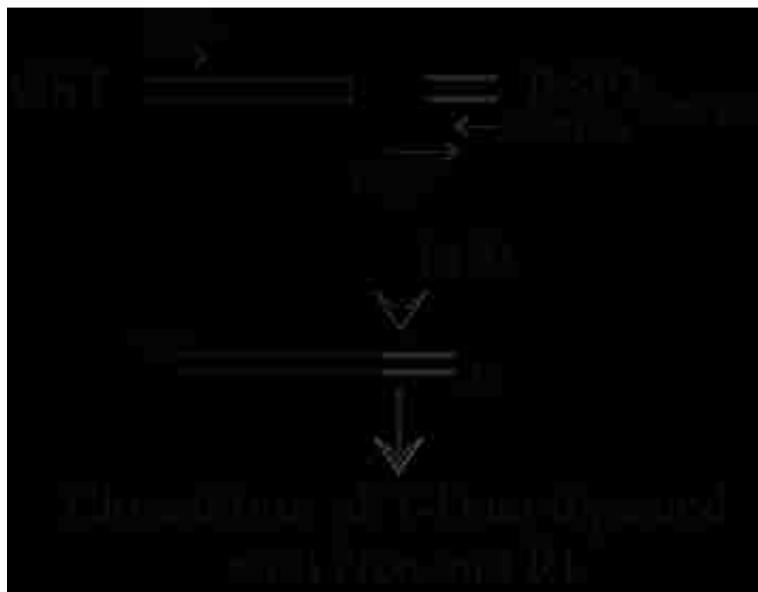


**Figure 2-1. The PCR strategy for fusing the sequences encoding a large tag and a small amphipathic helix.**

This method is developed to overcome the difficulty in cloning a small DNA fragment for protein expression. The templates for PCR amplification include the PCR fragments for GST and for RSP3's AH. Three primers for PCR amplification: the NcoS primer, the RSP3AS primer and the hybrid primer (HybS) which contain the 3' end sequence of GST DNA and the 5' end sequence of RSP3's AH. The PCR product generated from this reaction is purified and inserted into pET-Duet vector digested between the NcoI site and EcoRI site.

and inserted into NcoI site in pGEM-T Easy vector (Promega). The SacI site and its downstream sequence in the 3' flanking region were eliminated by limited restriction digest followed by treatment with T4 DNA polymerase. PCR with modified primers was performed to add the sequence for 6 His codons flanked by XhoI site at one end and stop codon followed by Xba site at the other end. Subsequently, a PCR product containing 3HA-6His coding sequence flanked by XhoI sites was ligated into the XhoI site. This fragment was amplified using p3HA plasmid (Silflow et al., 2001) as a template. The final RSP3 genomic construct, pRSP3-HAHis expressed a polypeptide with a 3HA and 12His tag. This construct was used to create all the mutant constructs. All the strains were generated using a PCR based approach.

#### **Δ1**

The nucleotide sequences flanking Coil1 (171-244 a.a.) were amplified from pRSP3-HAHis vector using the following primer pairs: XbaS, XhoAS and XhoS, AS. The PCR fragments were digested with XbaI and XhoI; and with XhoI and NotI. The two digested fragments, i.e. Xba-Xho and Xho-Not, were ligated into pRSP3-HAHis vector digested with SpeI and NotI. XbaI and SpeI generate complementary free ends that allow ligation and distinction between the parental DNA and the ligated DNA. For single plasmid transformation in *Chlamydomonas*, this construct was further modified by adding the paromomycin (PMM) resistance cassette from pSI 103 plasmid (Yang et al., 2008) into the AatII site. This vector is designated as pΔCoil1PMM.

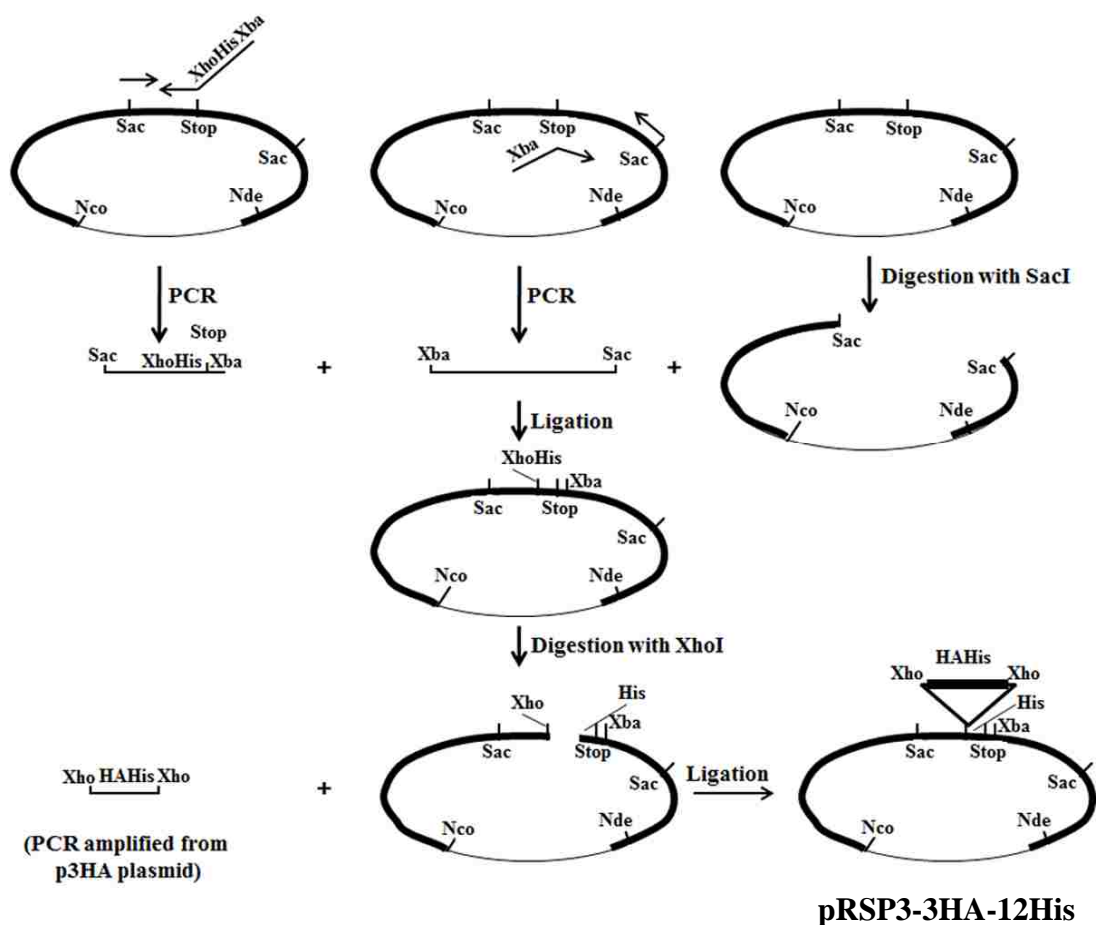


**Figure 2-2. Cloning Strategy for the generation of pRSP3-3HA-12His.**

The pGEM T- Easy vector that contained the sequence encoding the RSP3 genomic DNA (bold line) was amplified using primers with 6 His codons flanked by XhoI site at one end and a stop codon followed by a Xba site at the other end. This PCR fragment along with the Xba-SacI piece was ligated into the SacI site in the pGEM T-Easy vector. The sequence encoding the 3 HA tag was amplified from p3HA plasmid with primers that contained built in XhoI sites at both ends and also the sequence for 6 His codons. The resulting fragment which contained the sequence for 3HA tag and 6 His codons flanked on either side by Xho I site was cloned into the XhoI site thus generating pRSP3-3HA-12His.

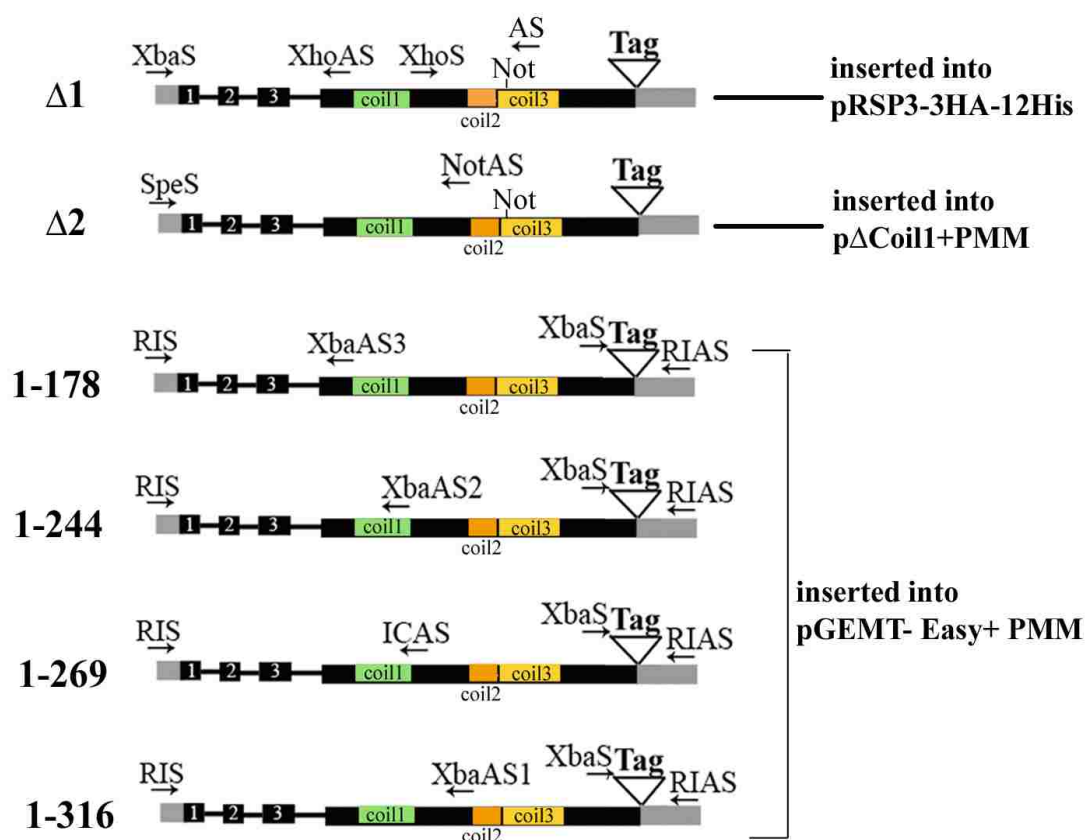


**Figure 2-3. Strategy for the generation of RSP3 truncation constructs.**

Schematic representing the cloning strategy that was applied to generate the various RSP3 truncation constructs. The grey boxes represent the 5' and 3' UTR; the black boxes depict the exons and the black lines depict the introns. The three coils in RSP3 are shown as the colored boxes. The primer pairs utilized to generate each construct are also depicted.

**Δ2**

The nucleotide sequences flanking coil2 were amplified from the pRSP3-HAHis vector using SpeS and NotAS primers. The amplified fragment was ligated into pΔCoil1PMM vector digested with Spe and Not.

The PMM cassette was also cloned into the AatII site in pGEM-T Easy, and this vector (pGEM-T Easy + PMM) was used to generate the remaining RSP3 constructs.

**1-178**

To create the RSP3<sub>1-178</sub> construct, two fragments were amplified from the pRSP3-HAHis vector. The first fragment which extended from the 5'UTR to 178 aa was generated using a EcoRIS primer with a built in EcoRI site and an antisense primer (XbaAS3) with a built in Xba site. The second fragment which extended from the 3HAHis tag to the 3'UTR was generated using a sense primer with a built in Xba site (XbaStag) and an antisense primer with a built in EcoRI site (RIAS). The two fragments (RI-Xba and Xba-RI) generated by PCR were ligated into the pGEM-T Easy + PMM template digested with RI.

**1-244**

To create the RSP3<sub>1-244</sub> construct, flanking sequences were amplified using the same set of primers that were used to make RSP3<sub>1-178</sub>, except XbaAS3 primer was replaced with the XbaAS2 primer, which resulted in a fragment extending from the 5'UTR to 244 aa. The second fragment which extended from the 3HAHis tag to the 3'UTR was generated using a sense primer with a built in Xba site (XbaStag) and an antisense primer with a built in EcoRI site (RIAS). The two fragments (RI-Xba and Xba-RI) generated by PCR, were ligated into the pGEM-T Easy + PMM template digested with RI.

**1-316**

To create the RSP3<sub>1-316</sub> construct, flanking sequences were amplified using the same set of primers that were used to make RSP3<sub>1-178</sub>, except XbaAS3 primer was replaced with the XbaAS1 primer which resulted in a fragment extending from the 5'UTR to 316 a.a. The second fragment which extended from the 3HAHis tag to the 3'UTR was generated using a sense primer with a built in Xba site (XbaStag) and an antisense primer with a built in EcoRI site (RIAS). The two fragments (RI-Xba and Xba-RI) generated by PCR, were ligated into the pGEM-T Easy + PMM template digested with RI.

**1-269**

To create the RSP3<sub>1-269</sub> construct, two fragments were amplified from the pRSP3-HAHis vector. The first fragment which extended from the 5'UTR to 269 a.a. was generated using the EcoRIS primer and ICAS primer with a built in Xho site. The second fragment which extended from the 3HAHis tag to the 3'UTR was generated using a sense primer with a built in Xho site and RIAS primer. The two fragments (RI-Xho and Xho-RI) generated by PCR, were ligated into the pGEM-T Easy + PMM template cut with RI.

**2.3.3 Engineering cDNA Constructs****i) GST-tagged RSP3<sub>96-180</sub>; RSP3<sub>245-316</sub> and RSP3<sub>269-316</sub>**

The constructs expressing GST tagged RSP3<sub>96-180</sub>, RSP3<sub>245-316</sub> and RSP3<sub>269-316</sub> were made by first amplifying the corresponding sequences from GST-RSP3 cDNA as a template (Diener et al.,1993) using a sense primer with a built in Bam site and an antisense primer with a built in RI site. The PCR products were then inserted into pGEX-2T vector digested with Bam and RI.

**ii) GST-tagged RSP3<sub>269-298</sub>**

RSP3<sub>269-316</sub> in pGEX-2T was used as the template. The sequence corresponding to RSP3<sub>269-298</sub> inclusive of the GST tag was amplified. The NcoS primer with a built in Nco site annealed to the GST tag and the 298RIAS primer was used to amplify the RSP3 sequence. The resulting fragment which consisted of GST-RSP3<sub>269-298</sub> was inserted into pET-Duet vector (Novagen) digested with Nco and RI.

**iii) GST- tagged RSP3<sub>280-316</sub>; RSP3<sub>280-306</sub> and RSP3<sub>280-308</sub>**

The constructs for expressing these short fragments were modified from the pGEX-RSP3<sub>245-316</sub>. The PCR fusion strategy was employed to fuse the coding sequences for GST and a RSP3 fragment. The fused PCR fragment was inserted into pET-Duet vector digested with Nco and RI.

**iv) RSP3<sub>280-316</sub>V300P**

The pRSP3<sub>280-316</sub> was used as the template to replace V300 into P using QuikChange Site-Directed mutagenesis strategy (Stratagene). The resulting plasmid is named pRSP3<sub>V300P</sub>.

**v) His-tagged full length Dpy-30 (FL)**

To create the His –tagged Human Dpy-30 full-length construct the sequence was amplified from a commercially available cDNA clone using a sense primer with a built-in NdeI site and an antisense primer with a built-in XhoI site. The fragment was inserted into pET-28a vector digested with NdeI and XhoI. The resulting construct expressed N-terminally- tagged Dpy-30.



**vi) His- tagged Dpy-30<sub>45-99</sub>**

The Dpy-30<sub>45-99</sub> construct expresses the Dpy-30 domain in the Dpy-30 protein. The sequence was amplified using a sense primer with a built-in PstI site and an antisense primer with a built-in NheI site. The PCR fragment is inserted into a modified pET-28a vector that has a coding sequence for TEV protease cleavage site inserted downstream to 8 His codons, pET28a-H8-TEV (kindly provided by Dr. St.Maurice).

**vii) GFP- tagged Ash2**

The coding sequence for Ash2's AH was PCR-amplified from a human cDNA clone obtained from Open Biosystems. GFP sequence was amplified from a plasmid obtained from Lehtreck and Witman (2009). The PCR products were fused together using the PCR fusion strategy and cloned into the PstI site in the pET28a-H8-TEV vector.

**2.3.4 Transformation of *Chlamydomonas***

All genomic constructs were transformed into the RSP3 mutant strain, *pfl4* using the glass beads method (Kindle, 1990). Cells were grown in ~350 ml TAP media under light and dark cycle to a mid-log phase and for an additional 24 hours under constant light. The cells were spun down at 1,500 rpm for 5 minutes and treated with autolysin at a concentration of  $1 \times 10^7$  cells/ml until > 50% of the cells were lysed by 0.5% Nonidet-P40. The autolysin-treated cells were washed with TAP medium and resuspended in the same solution to a final concentration of  $1 \times 10^8$  cells/ml. Aliquots of 300  $\mu$ l cells were added into each tube. Glass beads, 1-3  $\mu$ g plasmids and 100  $\mu$ l freshly prepared 20% PEG 8000 were then added to the tubes, followed by vortexing for 45 sec at speed 8 (Mini Vortexer, VWR). Afterwards, 10 ml TAP media was added into the tube immediately. The cells

were spun down gently in IEC clinical centrifuge at #3 setting for 5 min and resuspended in fresh TAP media (5 ml) and recovered under light overnight. The next day the cells were spun down again and the pellet was resuspended in 500  $\mu$ l TAP and plated on TAP agar plates with 10  $\mu$ g/ml PMM. Individual colonies became visible in 5 days. The colonies were re-streaked onto a fresh TAP plate.

## ***2.4 Cell Biology***

### **2.4.1 Microscopic Screening of Transformants**

A small fraction of the growth from single colonies was resuspended in TAP medium or water (200  $\mu$ l) in 96-well plates for motility analysis using the inverted compound microscopes (Olympus IX51).

### **2.4.2 Electron Microscopy**

Purified axonemes were spun down at 15,000 rpm for 20 minutes in a microfuge. The supernatant was discarded and the pellet was fixed with the primary fixative (25% glutaraldehyde and 10% tannic acid/0.2 M cacodylate buffer, pH 7.4) for 1 hour on ice. The primary fixative was discarded and the pellet was washed twice for 5 minutes each with 0.1 M cacodylate buffer. After washing, the pellet was fixed with the secondary fixative (4% osmium tetroxide/0.2 M cacodylate buffer, pH 7.4,) for 1 hour at room temperature. After two washes, 5 minutes each, with 0.1 M cacodylate buffer, the pellet was dehydrated sequentially with 50, 70, 80, 95 and 100% ethanol. The pellet was then transferred to a glass vial containing 10:1 ratio of epoxy resin mixture (EMBed 812, 20 ml; DDSA, 9 ml; NMA, 12 ml; and DMP30, 0.62-0.82 ml) and propylene oxide. The resin was allowed to infiltrate the pellet for 24 hours at room temperature. The pellet was

transferred to a glass vial containing fresh epoxy resin and incubated at 60°C under vacuum for 48 hours. The blocks were sectioned, stained and the images were taken as described (Yang et al., 2008). The blocks were prepared by us while the sectioning and images were taken by our collaborators at Oklahoma State University.

## ***2.5 Biochemistry***

### **2.5.1 Screening of Transformants: Flagella Miniprep**

The growth from one re-streaked single colony was resuspended in 1 ml TAP media and plated on a TAP plate. After 5-6 days of growth, the cells were recovered and resuspended in 1 ml water containing 5.44 mM CaCl<sub>2</sub>. The resuspended cells were placed under light for about 1-2 hours to allow hatching and flagella generation. The cells were spun down at 1,500 g for 10 minutes (Sorvall RC6+, Thermo Scientific). The pellet was resuspended in 5 ml HMDS (10 mM Hepes, 5 mM MgSO<sub>4</sub>, 1 mM dithiothreitol and 4% sucrose) solution and 0.013 mM dibucaine was used to deflagellate the cells. The cells were spun down at 1,500 g for 10 minutes and the flagella-containing supernatant was collected. A 25% sucrose cushion in HMDS was added to the supernatant and centrifuged at 1,500 g for 7 minutes (Clinical centrifuge, IEC, Swinging bucket rotor). The supernatant was centrifuged at 13,000 g for 5 minutes. The pellet which contains the flagella was resuspended in Buffer A (10 mM Hepes, 5 mM MgSO<sub>4</sub>, 1 mM dithiothreitol, 0.5 mM EDTA, 30 mM NaCl, 0.1 mM PMSF, 0.5 TIU/ml Aprotinin, pH 7.4). The samples were fixed with 5X sample buffer for SDS-PAGE and were analyzed by western blot.

### **2.5.2 Extraction of Axonemal Proteins**

*Chlamydomonas* cells were grown in ~ 350 ml TAP liquid medium for about three days in 14/10 hour light and dark cycle. The cells were harvested by centrifugation at 1500 g for 5 minutes (TA-10 rotor; Allegra 25R centrifuge; Beckman Coulter). The pellet was resuspended in 20 ml HMDS solution (10 mM Hepes, 5 mM MgSO<sub>4</sub>, 1 mM dithiothreitol and 4% sucrose). The cells were deflagellated using 50 mM dibucaine (1 ml/ L cell culture) followed by the addition of protease inhibitors, including 0.1 mM PMSF, 0.5 TIU/ml aprotinin and 0.5 mM EGTA. The cell bodies were separated from the flagella by centrifugation in a clinical centrifuge at speed #4 for 7 minutes. The supernatant was underlayered with 5 ml 20% sucrose and centrifuged at 1500 g for 7 minutes (Clinical Centrifuge, IEC). The upper layer was centrifuged at 12,000 g for 10 minutes using TA-14 rotor; Allegra 25R centrifuge. The pellet containing flagella was resuspended in Buffer A (10 mM Hepes, 5 mM MgSO<sub>4</sub>, 1 mM dithiothreitol, 0.5 mM EDTA, 30 mM NaCl, 0.1 mM PMSF, 0.5 TIU/ml Aprotinin, pH 7.4) and demembrated with 0.5% Nonidet-P40 for 20 minutes. The axonemes were recovered by centrifugation at 12000g for 10 minutes. The pellet was resuspended in ~300µl Buffer A. The protein concentration was determined using the Bradford assay. The axoneme samples were resuspended in Buffer A and fixed in sample buffer for SDS-PAGE at a concentration of 2 mg/ml.

### **2.5.3 Fractionation of Axonemal Proteins**

To extract radial spoke complex, the isolated axonemes were resuspended in 0.6 M potassium iodide (KI) / buffer A at 5 mg/ml for 30 minutes on ice. The mixture was

centrifuged at 12,000 g for 10 minutes. The supernatant was dialyzed in Buffer A for 30 minutes on ice. The dialyzed liquid was centrifuged at 12,000 g for 10 minutes. The supernatant was overlaid on an 11 ml 5-20% sucrose gradient. The gradient was subjected to velocity sedimentation at 36,000 rpm (SW41 rotor, Beckman Coulter) for 10-16 hours at 4°C. 500 µl fractions were collected using the Econo peristaltic pump (Bio-Rad). The fractions were fixed with 5X sample buffer for SDS-PAGE.

#### **2.5.4 SDS-PAGE**

Protein samples fixed with 5X sample buffer (10% SDS, 50% glycerol, 0.3 M Tris pH 6.8, 5% β-mercaptoethanol, 0.05% bromophenol blue) were boiled for 5 minutes at 100°C. The samples were loaded onto different percentage 8cm X 7cm minigels. The electrophoresis was performed using 1X running buffer (27 mM Tris Base, 0.1% SDS and 170 mM Glycine) as described by Laemmli (1970, 1973). A 5µl aliquot of molecular weight marker (Fermentas) was used. Electrophoresis was carried out with Protean III mini-gel apparatus (Bio-Rad) at 190 V for 0.5- 1 hour.

#### **2.5.5 Native-PAGE**

Protein samples were fixed with 5X sample buffer (50% glycerol, 0.3 M Tris pH 6.8, 5% β-mercaptoethanol, 0.05% bromophenol blue). The samples were loaded onto different percentage 8cm X 7cm native gels. Electrophoresis was performed using 1X running buffer (27 mM Tris Base and 170 mM Glycine) (Ornstein, 1964; Davis, 1964). 1 mg/ml BSA was fixed with 5X sample buffer for Native-PAGE and used as the marker.

Electrophoresis was carried out with Protean III mini-gel apparatus (Bio-Rad) at 190 V for 0.5- 1 hour.

### **2.5.6 Western Blot**

After gel electrophoresis, the proteins fractionated in the gel were transferred onto a nitrocellulose membrane. Depending on the size of the protein being transferred a 0.45  $\mu\text{m}$  pore size membrane ( $> 40$  KDa) or a 0.2  $\mu\text{m}$  pore size membrane ( $< 40$  KDa) (Pall Corporation) was used. The transfer cassette which consisted of sponge, filter paper, gel and membrane was placed into the gel box. The transfer was carried out using either Big protein transfer buffer ( $> 40$  KDa) (0.38 M glycine, 50 mM Tris base, 10% SDS, 20% methanol) or small protein transfer buffer ( $< 40$  KDa) (0.19 M glycine, 25 mM Tris base, 20% methanol). The transfer was carried out at 100 V for 50-60 minutes in a mini-gel transfer apparatus (Bio-Rad). Following transfer, the membrane was stained with Ponceau S (0.2% Ponceau S, 3% trichloroacetic acid, 3% sulfosalicylic acid) for about 2 minutes. The membrane was destained with deionized water. Subsequently the membrane was blocked with 5% non-fat milk in 1X TBS, pH 7.4 (0.14 M NaCl, 2.6 mM KCl, 25 mM Trizma base) for 1 hour at room temperature. The blocked membrane was incubated with primary antibody for 2 hours at room temperature. The blot was washed thrice, 5 minutes each, with 1 X TBS, followed by incubation with secondary antibody for 2 hours at room temperature. The blot was washed again thrice with 1 X TBS. The protein bands were then revealed by enhanced chemiluminescence (ECL) using a mixture of two solutions: solution 1 (0.5 ml 1 M Trizma base pH 8.8, 50  $\mu\text{l}$  44 mg/ml luminol, 22  $\mu\text{l}$  15 mg/ml *p*-coumaric acid and 4.4 ml  $\text{H}_2\text{O}$ ) and solution 2 (0.5 ml 1 M Trizma base, pH 8.8,

3  $\mu$ l 30%  $H_2O_2$  and 4.5 ml  $H_2O$ ). The blot was incubated with this mixture for 1 minute. The blot was then exposed to autoradiography film (Denville Scientific) for different periods of time and developed with an automatic film processor CP1000 (AGFA healthcare).

### **2.5.7 Ni-NTA Affinity Purification**

The vectors encoding GST-tagged RSP3 constructs and the His-tagged Dpy-30 constructs were co-transformed into BL21 (DE3) cells. The transformants were inoculated into 5 ml LB liquid medium supplemented with appropriate antibiotics. The liquid cultures were incubated at 37°C in a shaker for ~2-3 hours (OD ~0.4-0.6). Following this the culture was induced using 1mM IPTG, overnight at 16°C. Following induction, the cells were spun down at 10,000 g for 1 minute. The cell pellet was resuspended in 750  $\mu$ l Lysis Buffer (50 mM  $NaH_2PO_4$ , 300 mM NaCl, 10 mM imidazole, pH 8.0) and sonicated using a Branson digital sonifier. The sonicated cells were spun down at 12,000 g for 25 min at 4°C. 50  $\mu$ l of the supernatant was saved as 'pre'. The rest of the supernatant was applied to Ni-NTA matrix (100  $\mu$ l) and incubated at room temperature for 1 hour. Following incubation the mixture was spun down and 50  $\mu$ l of the supernatant was saved as flow through or 'post'. The rest of the supernatant was discarded. The beads were washed thrice using the wash buffer (50 mM  $NaH_2PO_4$ , 300 mM NaCl, 20 mM imidazole, pH 8.0). Following the washes the bound protein was eluted using the elution buffer (50 mM  $NaH_2PO_4$ , 300 mM NaCl, 250 mM imidazole, pH 8.0). The samples were fixed in 5X sample buffer and fractionated on SDS PAGE gels. The gels were blotted onto nitrocellulose membranes and probed using the monoclonal GST antibody (Genscript).

### **2.5.8 Overlay**

Axonemal samples or bacterial samples were fractionated on SDS-PAGE gels. The gels were transferred to nitrocellulose membrane (Ponceau staining is omitted). The blot was blocked with 5% non-fat milk pH 7.4 in 1X TBS (0.14 M NaCl, 2.6 mM KCl, 25 mM Tris base) for 30 minutes at room temperature. The blot was probed with 2  $\mu$ g/ml purified Dpy-30 protein for 2.5 hours at room temperature. The blot was washed once with 1 X TBS. Subsequently the blot was probed with anti-Dpy30 antibody. The blot was washed once with 1 X TBS and then incubated with horse radish peroxidase-conjugated anti-rabbit secondary antibody. The blot was washed once with 1 X TBS and developed using enhanced chemiluminescence. The No ligand control was processed identically except that the blot was not probed with Dpy-30 protein.

### **2.5.9 Chemical Blocker Screening with Native Gel Electrophoresis**

The mixture of 2  $\mu$ g of each protein in PBS was incubated at room temperature for 1.5 hours. Subsequently the reaction mixture was fixed with 5X native gel sample buffer. The samples were fractionated on a native gel and visualized by Coomassie staining.

To identify compounds that inhibit the RSP3-Dpy-30 interaction, 2  $\mu$ g purified Dpy-30 was incubated with different compounds, at 25  $\mu$ M, for 1 hour at room temperature. Subsequently, purified GST-tagged RSP3 peptides were added to the mixture to a final concentration of 1  $\mu$ g/ $\mu$ l. After 1-hour incubation at room temperature, the samples were fixed with sample buffer for Native PAGE and fractionated on a native gel. The proteins were visualized by Coomassie stain.



### **2.5.10 Chemical Blocker Screening with Ni-NTA Pull-Down**

Aliquots of purified Dpy-30 protein were incubated with 50  $\mu$ M compound for 1 hour at room temperature. Following the incubation, the mixture was incubated with purified GST-tagged RSP3 peptides at room temperature for 1 hour. A fraction of the mixture is saved as 'pre' sample. To the remaining mixture, 20  $\mu$ l Ni-NTA matrix were added and the sample was incubated at room temperature for 1 hour. Following the incubation, the reaction mixture was spun down and a fraction of the supernatant was saved as 'post' sample. 5X sample buffer for SDS-PAGE was added to the rest of the beads and spun down. The supernatant along with the pre and post samples were fractionated on a SDS-PAGE gel and visualized by Coomassie stain.

### **2.6 Sequence Analysis**

Sequence alignments were generated using ClustalW2 program (<http://www.ebi.ac.uk/Tools/msa/clustalw2/>). Coils program was used to define regions with high propensity to form coiled coils ([http://www.ch.embnet.org/software/COILS\\_form.html](http://www.ch.embnet.org/software/COILS_form.html)). PyMOL (DeLano, 2002) was used to visualize the crystal structures of RIIa clan domains and also align the structures. Secondary structure predictions were made using HNN ([http://npsa-pbil.ibcp.fr/cgi-bin/npsa\\_automat.pl?page=npsa\\_nn.html](http://npsa-pbil.ibcp.fr/cgi-bin/npsa_automat.pl?page=npsa_nn.html)). Pfam database (<http://pfam.sanger.ac.uk/>) was used to define proteins that contain RIIa clan domains.

## **Chapter 3: RSP3 Forms the RS Scaffold with Two Distinct Sites that Anchor RIIa Clan Domains**

### ***3.1 Introduction***

Anchoring proteins are used by eukaryotic cells to localize molecules involved in signal transduction, such as kinases, phosphatases, GTPases and phosphodiesterases (Scott and Pawson, 2009; Klauck et al., 1996). This concept was founded on the discoveries of anchoring proteins for cAMP-dependent protein kinase (PKA), the key effector mechanism for cAMP (Theurkauf and Vallee, 1982). The PKA holoenzyme contains two catalytic subunits and two regulatory subunits, RI or RII. Although PKA plays a central role in the regulation of many cellular reactions, it has broad substrate specificity. It was discovered that cells contain various A-Kinase Anchoring Proteins (AKAPs) to target this promiscuous enzyme to specific sub-cellular locations (Welch et al., 2010).

Anchoring of PKA is mediated by a 14-18 a.a. amphipathic helix in AKAPs and the RIIa domain in the regulatory subunit, RI or RII, in PKA (Carr et al., 1991). Many AKAPs were identified solely based on the presence of an AH and the binding of RII *in vitro*. However, the RIIa domain is not restricted to PKA alone. It has been found in numerous proteins associated with various flanking sequences. Another RIIa like domain known as the Dpy-30 domain is also found in equally numerous molecules with diverged architectures. Together, all these proteins are classified into two subfamilies under the RIIa clan in the Pfam database.

Interestingly, two proteins from each subfamily are subunits of the radial spoke complex, a key regulatory element within the 9+2 axonemal machinery. RSP7 and RSP11 contain a RIIa domains while RSP2 and RSP23 contain Dpy-30 domains (Yang et

al., 2006). These four proteins may contribute partly to the mechanism of this molecular complex.

During flagellar beating, the RS couples the mobile CP with the dynein motors that are attached to the outer doublets (Warner and Satir, 1974; Smith and Yang, 2004). Precise coupling of these elements is critical for flagella to bend and to propagate the bend. Consistently, RS appears rather rigid with slight elasticity under electron microscopy. We reason that the rigidity for effective coupling of RS and the mobile CP must be based on a single molecule extending throughout the spoke stalk as a core to associate with other RS constituents that confer the effector mechanisms of the RS. The first generation models in which the stalk is comprised of a string of RSPs (Yang et al., 2006) are not likely to provide the necessary rigidity. Among the 23 RSPs, the best candidate for this scaffold protein is RSP3.

First of all, a 300-a.a. region near the N-terminus is evolutionarily conserved, in sequence as well as in length. The homology in length is consistent with the extraordinarily conserved dimension of the RS and 9+2 axonemes from diverse organisms (Mastrorade et al., 1992; Nicastro et al., 2006). Secondly, it was demonstrated that RSP3 is essential for the assembly of the radial spoke (Huang et al., 1981; Williams et al., 1989). Its N-terminus directly binds to the axonemes (Diener et al., 1993). In addition, a downstream AH interacts with the RIIa domain (Gaillard et al., 2001), presumably for binding the two RIIa RSPs. If RSP3 is the scaffold, sequence toward the C-terminus will bind the Dpy-30 domain in RSP2 and RSP23. Thus we hypothesize that the dimeric spoke AKAP, RSP3, forms the radial spoke scaffold and contains two distinct sites that anchor the RIIa clan RSPs.

This chapter describes in two sections the two main strategies that were taken to test this hypothesis. The results from independent approaches consistently support the hypothesis and demonstrate that RSP3 contains two distinct sites that associate with the RIIa domain and the Dpy-30 domain respectively. Anchoring through these sites and the RIIa clan domains localizes the rest of the molecular modules in these four RSPs to precise locations for the assembly and modulation of the RS. The *in vitro* investigation further defined the amphipathic binding site for the Dpy-30 domain.

### ***Section 1: In vivo approach***

Sequence analyses were performed to identify the regions that may bind the Dpy-30 domain. Based on the prediction, truncation constructs of RSP3 genomic DNA were engineered and *Chlamydomonas* mutants were generated. The mutant strains were subjected to motility, biochemical and morphological analyses.

## **3.2 Results**

### **3.2.1 Sequence Analysis of RSP3**

We reason that the organization of the four RIIa clan members in the RS stalk must be conducive to the predicted key property of the stalk-- rigidity—in order for the RS to mechanically couple the mobile CP and outer doublets at a high frequency (Warner and Satir, 1974). Higher rigidity may come from a RS with all four RIIa clan members docking to a single or dimeric fibrous molecule extending throughout the complex than a RS made from a continuous chain of individual RIIa clan members. The core molecule that anchors the RIIa clan members should be long enough to span the distance from the outer doublets to the CP. Furthermore, it should be conserved, as the dimension of various axonemes is similar (Mastronarde et al., 1992; Nicastro et al., 2006). Sequence analyses showed that among the 19 spoke components, the best candidate is RSP3, the dimeric spoke AKAP which has the dimensions necessary to span the distance of the spoke stalk (Discussed in Chapter 5) (Wirschell et al., 2008; Gaillard et al., 2001).

The AH<sub>R</sub> (a.a.# 161-178) (Gaillard et al., 2001) separates RSP3 into two segments (Figure 3-1A): the N-terminal disordered region that binds axonemes (Diener et

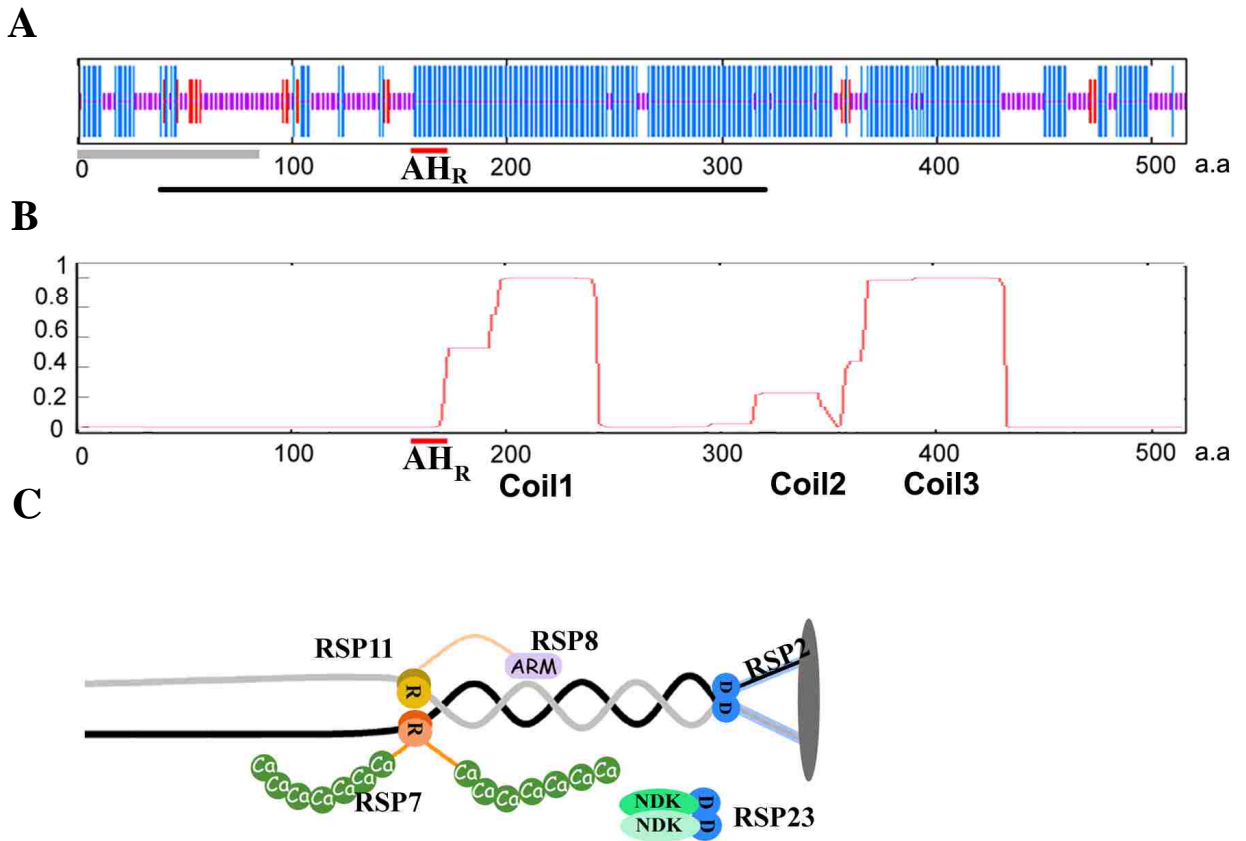


**Figure 3-1. Sequence analyses and the model of RS.**

(A) The secondary structure of RSP3 appears to be divided into two distinct areas by the RIIa-binding site (red underline). The N-terminal 160 a.a. contains random coils (purple) interspersed with short  $\alpha$ -helices (blue) and  $\beta$ -strands (red), while the C-terminus is primarily composed of  $\alpha$ -helices. Black bar, the RSP3 domain highly conserved among RSP3 orthologues; Grey bar, the axoneme-binding region. (B) RSP3 contains three areas with propensity to form coiled coils. The prediction was made by Coils program using the window size of 28 a.a.. (C) A model depicting RSP3 dimer (black and gray lines) as the core in the RS, with two sites for anchoring RIIa (R) and Dpy-30 (D), dimerization and docking domains in two pairs of RSPs. Each domain tethers distinct molecular moieties as effector mechanisms, like an armadillo repeat protein (ARM), the calcium-binding EF-hands (Ca), coiled coils (blue bars), nucleoside diphosphate kinase (NDK), RIIa binding amphipathic helix (AH<sub>R</sub>).

al., 1993; the grey bar) and a stack of LC8 dimers (Gupta et al., unpublished); and the C-terminus that is largely helical with a propensity to form three coiled coils (Figure 3-1B). Coiled coils are known to promote protein-protein interactions. The N-terminal ~320-a.a. region, upstream to Coil 2, is highly conserved and is recognized as a RSP3 domain by the Pfam database (the black bar). Coil 2 is mildly conserved, whereas the C-terminus including Coil 3 is unique to *Chlamydomonas* and is dispensable (Diener et al., 1993). Thus we postulate that the dimer of the conserved region in RSP3 forms the core of the RS, with binding sites for the axoneme as well as RIIa domain, Dpy-30 domain and possibly the spokehead (Figure 3-1C).

### **3.2.2 RSP3 Truncation Mutagenesis Clarifies the Binding Region for the RIIa Domain and its Tethered Moieties**

Although point mutations in RSP3's AH<sub>R</sub> abrogates the interaction of RSP3 with RII in an overlay assay (Gaillard et al, 2001), the mutant strain expressing the same mutated RSP3 polypeptide did not perturb the assembly of the RIIa-domain containing proteins RSP7 and RSP11 (Gaillard et al., 2006). We predict that the inconsistency is because RSP7 and RSP11 engage in multiple interactions with RSP3 and hence an alteration in the AH<sub>R</sub>-RIIa interaction alone is insufficient to prevent their assembly. Therefore in order to test whether the AH anchors the RIIa domain in RSP7 and RSP11, it is also necessary to delete the area associated with their effector mechanisms. If the hypothesis is correct, deletion of all involved sequences in RSP3 will result in an axoneme devoid of these two molecules and possibly their associated molecules, such as RSP8 with ARM repeats that are known to promote protein-protein interactions. Alternatively, retention of the AH<sub>R</sub> alone may be sufficient to restore these two molecules. To alleviate folding

issues due to inappropriate deletions, the designs of RSP3 deletion constructs were guided by the predicted secondary structure.

Toward this end, we first created two complementary strains: the 1-178 strain that terminates at the end of the AH<sub>R</sub>; and  $\Delta$ 1 strain lacking Coil 1 (a.a.# 171-244) and part of the AH<sub>R</sub>. The third strain,  $\Delta$ 2, that lacks the small Coil 2 (#316-354), served as a control. All truncated polypeptides retained the axonemal binding region at the first 80 a.a. and thus could be assembled into the axoneme. To protect the truncated ends and to detect the truncated polypeptide, the C-terminus of all RSP3 polypeptides was tagged with 3 HA epitopes and 12 His residues. The tag also allowed quantitative comparison of the truncated RSP3 variants in the axoneme.

All of the constructs for creating RSP3 mutant strains were modified from a plasmid carrying the wild type (WT) RSP3 genomic DNA that was recovered from a BAC clone. The truncated constructs were transformed individually into the RSP3 mutant *pf14* in which a premature stop codon results in diminished expression of the RSP3 polypeptide missing the axonemal binding site at the N-terminus (Williams, et al., 1989; Diener et al., 1993). Since RSP3 mutants defective in the conserved region are paralyzed like *pf14* (Diener, et al., 1993), some of the truncated strains were expected to be paralyzed as well. To aid the differentiation of paralyzed RSP3-positive clones from paralyzed parental cells, an antibiotic resistance cassette was inserted into the plasmid for single-plasmid transformation. The transformants were first selected for antibiotic resistance. More than 100 antibiotic-resistant clones for each construct were screened microscopically. All clones in both  $\Delta$ 1 and 1-178 groups were paralyzed. On the other



Construct	# observed	# Motile <sup>a</sup>	# for flagella prep. <sup>b</sup>	# HA +
Δ1	160	0/160	23	5/23
Δ2	118	50/118	16	7/16
1-178	40	0/40	10	2/10

<sup>a</sup> The suspension contains swimmers.

<sup>b</sup> The quantity from each quick flagellar preparation varied. The yield of some clones was low because of fewer flagellated cells or had difficulties in shedding flagella.

**Table 3-1. Screening of RSP3 truncation mutants.**

Single colonies of antibiotic-resistant transformants were randomly picked and re-streaked on agar plates. A fraction of each colony was resuspended for light microscopy. A crude flagella preparation was made from a plate of clones randomly selected from the group of Δ1 and 1-178 that were 100% paralyzed; or from the clones with swimmers from the group of Δ2. The samples were then assessed by HA western blots. #, colony numbers.

hand, among the 118  $\Delta 2$  clones screened, 50 clones contained motile cells (Table 3-1), indicating substantial amount of  $\Delta 2$ -RSP3 polypeptides were restored to the axoneme of 40% of the antibiotic-resistant strains. In the case of the paralyzed clones, the plasmid may not have inserted into the genome properly to express the truncated RSP3 in sufficient quantity. These data suggest that  $\Delta 2$ -RSP3 can restore the motility to *pf14* flagella, whereas  $\Delta 1$  RSP3 cannot rescue the motility, even if the truncated polypeptides are restored to the axonemes.

A quick preliminary screen was conducted to identify clones with truncated RSP3 in their flagella. 10 clones were randomly selected from the paralyzed  $\Delta 1$  and 1-178 groups; and from the motile clones in the  $\Delta 2$  group. A small crude flagella preparation was made from a plate of each clone for HA western analysis (not shown). The clones with HA-positive flagella were cultured in liquid media for axoneme preparations. Western blots of near equal loads of axonemes were probed for representative RSPs (Figure 3-2). The clone expressing wild type (WT) RSP3-HAHis served as the positive control. The negative control was the spoke-less *pf14*. The representative HA western blots showed that in all strains except *pf14*, the amount of RSP3 variants in axonemes were similar. For the  $\Delta 1$  strain that was missing Coil 1 (a.a.# 171-244) that includes part of the AH<sub>R</sub> (a.a.# 161-178) in RSP3, both the RIIa-containing RSP7 and RSP11, as well as RSP8, the ARM repeat protein, were absent (Figure 3-2), while all the proteins in the spoke head and neck region were present at normal levels. The assembly of the Dpy-30-containing RSPs at the neck when the RIIa-containing RSPs located between the neck and the base are absent indicates that the RS is not comprised of a string of individual RIIa clan RSPs. Conversely the 1-178 axonemes, in which the entire AH<sub>R</sub>

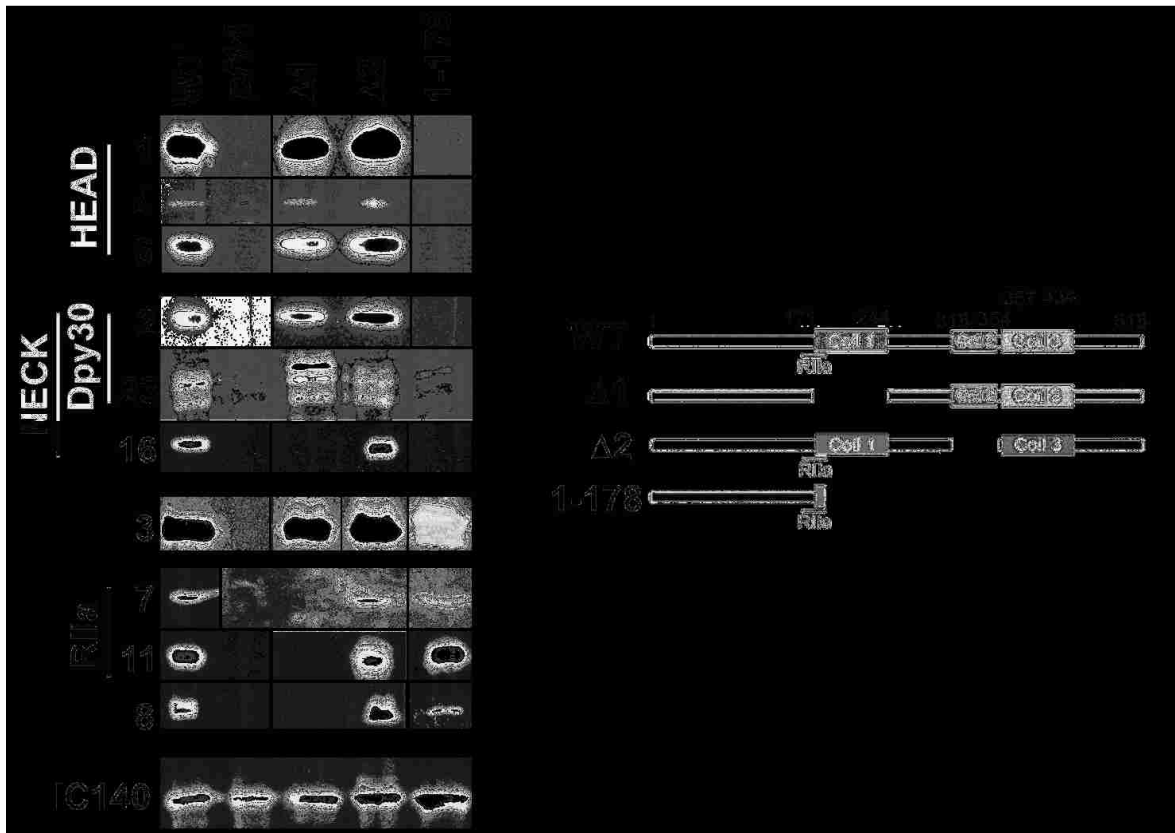


**Figure 3-2. Truncation around the Coil 1 region results in deficiencies in RIIa-domain-dependent assembly.**

Western blots of axonemes (left panel) from WT and the RSP3 strains defective in the region around coiled coils (right panel) were probed for relevant RSPs as indicated. The RIIa proteins (RSP7 and 11) and the ARM (RSP8) were missing in the  $\Delta 1$  strain in which half of the RIIa-binding AH is truncated. These proteins appeared normal in  $\Delta 2$  axoneme. The 1-178 axonemes that contains RSP3 sequence up to the AH lacked all the proteins in the spokehead and spokeneck but contained the RIIa proteins (RSP7 and RSP11). Note RSP8 was less abundant. The spoke-less *pf14* was the negative control. IC140, an inner dynein arm subunit, indicated the protein loading.

(a.a.# 161-178) was retained, both RSP7 and RSP11 were present, but the spoke head proteins (RSP1, RSP4, RSP6) and neck proteins (RSP2, RSP23 and RSP16) were absent (Figure 3-2). Therefore, AH<sub>R</sub> is sufficient to anchor the two non-PKA RIIa proteins. Note RSP8 was less abundant in 1-178 axonemes than in the WT, like the axoneme of the RSP11 mutant *pf25* that lack RSP11 (Yang et al., 2006). The RSP8 deficiency in the axoneme defective in Coil 1 (1-178 or  $\Delta 1$ ) or lacking RSP11 supports the prediction that RSP11 and RSP8 form a tri-molecular sub-complex with RSP3 Coil 1 region (Figure 3-1C). Furthermore, the fact that the C-terminus up to Coil 3 is dispensable (Diener et al., 1993); and Dpy-30-domain-containing RSP2 and RSP23 are absent in 1-178 strain but normal in  $\Delta 1$  and  $\Delta 2$  strains suggest that the Dpy-30-domain-binding site is located between Coil 1 and Coil 2.

### **3.2.3 A Downstream Helical Region Associates with Dpy-30 Domain Containing Proteins**

To define the Dpy-30-domain-binding region in RSP3, we took the same strategy to generate three more strains in which RSP3 terminated at different residues between Coil 1 and Coil 2, i.e. a.a.# 244, 269, 316 respectively. As expected, all clones in the 1-244 and 1-269 groups were paralyzed (Table 3-2). As the  $\Delta 2$  group, approximately 40% of the clones in the 1-316 group contained swimmers. This further confirms that the less conserved Coil 2 region is dispensable. Preliminary western blots of flagella from selected clones identified the RSP3 (HA)-positive clones. The axonemes from these clones were subjected to detailed analyses.

Western blots showed that the axonemes from the paralyzed 1-244 and 1-269 strains, like the 1-178 strain, were deficient in the neck proteins (RSP2, RSP23 and

Construct	# observed	# Motile <sup>a</sup>	# for flagella prep. <sup>b</sup>	# HA +
1-244	50	0/50	10	3/10
1-269	92	0/92	10	2/10
1-316	114	47/114	10	7/10

<sup>a</sup> The suspension contains swimmers.

<sup>b</sup> The quantity from each quick flagellar preparation varied. The yield of some clones was low because of fewer flagellated cells or had difficulties in shedding flagella.

**Table 3-2. Screening of RSP3 truncation mutants.**

Single colonies of antibiotic-resistant transformants were randomly picked and re-streaked on agar plates. A fraction of each colony was resuspended for light microscopy. A crude flagella preparation was made from a plate of clones randomly selected from the group of 1-244 and 1-269 that were 100% paralyzed; or from the clones with swimmers from 1-316 group. The samples were then assessed by HA western blots. #, colony numbers.

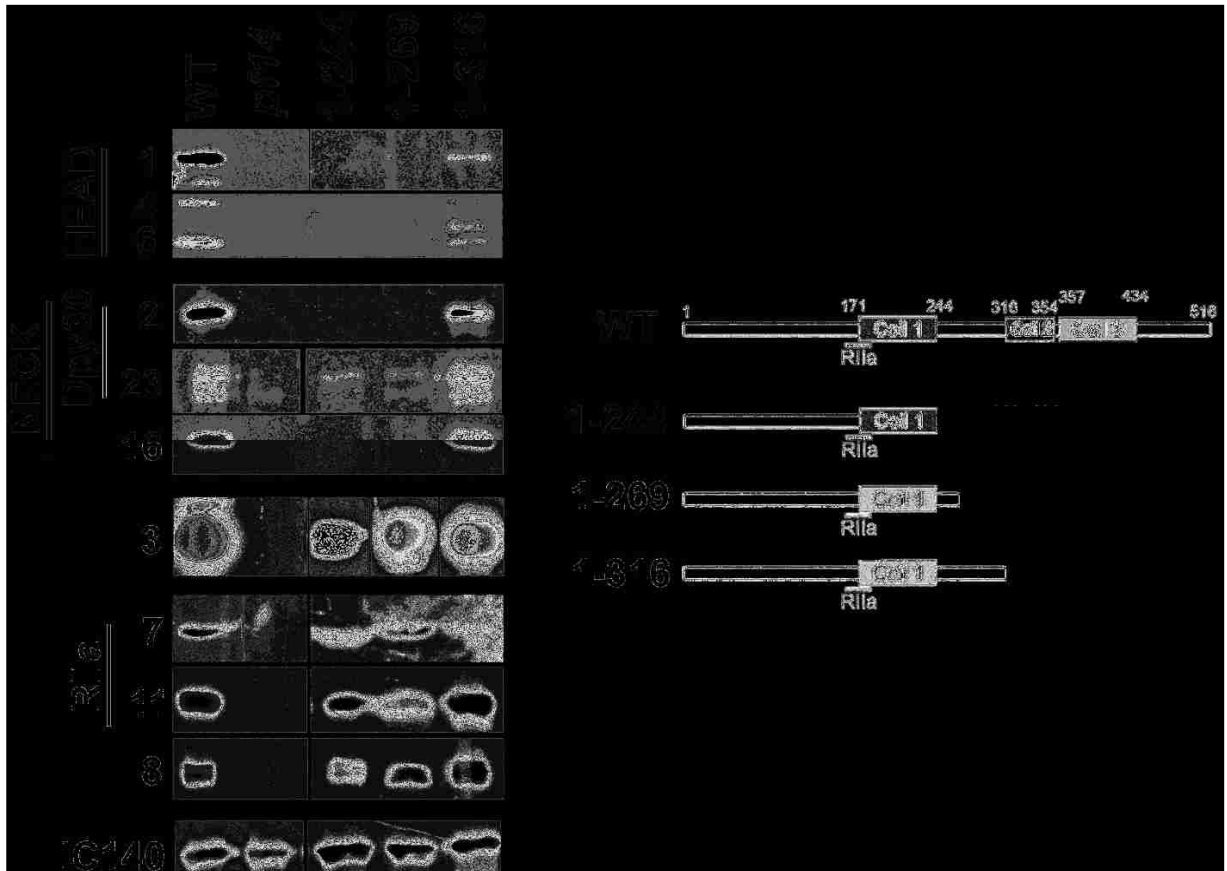


**Figure 3-3. Truncation between the first two coils results in deficiencies in Dpy-30-domain-dependent assembly.**

Western blots of axonemes (left panel) extracted from WT and three mutants with different truncations distal to Coil 1 (right panel) were probed for relevant RSPs as indicated. 1-244 strain and 1-269 strain were deficient in the spokehead proteins and the spokeneck proteins including RSP16 and the two Dpy-30-domain-containing RSP2 and RSP23. These proteins were present in 1-316 strain but the spokehead proteins were less abundant than that in the WT control. The spoke-less *pf14* was the negative control. IC140, an inner dynein arm subunit, indicated the protein loading.

RSP16) and the head proteins (RSP1, RSP4 and RSP6) (Figure 3-3). This suggests that the region involved in the head-neck assembly and anchoring the Dpy-30 domain is within a.a.# 269-316 in RSP3. For the 1-244 and 1-269 strains that retain both AH<sub>R</sub> and Coil 1, the axoneme had normal amounts of RIIa-domain-containing RSP7 and RSP11 as well as the ARM repeat protein RSP8. This result further supports the prediction that the mutually interacting RSP11 and RSP8 bind to AH<sub>R</sub> and Coil 1.

In 1-316 axonemes in which RSP3 lacks both Coil 2 and Coil 3, the Dpy-30-domain- containing RSP2 and RSP23, and RSP16 were present in normal levels as expected (Figure 3-3). The head proteins (RSP1, RSP4 and RSP6) were also present, yet their amounts were drastically reduced compared to WT axonemes. These head proteins were also less abundant in the RSP2 mutant *pf24* (Huang et al., 1981; Patel-King et al., 2004; Yang et al., 2006). The same spokehead deficiencies due to the defect either in RSP2 or in the C-terminus of RSP3 suggests that RSP2 and RSP3 Coil 2 region are both involved in the assembly of the spokehead. Furthermore, the 47-a.a. RSP3<sub>269-316</sub> may anchor the Dpy-30 domain directly. The precise binding site was determined by in vitro experiments described later.

### **3.2.4 Truncations in RSP3 Lead to Smaller Spoke Particles**

To assess the RSs with truncated RSP3 independently, we took two more approaches. Firstly, RSs were extracted from axonemes with KI buffer and the dialyzed extract was fractionated by sucrose gradient velocity sedimentation. The fractions of the gradient were then assessed by western blots (Figure 3-4). The RS complex from the WT control sample sedimented as an intact particle with a single 20S peak (Yang et al., 2001). For all

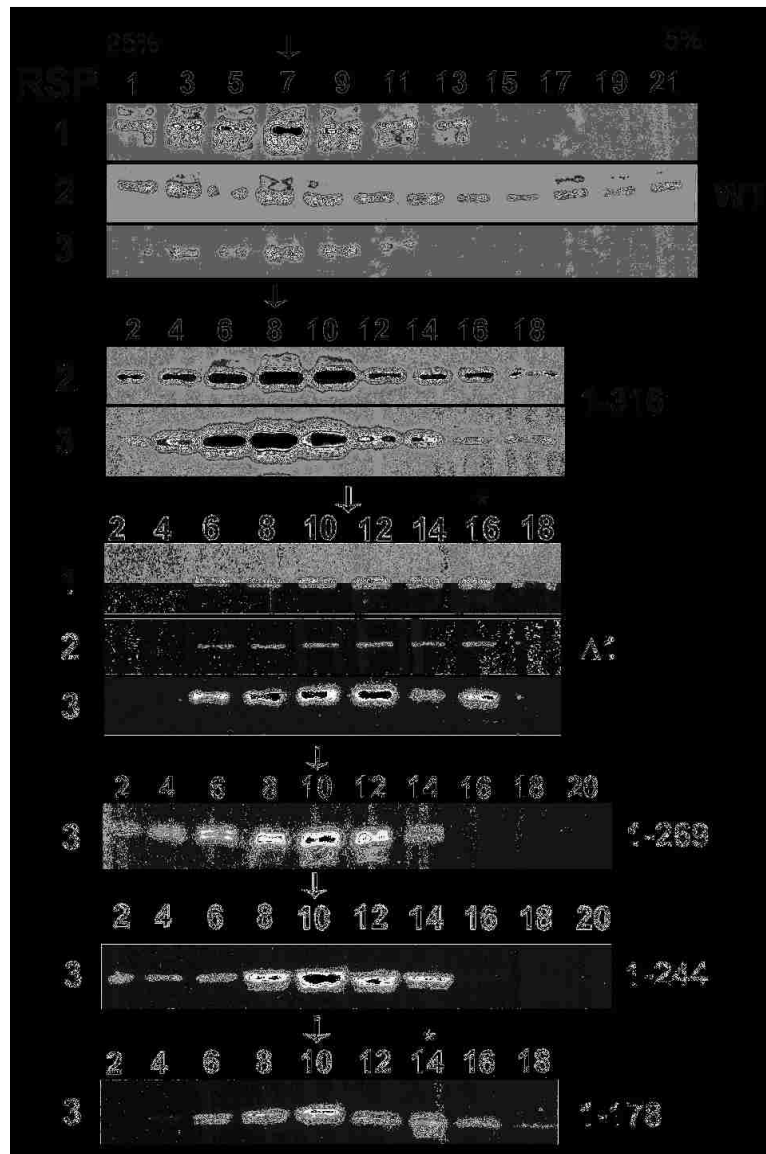


**Figure 3-4. Radial spokes extracted from mutants largely sedimented as smaller particles.**

The KI axonemal extracts from the indicated strains were sedimented through a 5-25% sucrose density gradient and the fractions were assessed by western blots probed for relevant RSPs. The major peaks were indicated by arrows. The extracted RSPs from all truncation mutants sedimented together as intact particles smaller than WT RSs. A second RSP3 peak (asterisk) was present in the gradients from  $\Delta 1$  and 1-178 strains that lacked Coil 1.



the mutants, RSs with truncated RSP3 sedimented as smaller particles, similar to or smaller than RS stalk particles from the mutants lacking the head proteins (Yang et al., 2001). While the gradients of 1-244, 1-269 and 1-316 strains contain a single RSP3 peak, the gradients of the  $\Delta 1$  and 1-178 strains that lack Coil 1 contained another minor peak, suggesting that Coil 1 is critical to the unusual stability of the RS complex, possibly for the formation of a dimeric coiled coil.

### **3.2.5 Electron Microscopy Reveals Distinct Dwarf RSs in RSP3 Mutant Axonemes**

To verify the hypothesis independently, the morphology of the RS with truncated RSP3 was assessed by electron microscopy (EM). Due to the resolution of EM and the similar sizes of the RS particles in the mutants, we only compared the axonemes of WT,  $\Delta 1$  and 1-178 strains (Figure 3-5A). If the proposed model is correct, the two RSP3 truncation mutants would have shorter RSs with and without the spokehead respectively (Figure 3-5B).

The EM images of axoneme cross sections revealed two main defects, a lateral shift of the CP, a signature of prominent RS defects (Witman et al., 1978); and stubby RSs (Figure 3-5A and Table 3-3). Importantly, some RS stubs in  $\Delta 1$  axonemes but not 1-178 axonemes exhibited an enlarged head (Insets), consistent with the presence of head proteins only in the  $\Delta 1$  axonemes (Figure 3-2) and the proposed model (Figure 3-5B). The RSs, measured to outer doublets, are the longest in the WT and the shortest in 1-178 (Figure 3-5C). About 92% of  $\Delta 1$  images and about 69% of 1-178 images had deviated CP (Table 3-3). The more prominent shift of the CP in  $\Delta 1$  despite longer RS may be due to their spokeheads that could adhere and actively detract the CP off the center.

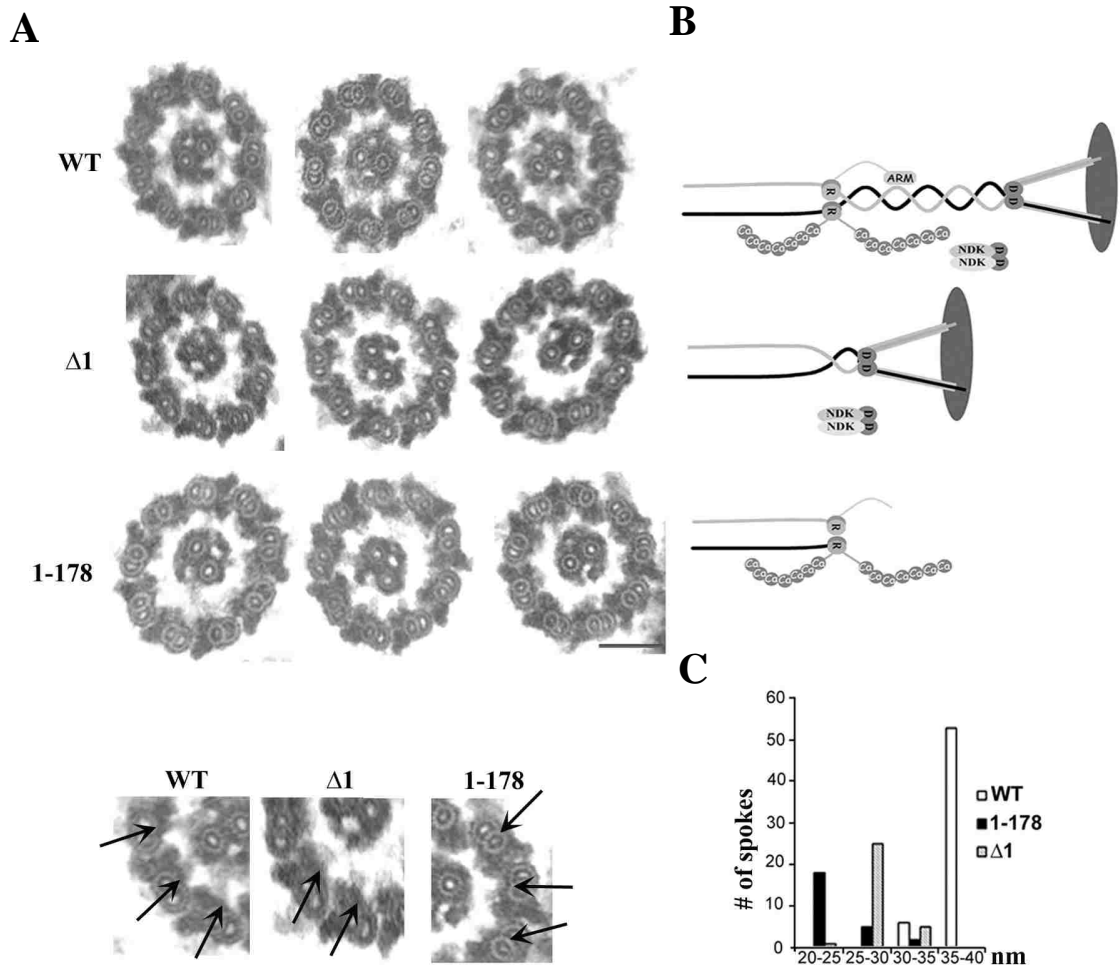


**Figure 3- 5. Distinct stubby spoke in the axonemes from the  $\Delta 1$  and 1-178 mutants.**

(A) The representative images of cross-sectioned axonemes revealed by transmission electron microscopy. Full length RSs on each outer doublet tug the central pair apparatus to the center of the WT axonemes. The RSs in the axonemes of  $\Delta 1$  and 1-178 strains were shorter, resulting in the lateral shift of the central pair apparatus in some axonemes. However, only the dwarf RSs in  $\Delta 1$  axonemes contain slightly enlarged spokehead. The bottom panel gives an enlarged view of the axoneme cross sections. The arrows highlight the defective radial spokes. (B) Schematic pictures depicting the RSs in each strain. (C) The lengths of RSs in cross sectioned axonemes.

Strain	% of axonemes with deviated CP	# of Axonemes measured <sup>a</sup>	% deviation of the CP
WT	3.7% (n=27)	-	-
$\Delta 1$	92% (n=38)	14	16.6%
		3	15%
		2	20%
1-178	69% (n=39)	9	16.6%
		5	20%

n, the total number of cross-sectioned axoneme images that were visually inspected.

<sup>a</sup> The number of axonemes with a deviation that was large enough to be measured

**Table 3-3. The incidence of lateral-shifted central pair (CP) apparatus in axonemes and the extent of deviation.**

The combined results from motility, biochemical and morphological analyses support the proposed model (Figure 3-1C) -- RSP3 dimer extends throughout the spokestalk with two discrete regions for anchoring the two types of D/D domains in four RSPs. A region near Coil 2 anchors the Dpy-30 domain present in RSP2 and RSP23. The helices downstream to the binding region in both RSP2 and RSP3 may form coiled coils with each other and with the head components. As for RSP23, the Dpy-30 domain could tether the associated NDK to the RS complex. Finally, the coiled coils adjacent to the docking and anchoring region in RSP2 and RSP3 associate with the spokehead (Yang et al., 2008). Through these multiple interactions, the head, neck and stalk are linked together.

For the two RIIa-containing proteins, RSP11's RIIa domain docks onto the AH<sub>R</sub> in RSP3 while its short flanking sequence tethers the ARM repeat protein (RSP8) to interact with the Coil 1 region in RSP3 directly or indirectly. We speculate that this may enhance the rigidity of the dimeric RSP3 core, since the mutants defective in RSP11 can swim but become paralyzed in the exhausted media (Yang and Yang, 2005). By the same token, RSP7's RIIa domain docks to AH<sub>R</sub> in the other RSP3 monomer. Yet contrary to the constitutive function of RSP11, RSP7's EF-hands could allosterically modulate the stalk when calcium increases, analogous to the cAMP-induced release of the PKA catalytic subunit. These various effector mechanisms of the four RSPs are all docked through the D/D domains to the two regions in RSP3.

Taken together, with all these molecular interactions throughout the RS, including the association with the axonemal outer doublets (Diener et al., 1993), the dimeric RSP3 clearly is a bona fide core scaffold of the entire RS complex. The effectors anchored

through AH-D/D domains facilitate the assembly of the rest of RSPs and modulate the scaffold itself in calcium-dependent and independent manner. Such a model depicts the RS with sufficient rigidity to mechanically couple the CP and outer doublets during oscillatory beating and can be modulated when calcium induces changes in oscillatory beating.

There are several alternative models. For instance, each 96-nm repeat contains two RSs and each of the two RSPs with the same D/D domain may reside in only one RS. However, this model is inconsistent with the co-assembly and direct interaction of the Dpy-30-domain containing RSPs. RSP23 is diminished when RSP2 is diminished in the axoneme of RSP2 mutant *pf24*. Furthermore, these two molecules and their human counter parts, directly interact with each other in the pull-down experiments and in the yeast two-hybrid system (Kohno et al., 2011; Rual et al., 2005). The second possibility is that the RIIa clan domain containing proteins can form heterodimers. However, we have not succeeded in coercing the formation of hetero-dimers. Recently it was shown that RSPs form smaller sub-particles in the cell body of the RSP3 mutant *pf14* (Diener et al., 2011). Perhaps, homodimers of RSP2 and RSP23 form a hetero-tetramer prior to docking to the RSP3 dimer. Preformed sub-complexes may ensure each RS contains both RIIa-RSPs and both Dpy-30-RSPs.

## ***Section 2: In vitro approach***

Although the in vivo approach provides results with in vivo relevance, it is not possible to demonstrate unequivocally the direct interaction because of the inherent assembly mechanism of axonemal complexes in the cell body. For example, the five spokehead components pre-assembled as a unit (Diener et al., 2011). All five proteins are absent even when one protein is defective (Huang et al., 1981). Thus, to test the direct interaction between RSP3 and the RIIa clan domains we took an in vitro approach. In addition, it is possible to express small fragments of interest in vitro while in the in vivo setting deleting the N terminus of RSP3 which is essential for the assembly of the RS is not feasible (Diener et al., 1993).

Short fragments of RSP3 were synthesized as a fusion protein with a glutathione S-transferase (GST) tag at the N-terminus. The GST tag was chosen for several reasons; to serve as a carrier that would protect the short fragment from degradation, the highly soluble GST tag would aid in the efficient expression of the peptides in the bacterial system. Furthermore, the tag would serve as a marker for the detection of the peptides. Lastly, its affinity to glutathione can be exploited to purify the peptides using glutathione agarose beads.

Conversely, the polypeptides with the RIIa domain or the Dpy-30 domain were fused to a 6 His sequence for similar reasons. The affinity of the His tag for Ni<sup>2+</sup> ion enables the pull-down and affinity chromatography of the fusion proteins using Ni-NTA matrix. To test the interaction between the peptides of interest and the RIIa or Dpy-30 domain, a vector that encodes the GST tagged truncated RSP3 constructs was co-transformed into bacteria along with a vector that encodes the His tagged RIIa or Dpy-30

domain. This system allowed us to test with either the glutathione affinity matrix or the nickel affinity matrix. If the two fusion proteins interact, then both molecules should be pulled down using either glutathione or nickel affinity matrix. In this project, Ni-NTA affinity matrix was primarily used.

### **3.3 Results**

#### **3.3.1 RSP3 Directly Interacts with RIIa domain of RSP7 and Dpy-30 Domain**

Previous studies have shown that N-terminus of RSP3 (161-178 a.a) interacts with RII (Gaillard et al., 2001), while RSP3 can be co-purified with RSP11 (Yang et al., 2006). However, perturbing this RIIa binding site did not abolish the assembly of RIIa-domain containing RSP7 or RSP11 (Gaillard et al, 2006). The results from the in vivo approach have verified that the AH sequence is used to anchor the RIIa domain in these two non-PKA proteins. Hence we used the RIIa domain of RSP7 as an example to demonstrate the direct interaction between the AH and the RIIa-domain from these non-PKA proteins. For the Dpy-30 domain, the in vivo studies have mapped its binding sequence to a helical region (269-316 a.a) downstream to the RIIa-binding AH.

Three short peptides within these two regions in RSP3 were generated, RSP3<sub>96-180</sub>, RSP3<sub>245-316</sub> and RSP3<sub>269-316</sub>. The coding sequence for these fragments were PCR-amplified and cloned into pGEX-2T vector, resulting in the expression of fusion proteins with a GST tag at the N terminus. The RIIa domain of RSP7 as well as Dpy-30 was cloned into pET-28a vector, resulting in the expression of a N-terminally His-tagged polypeptide in the case of Dpy-30 and C-terminally tagged polypeptide in the case of RIIa.

The constructs for GST-tagged RSP3<sub>96-180</sub>, which contained the RIIa-binding AH at a.a.#161-178 a.a, and for the His-tagged RIIa were co-transformed into BL21(DE3) cells. The transformants were screened by double selection using culture plates that contained both carbenicillin (pGEX-2T) and kanamycin (pET-28a). The surviving clones were cultured and the proteins were induced by IPTG. As predicted, GST-tagged RSP3<sub>96-180</sub> was co-purified with the His-tagged RIIa domain by Ni-NTA (Figure 3-6A). This result served as a positive control and confirmed the interaction between the AH (161-178 a.a) and the RIIa domain.

The Dpy-30 domain containing RSPs, RSP2 and RSP23, were not amenable for this study due to their tendency to precipitate. Hence human Dpy-30 protein was co-expressed with RSP3 polypeptides. The human Dpy-30 protein was cloned into pET-28a vector which resulted in a His-tagged polypeptide. GST-tagged RSP3<sub>245-316</sub> and RSP3<sub>269-316</sub> were co-transformed into BL21(DE3) cells along with His-tagged human Dpy-30 protein. The transformants were induced with IPTG overnight at 16°C. The His-tagged human Dpy-30 proteins were pulled down using nickel beads. The samples which included 'pre', 'post' and the 'elute' were fractionated on SDS PAGE gels and visualized by Coomassie staining. Both RSP3<sub>245-316</sub> and RSP3<sub>269-316</sub> were pulled down along with human Dpy-30 protein (Figure 3-6 B and C). This result confirms the direct interaction between the candidate region (269-316 a.a) and human Dpy-30 protein. As a negative control, pGEX-4T vector with no insert was also co-expressed with human Dpy-30 protein to demonstrate that GST tag on its own does not interact with human Dpy-30 protein (Figure 3-6 D).



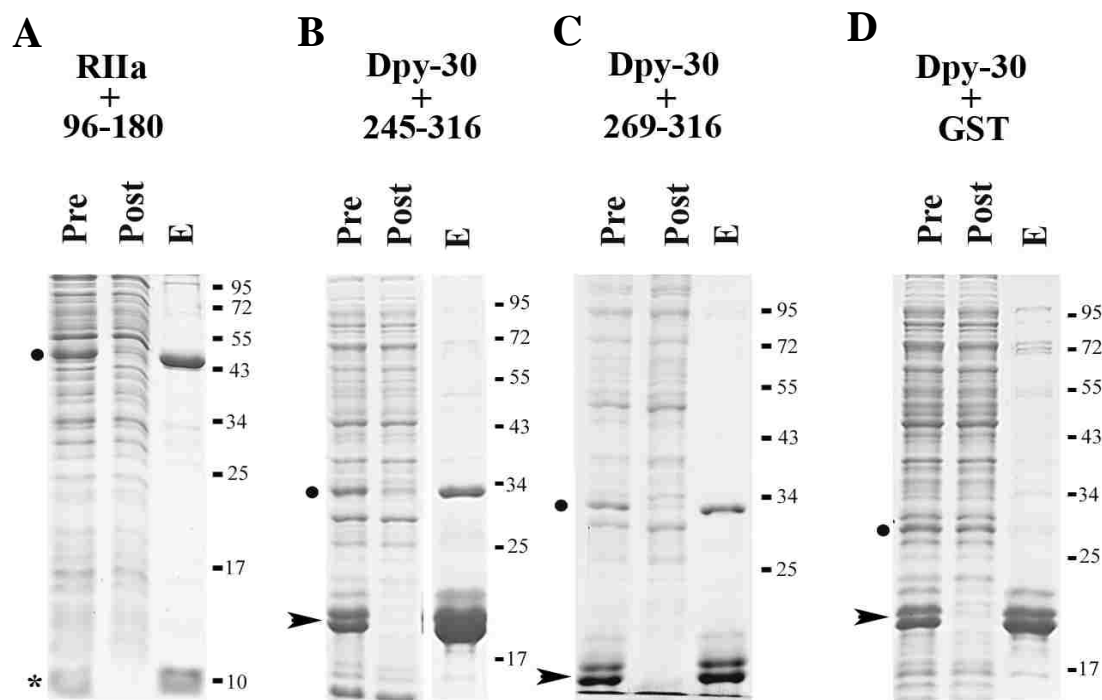


**Figure 3-6. Two regions in RSP3 bind to the RIIa and the Dpy-30 domain in vitro.**

(A) His-tagged RIIa from RSP7 (asterisk) or His-tagged Dpy-30 protein (arrowhead) were co-expressed with a RSP3 peptide tagged to GST (dot). The Ni-NTA pull-down was analyzed by Coomassie stained protein gel. (A) The positive control, the co-purification of the RIIa domain and the 96-180 fragment containing the RIIa-binding AH (Gaillard, 2001). (B) and (C) The co-purification of Dpy-30 protein and GST tagged RSP3 fragments (dot). (D) The negative control, showing that GST alone does not interact with Dpy-30 protein. Pre, the bacterial extract; Post, the flow through from Ni-NTA matrix; and E, the eluate.

These co-expression studies provided evidence for the direct interaction of the AH with the RIIa domain and RSP3<sub>269-316</sub> with the Dpy-30 protein.

### 3.3.2 Defining the Dpy-30 Domain Binding Site

In order to compare the binding sites of the RIIa clan domains we defined the exact Dpy-30 binding site within 269-316 a.a. Smaller constructs were engineered that expressed different regions within 269-316 a.a. All the RSP3 polypeptides were tagged with GST at the N terminus and cloned into the pET-Duet vector. The GST tagged RSP3 polypeptides were co-expressed in BL21(DE3) cells along with His-tagged human Dpy-30 protein. The human Dpy-30 protein was subjected to affinity purification and pulled down using Ni<sup>2+</sup> beads. The samples which included the 'pre', 'post' and the 'elute' were fractionated on SDS PAGE gels and RSP3 polypeptides were detected using the  $\alpha$ -GST antibody. RSP3<sub>280-316</sub> and RSP3<sub>280-308</sub> were effectively pulled down by human Dpy-30 protein (Figure 3-7). RSP3<sub>280-306</sub> however was not able to pull-down human Dpy-30 protein (Figure 3-7). Thus the Dpy-30 protein binding site was narrowed to the 28 a.a. region between #280-308.

AKAPs interact with the RIIa domain through a 14-18 residue amphipathic helix (Carr et al., 1991). Hence the 18 residue RIIa domain binding site in RSP3 (161-178 a.a) forms an amphipathic helix. Previous studies have shown that when the amphipathic helix is disrupted by introducing point mutations, the binding with the RIIa domain is abrogated (Carr et al., 1992; Gaillard et al., 2001). We speculate that the other member of

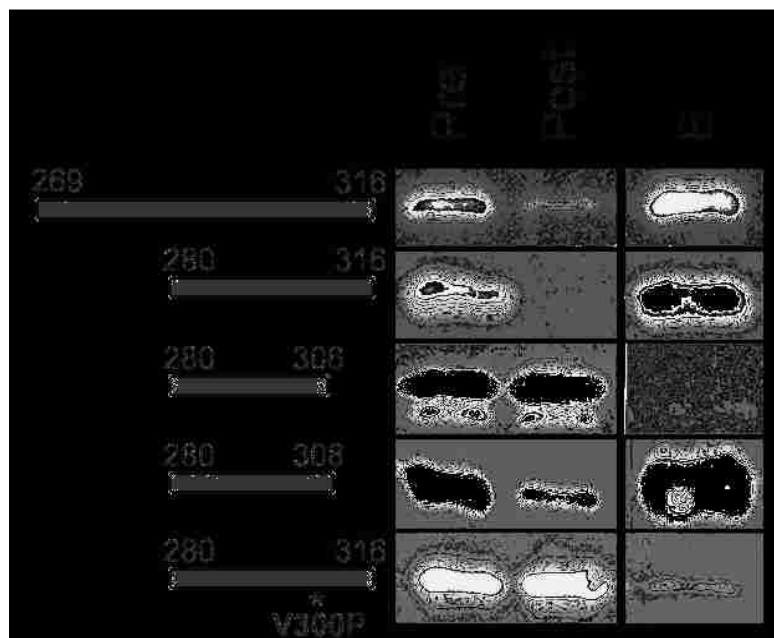


**Figure 3-7. The Dpy-30 protein binds to a.a.# 280-308 in RSP3.**

His-tagged full-length Dpy-30 protein was co-expressed with GST-tagged RSP3 peptides and then subjected to Ni-NTA pull-down. The protein samples fractionated by SDS-PAGE were probed for GST. The smallest region that bound the Dpy-30 protein was a.a. # 280-308. The interaction was perturbed by V<sub>300</sub>P mutation. Pre, the bacterial extract; Post, the flow through from Ni-NTA matrix; and E, the eluate.

the RIIa clan, Dpy-30 domain would also bind to similar amphipathic helices. Thus creating point mutations within the Dpy-30 binding site that disrupt the helicity of the region should abrogate its binding with the Dpy-30 domain. To test this we generated RSP3<sub>280-316</sub> polypeptide that contained a point mutation which replaced valine at 300 with a proline. The RSP3 polypeptide containing the mutation was cloned into the pET-Duet vector. The vector containing mutated RSP3 protein was transformed into BL21-DE3 cells along with His tagged human Dpy-30 protein. The transformants were expressed and subjected to affinity purification (as described before). The mutated RSP3 polypeptide was not able to pull-down human Dpy-30 protein (Figure 3-7). This suggests that the binding principles of both the RIIa clan domains are very similar.

### **3.3.3. Dpy-30 Protein Interacts with RSP3 through the Dpy-30 Domain**

The co-expression studies were carried out with full length human Dpy-30 protein. However, Dpy-30 protein is 99 amino acids in length. In addition to the 40 a.a. Dpy-30 domain in its C terminus, it has 59 additional residues. To clarify that the interaction between RSP3 polypeptides and the human Dpy-30 protein occurred through the 40 a.a. Dpy-30 domain, we engineered a construct that expresses the Dpy-30 domain alone. This construct (Dpy-30<sub>45-99</sub>) was cloned into the pET-28a vector resulting in a His tagged protein. Dpy-30<sub>45-99</sub> was co-transformed into BL21(DE3) cells along with the GST-tagged RSP3 constructs. The transformants were subjected to affinity purification using Ni-NTA matrix. The 'pre', 'post' and 'elute' samples were fractionated on SDS PAGE gels and detected by probing with  $\alpha$ -GST antibody. As anticipated the results obtained using full length human Dpy-30 protein were replicated using Dpy-30<sub>45-99</sub> (Figure 3-8).

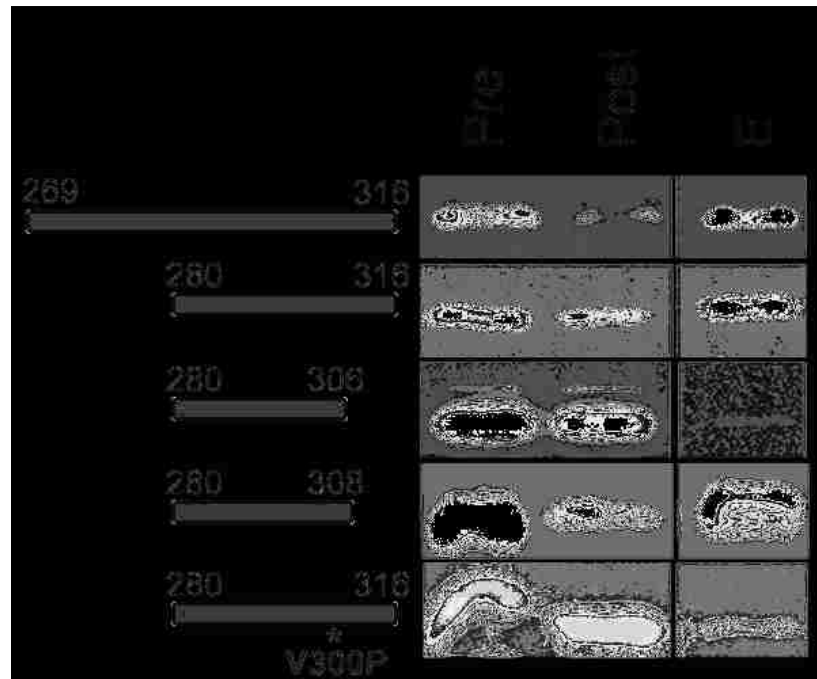


**Figure 3-8. The Dpy-30 domain binds to a.a.# 280-308 in RSP3.**

His-tagged Dpy-30 domain was co-expressed with GST-tagged RSP3 peptides and then subjected to Ni-NTA pull-down. The protein samples fractionated by SDS-PAGE were probed for GST. The smallest region that bound the Dpy-30 domain is a.a. # 280-308. The interaction was perturbed by V<sub>300</sub>P mutation. Pre, the bacterial extract; Post, the flow through from Ni-NTA matrix; and E, the eluate.

This suggests that the interaction between RSP3 polypeptides and the human Dpy-30 protein occurs through the Dpy-30 domain. Thus the co-expression studies allowed us to narrow down the Dpy-30 binding site to 28 a.a between residues 280 and 308 and also demonstrate that the binding principle of both the RIIa clan domains is highly similar.

### **3.3.4 Construction of a Dpy-30/RSP2 Hybrid Molecule**

The low expression and precipitation propensity of RSP2 and RSP23 precludes their usage in co-purification experiments. We speculate that these problems can be overcome by creating a hybrid molecule, using the N-terminal half of the Dpy-30 protein to carry RSP2's Dpy-30 domain. The hybrid molecule might remain soluble and could be used to test if the RSP2's Dpy-30 domain can bind to the partner sequence in RSP3.

Swapping the Dpy-30 domain in these two molecules is not straightforward, since the domain is at opposite positions in these two molecules. For RSP2, it is located in the N-terminus. For Dpy-30 protein, it is located at the C-terminus. The N-terminal region (1-45 a.a) of Dpy-30 protein and the Dpy-30 domain of RSP2 were PCR-amplified and cloned into pET-28a vector. The final construct would express a His-tagged hybrid polypeptide including the first 45 a.a. residues from the N-terminus of Dpy-30 protein preceding RSP2's Dpy-30 domain. To test its interaction with the RSP3 sequence, the hybrid construct was subjected to co-expression and co-purification with the GST-RSP3<sub>280-308</sub> construct.

While the hybrid did bind RSP3<sub>280-308</sub>, its binding efficiency was poorer than that

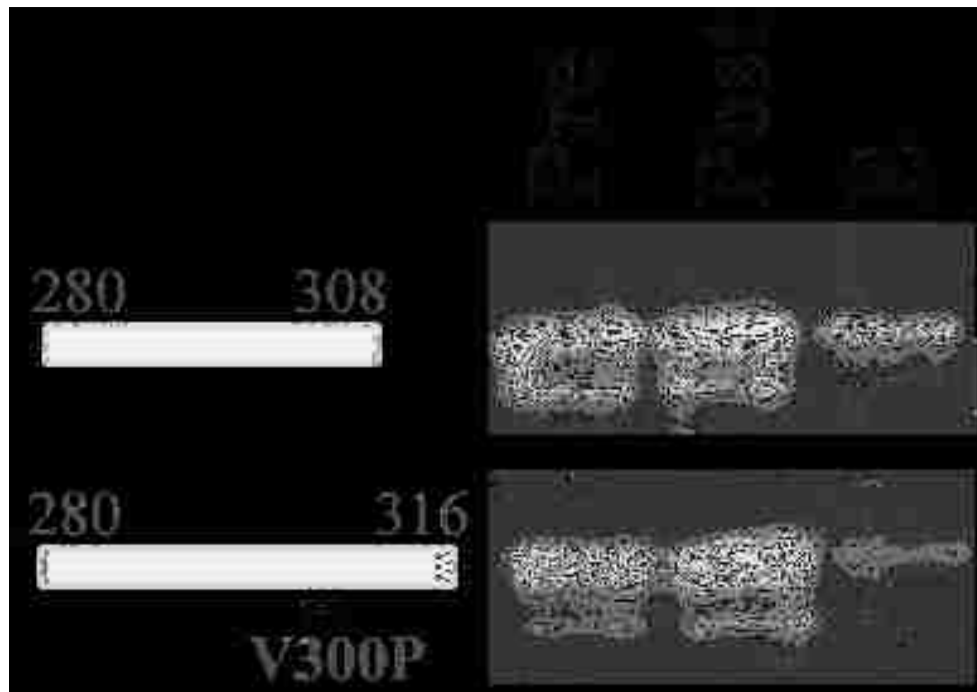


**Figure 3-9. The Dpy-30 binding domain (RSP3<sub>280-308</sub>) binds to the hybrid molecule albeit with low affinity.**

His-tagged hybrid construct which contains the Dpy-30 domain of RSP2 was co-expressed with GST tagged RSP3 polypeptides and subjected to Ni-NTA pull-down. The samples were fractionated on SDS-PAGE gels and probed for GST. The Dpy-30 binding region was pulled down by the hybrid construct while the construct harboring the point mutation was not co-purified. 'Pre' the bacterial extract, 'Post' the flowthrough from Ni-NTA matrix, 'E' the eluate.

of Dpy-30 protein (Figure 3-9). However, the binding was even poorer when GST-RSP3<sub>280-308</sub> was co-expressed with the V<sub>300</sub>P mutation construct (Figure 3-9). This suggests that RSP2's Dpy-30 domain binds RSP3<sub>280-308</sub>, albeit with low affinity.

Although, the hybrid protein allowed us to circumvent the solubility and expression problems of the RSP2 polypeptide, its affinity for RSP3<sub>280-308</sub> was not as high as that of Dpy-30 protein. This lesser efficiency could be attributed to the tethered sequence in RSP2. The last helix in RSP2's Dpy-30 domain forms a continuous helix of coiled coil propensity with flanking sequence. In engineering the hybrid construct this continuous helix was perturbed and may account for the low binding affinity of the hybrid construct. Additionally, recent studies on RIIa domains have shown that the sequences outside the domain do participate and contribute to the specificity and affinity of binding (Christian et al., 2011). In the same vein, utilizing the Dpy-30 domain of RSP2 without the downstream flanking sequence could severely compromise the binding affinity.

### **3.3.5 Comparing the RIIa Clan Domains**

Sequence alignment of RIIa and Dpy-30 domains from different proteins showed that there is considerable similarity between these domains (Figure 3-10). Both of the domains adopt a helix-loop-helix morphology. The RIIa domain structure is described as a X-shaped four helix bundle. It consists of two helix-loop-helix monomers that dimerize to form a hydrophobic groove to which the amphipathic helix of AKAP binds (Figure 3-11 A) (Newlon et al., 2001; Gold et al., 2006). The N terminus of the RIIa domain of RII-PKA is considered to be disordered and has been shown to form key contacts with



	<u>Helix I</u>	<u>Loop</u>	<u>Helix II</u>
<b>Dpy-30</b>			
KAD7_HUMAN/679-720	PLRNYLMTYVMPTLIQGLNECCNVRPE----	DPVDFLAEYLFKNNP---	
NDK5_HUMAN/156-197	AAKDYLNLHIMPTLLEGLTELCKQKPA----	DPLIWLADWLLKNNP---	
DPY-30_HUMAN/52-93	PTRAYLDQTVVPIILQGLAVLAKERPP----	NPIEFLASYLLKKA---	
DPY30_CAEEL/69-110	PTRQYLDSTVVPPIILQGLGALAKDRPE----	NPIEFLANFLLREKD---	
RSP2_CHLRE/8-49	HDTAYLKETVGEALARGCAAISAQPN----	DPVEYLGWLWLLKYVK---	
RSP23_CHLRE/152-197	AAAEYITKRIQPALAKALAAALAREKPSADKFEAITFVAGYLLQNNP---		
<b>RIIa (RI)</b>			
Q17QF5_BOVINE/25-62	-----RGIQQVLKDCIVQLCLAKPE----	RPMRFLREHFERLEKEEN	
KAP1_RAT/25-62	-----HGIQQVLKECIVHLCVAKPD----	RPLRFLREHFEEKLEKEEN	
A6YCE2_HUMAN/25-60	-----HNIQALLKDSIVQLCTARPE----	RPMAFLREYFERLEKP--	
Q96P62_HUMAN/25-59	-----HNIQALLKDSIVQLCTARPE----	RPMAFLREYFERLEK---	
A2AI69_MOUSE/25-62	-----HNIQALLKDSIVQLCTTRPE----	RPMAFLREYFERLEKEEA	
<b>RIIa (RII)</b>			
KAP2_HUMAN/8-45	-----PGLTELLQGYTVEVLRQQPP----	DLVEFAVEYFTRLREARA	
KAP2_MOUSE/8-44	-----PGLTELLQGYTVEVG-QQPP----	DLVDFAVEYFTRLREARR	
Q6NW93_ZEFSH/7-44	-----AGLPELLRGFTLEVLRRQPA----	DLLEFSVRYFTGLRDTRS	
RSP11_CHLRE/16-50	-----PHNLADILKAYTKEVIRRQPT----	DLIAFSAKYFTNLAN---	
RSP7_CHLRE/13-50	-----EGFPQLLKAFTREILRNQPD----	NIYEFGAKYFEDLIEENK	
CABYR_HUMAN/12-49	-----YGLKTLLEGISRAVLKTNPS----	NINQFAAAYFQELTMYRG	

### Figure 3-10. Sequence Alignment of the RIIa clan domains.

Sequence alignment displays the similarities between the RIIa clan domains from various molecules. The regions forming helix-loop-helix structures are underlined. The conserved hydrophobic residues and prolines are highlighted. Accession numbers for Dpy-30 domain proteins: KAD7 (Q96M32), NDK5 (P56597), DPY-30 Human (NP\_115963), DPY-30 C.e. (NP\_506058), RSP2 (XP\_001702718.1), RSP23 (XP\_001698136). Accession numbers for RIIa (RI) domains: KAP1 (P81377), A6YCE2, Q96P62, A2AI69. Accession numbers for RIIa (RII) domains: KAP2 Human (P13861), KAP2 Mouse (P12367), RSP11 (ABC02022), RSP7 (ABC02026), CABYR (NP\_036321).

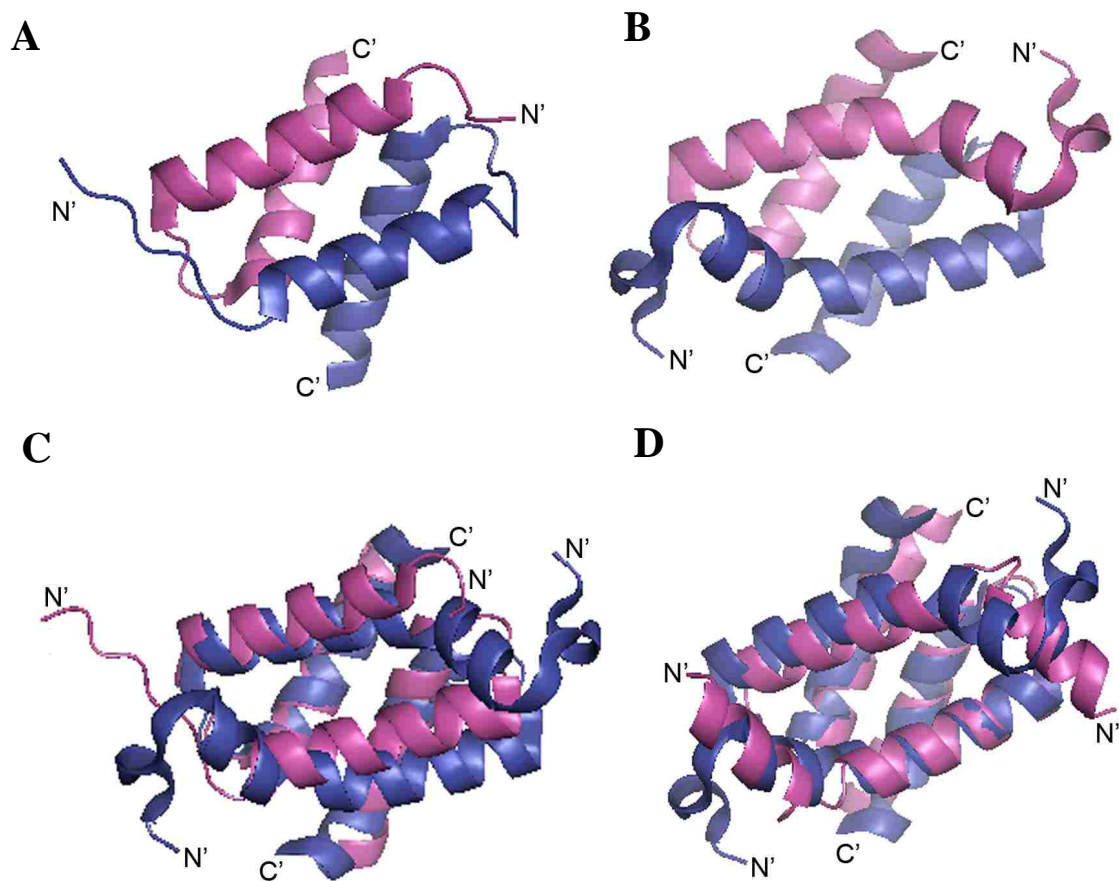


**Figure 3-11. Comparison of crystallographic structures of the Dpy-30 domain and the RIIa domains from PKA.**

(A) The domain from RII (PDB ID: 2HWN). (B) The domain from human Dpy-30 protein (PDB ID: 3G36). (C) and (D) The alignment of the Dpy-30 domain (blue) with the RIIa domain (pink) from RII and RI (PDB ID: 3IM4) respectively.

residues in AKAP (Kinderman et al, 2006). The RIIa domain of RI-PKA also adopts a X-shaped four helix bundle like structure. The hydrophobic groove that binds AKAP is created by the dimerization of two helix loop helix dimers (Banky et al., 2003; Sarma et al., 2010). The N terminus of the RIIa domain of RI-PKA differs from the RIIa domain of RII-PKA. It consists of key di-sulphide bridges that are essential for the dimerization of the domain. The RIIa domain of RI-PKA also contains an extended N terminus that folds inward resulting in a binding pocket that is much deeper than the RIIa domain of RII-PKA. It is speculated that the binding pocket of RI-PKA can accommodate bulky and aromatic residues unlike the flat hydrophobic groove of RII-PKA (Sarma et al., 2010).

The Dpy-30 domain structure is also described as a X-shaped four helix bundle. It also consists of two helix-loop-helix monomers that dimerize to form a groove or binding pocket (Wang et al., 2009) (Figure 3-11 B). This groove is primarily hydrophobic in nature. The structure of Dpy-30 in complex with its binding partner has not been solved; hence it is not known how the interacting protein occupies this hydrophobic groove. But drawing on analogies to the RIIa domain structure, it is reasonable to speculate that the interaction between Dpy-30 domain and its binding partner would be very similar to the interaction between RIIa domain and AKAP.

To compare the Dpy-30 domain and the RIIa domain of RI and RII-PKA, the structures were aligned using PyMOL (Figure 3-11 C and D). The alignment showed that although the core structure of the RIIa clan domains is similar, the Dpy-30 domain is more similar to the RIIa domain of RI-PKA (Figure 3-11 D). Like the RIIa domain of RI-PKA, the N terminal region of Dpy-30 domain also contains an extended helix that fold inwards resulting in a deeper binding pocket. The binding pocket of the Dpy-30 domain

has been described as less flat and less hydrophobic compared to the RIIa domain of RII-PKA (Wang et al., 2009). These differences may be key to afford specificity to these domains. Thus the RIIa clan domains exhibit several similarities and a few key differences.

### **3.3.6 Comparing the RIIa Clan Domain Binding Sites**

The similarities between the RIIa clan domains led us to compare the RIIa clan domain binding sites from various proteins in various organisms. The binding sites of RIIa clan domains were analyzed using helical wheel programs. The binding sites formed amphipathic helices with a distinctly hydrophobic face and a hydrophilic face. The amphipathic nature of RIIa domain binding sites is a well-documented finding. But the finding that this feature is also shared by Dpy-30 domain binding sites is novel (Figure 3-12 B). This finding reinforces the similarity in the binding principle of these domains.

Sequence comparison of RIIa and Dpy-30 domain binding sites did not reveal considerable identity. But when examined closer, it revealed conservation in the pattern of the sequences. Analyzing the RIIa and Dpy-30 binding sites from different proteins in different organisms we found that these binding sites contained hydrophobic residues that repeat in pairs interspersed by non-hydrophobic residues (Figure 3-12 A). These repeats were designated as ‘hydrophobic dyads’. Some binding sites contained four such pairs while some contained three pairs. This difference in number of pairs could depend on the number of contacts the binding peptide makes with the RIIa clan domains. Previous studies have shown that such a difference exists in the interaction between dual AKAP (AKAP that interacts with the RIIa domain of both RI-PKA and RII-PKA) and the RIIa



**Figure 3-12. Similarities of the RIIa- and Dpy-30-domain binding sequences.**

(A) Alignment of RSP3 sequences with the amphipathic helices that bind RIIa- (AH<sub>R</sub>) or Dpy-30-domain (AH<sub>D</sub>). Paired hydrophobic residues (black boxes) alternate with two varied residues. No particular residues are conserved to distinguish the two groups of sequences. D-AKAP2, a dual specific AKAP that binds the RIIa domain in RI and RII of PKA. Ash2 and BIG1, the Dpy-30-binding protein in histone methyltransferase complex and in the trans-Golgi network. RII-AKAP, Q12802; RI-AKAP, AAC24507 ; C.r., *Chlamydomonas reinhardtii*; C.e., *Caenorhabditis elegans*; D.r., *Danio rerio*; H.s., *Homo sapiens*; S.c., *Saccharomyces cerevisiae*. (B) Helical wheel plots of the sequences. The hydrophobic residues (bold and circled) are clustered to one side of the helix as expected for an amphipathic helix. AH<sub>R</sub> and AH<sub>D</sub>, the RIIa- and Dpy-30-binding sequences in RSP3.

domain of RI-PKA and RII-PKA. The crystal structures of both these complexes revealed that the same peptide undergoes one whole helical turn to bind the RIIa domain of RI-PKA (Sarma et al., 2010). Thus, in turn, the peptide makes more contacts with residues in the RIIa domain of RI-PKA.

The binding sites of RIIa domain from RII-PKA and RI-PKA have been studied extensively. These studies have shortlisted certain key residues that make a binding site specific for RII-PKA or RI-PKA (Banky et al., 2003; Sarma et al., 2010). In the same line, the Dpy-30 domain is not well studied and very few Dpy-30 domain binding sites have been characterized. Thus, it is difficult to compare the Dpy-30 binding sites with the RIIa binding sites and establish differences between these two domains.

The bioinformatics analysis revealed that similarities exist not just between the RIIa clan domains but also between the RIIa clan domain binding sites. This establishes the common binding principle behind these domains. Utilizing a common binding principle might stem from a common function of these domains which we speculate is targeting proteins to the appropriate location.

### ***3.4 Discussion***

The truncation strategies, using both the in vivo and the in vitro system, reveal the distinct binding sites for the RIIa and Dpy-30 domain in the RS. These distinct sites are amphipathic in nature, like all RIIa binding sites within AKAPs. In addition, the mutant phenotypes from the in vivo system also reveal the molecular interactions of the sequences tethered to these two domains. These findings elucidate the topology of the RS and explain the operational mechanism of this complex central for the motility control. In

addition, the results from the in vitro approach also revealed the common binding principle for anchoring the similar RIIa and Dpy-30 domains. The evidence and conclusions from this study are summarized below. The implications of these findings will be discussed in detail in the final chapter.

### **3.4.1 RSP3 Contains Binding Sites for the RIIa and Dpy-30 Domain**

The in vivo approach which involved generating RSP3 truncation mutants in *Chlamydomonas* was utilized to test if RSP3 could directly interact with all four RSPs with either a RIIa or Dpy-30 domain. The complementary phenotypes of the strains lacking major parts of RSP3 in the ( $\Delta$ 1) and 1-178 strains support this prediction. The analysis of the truncation mutants also revealed several details pertinent to the organization of the RS complex. It confirmed that the two RIIa RSPs, RSP7 and RSP11, are anchored through the AH that is known to anchor RII in vitro (Gaillard et al., 2001; Yang and Yang, 2006). This showed that these RIIa domains, identified based on sequence analysis, are functionally equivalent and are used for various molecules, aside from PKA. In the same token, this could be applicable to the Dpy-30 domain. Furthermore, the deficiency of armadillo repeat protein, RSP8 (ARM) that interacts with RSP11, in the  $\Delta$ 1 strain suggests that ARM associates with the coil 1 region of RSP3 either directly or through RSP11. These findings indicate that RSP11, RSP8 and RSP3 may form a tri-molecular complex. Most importantly, these results also suggest that the interaction between the AH and RSP11 tethers the ARM to RS complex and hence structurally reinforces the spoke scaffold. The deficiency of RSP7 in the  $\Delta$ 1 strain is identical to RSP11. Thus these two RIIa proteins are assembled similarly. We speculate

that RSP7 functions to tether the second ARM-containing RSP, RSP14. However, we could not verify this prediction due to lack of appropriate antibodies.

Lastly, these results also predicted that the candidate binding site for Dpy-30 domain should be downstream to the AH. Based on the mutants expressing RSP3 varying at the C-terminus, the Dpy-30 binding region was further delimited to be ~50 a.a. near the end of the conserved region in RSP3. Furthermore, the spokehead deficiency observed in these RSP3 truncation mutants is similar to the RSP2 mutants (Huang et al, 1981; Patel-King et al., 2004). This indicates that RSP3 collaborates with RSP2 in linking the spokehead to the stalk. This confirmed the prediction that RSP2 is not the only molecule connecting the head and stalk modules together. These predictions were strengthened by EM of the RS in truncated RSP3 mutants. Together, these findings provide the evidence for establishing the topography of the RS.

### **3.4.2 The Topography of the RS**

These results combined with the previous finding that RSP3 N-terminus is anchored to the outer doublets (Diener et al., 1993), support a model wherein dimeric RSP3 forms the scaffold of the RS complex. The two AHs in each RSP3 monomer anchor a protein with a RIIa domain and a Dpy-30 domain respectively. This model predicts the topology of the RS complex which couples the CP to the dynein motors on the outer doublets.

The dimeric core from a single protein extending throughout the RS provides the backbone to build a rigid complex. Docking of the RIIa domain at the AH at a.a.# 161-178 localizes within the RS complex the flanking sequences in RSP7 and RSP11 and the associated ARM RSPs. These tethered modules could possibly modulate or strengthen



the rigidity or other physical properties of the RS for appropriate mechanical transduction under a wide range of conditions. The docking of the Dpy-30 domain at the downstream AH at a.a.#280-308 enables the flanking coils in both RSP3 and RSP2 to interact with each other and to harness the multiple components in the spoke head and spokeneck. These multiple molecular interactions may be necessary to forge the two modules into one object that contacts the CP and endures the intermittent force occurring repeatedly from the mechanical transduction between the CP and the RS. The dimeric nature of RSP2 and RSP3 (Wirschell et al., 2008) makes it possible to form a symmetric spokehead that tilts back and forth around the circumference or along the length of the axonemes during each oscillatory beating. In addition, the docking also localizes the NDK in RSP23 to the neck. The localization of NDK at this position is unclear. However, it seems to be a valuable strategy since this molecule is also present in mammals. One possibility is that RS is a measure to distribute the NDK enzyme that balances the concentrations of ATP and GTP evenly throughout the flagellum. Or the enzymatic activity serves to solely regulate motility by modulating the local function of the RS or RS/CP system.

### **3.4.3 The In Vitro System Identified the RIIa- and Dpy-30 Binding Sequence.**

Using the in vitro approach, it was possible to confirm that the AH in RSP3 binds the RIIa domain from RII, RSP7 and RSP11. Most importantly, it also defined the precise Dpy-30 binding site from the 50-a.a. region as revealed in the *Chlamydomonas* RSP3 mutants. The Dpy-30 protein from human histone methyltransferase complex helped circumvent the solubility issues encountered with RSP2 and RSP23 in this system. The results are justified, as the AH<sub>R</sub> that was shown to bind recombinant RIIa domain in vitro

(Gaillard et al., 2001) also bound the RIIa domain of RSP7 and RSP11 (Yang et al., 2006). The AH for Dpy-30 domains were further confirmed by the V<sub>300</sub>P mutation.

#### **3.4.4 The Comparison of the RIIa and Dpy-30 Binding Sequences**

The well-defined binding sites made it possible to compare the binding sequences for the RIIa and Dpy-30 domains. The two RSP3 peptide sequences for binding RIIa and Dpy-30 domain were significantly different from each other and from other representative proteins. However sequence alignment showed that they do follow an identical pattern, repeats of  $\Phi\Phi XX$ , twin hydrophobic residues ( $\Phi\Phi$ ) interspersed by paired variable a.a.. Furthermore, the Dpy-30-domain binding helix can be plotted into an AH in a pattern similar to the RIIa binding sequences. This similar AH pattern is echoed by the similarity between the Dpy-30 domain and RIIa domain from both RI and RII. Thus, it is rather interesting that, although the two domains bind to RSP3, especially at two distinct sites, the principle of the interaction is quite similar if not identical.

## **Chapter 4: Development of tools for the study of Dpy-30-anchoring mechanism**

### ***4.1 Introduction***

This thesis and recent findings have demonstrated the similarities of the Dpy-30 and RIIa domain in sequence, structure and function (Chapter 3). Each domain is present in over 200 molecules that have additional diverged molecular architectures. These molecules mediate vital processes ranging from flagellar motility to membrane trafficking to epigenetic regulation. Like RII that binds many AKAPs, Dpy-30 protein itself binds to at least two vital molecules, BIG1 in the Golgi apparatus and Ash2 in histone methyltransferase complexes in the nucleus (Xu et al., 2009; Cho et al., 2007). The binding of human Dpy-30 protein to the Dpy-30-domain-binding AH in the radial spoke (RS) demonstrated the functional equivalence of these domains. Collectively, these findings raise three important questions. First of all, do the RIIa and Dpy-30 domains demonstrate specificity in terms of their binding partners? Secondly, aside from BIG1 and Ash2, how many more molecules anchor Dpy-30 proteins in various cells and organisms? Lastly, could the new findings on the Dpy-30 domain be applied for other research and therapy, such as the identification or perturbation of other anchoring proteins?

Similar questions have been thoroughly explored for the RIIa domain, cAMP-dependent protein kinase A (PKA) and numerous A-kinase anchoring proteins (AKAPs). The explosive discoveries in this field heavily relied on several powerful tools. The development of the labeled RII, a high-affinity blocking AH and the RII overlay catapulted the study of AKAPs and the differential targeting of RI type PKA and RII type

PKA. Similar tools for the Dpy-30 domain will likely simplify and accelerate the research of this domain and its anchoring proteins.

This dissertation has highlighted the insight that could be gained from exploring the anchoring proteins of Dpy-30 domain. As described in Chapter 3, identification of RSP3 as the anchoring protein for the Dpy-30-domain-containing RSP2 and RSP23 led to the elucidation of the molecular topography and mechanism of the RS. The reagents designed for these experiments could be modified into new tools towards understanding the Dpy-30 proteins and its molecular interactions.

Initially, recombinant human Dpy-30 and the RIIa domain that bind to the respective GST-tagged AHs could be used to test cross reactivity and to design the first-generation overlay assay. Subsequently, the existing constructs could be modified by adding different tags depending on the requirement of each assay. Each assay has distinct advantages and some of these assays need to be sensitive and quantitative. These new tools will pave the way for the development of specific and high affinity blocking AHs. The preliminary data for these assays will be described in this chapter.

## **4.2 Results**

The ultimate goal is to develop simple assays for identifying various proteins that anchor the Dpy-30 domain and high affinity AHs that block the interaction. These two goals are related. Simple assays will help the development of high affinity AHs. Conversely, high affinity AHs can verify the specificity of the interaction between the anchoring proteins and Dpy-30 in the assays. Studies on the *Chlamydomonas* flagellar RS complex described in Chapter 3 defined the RIIa and Dpy-30 binding AH in RSP3. These results were exploited to establish three strategies described below.

### **4.2.1 Strategies to Identify Dpy-30 Interacting Polypeptides**

Three strategies were taken to identify Dpy-30 interacting polypeptides: affinity co-purification, native gel electrophoresis; and a Dpy-30 overlay. All three methods can be used to test candidate Dpy-30 binding polypeptides. The overlay can be used to screen unknown samples.

#### 4.2.1.1 Affinity Co-Purification

This method relies on the interaction of two recombinant proteins that are co-expressed in bacteria; or expressed separately but mixed together once bacteria are lysed. This method has been used extensively in the study for PKA and AKAPs (Carr and Scott, 1992) and in this dissertation to identify the RIIa and Dpy-30 binding sites in RSP3. Specifically, His-tagged RIIa clan proteins and GST-tagged RSP3 peptides were co-expressed in bacteria and were pulled down together by Ni-NTA affinity chromatography. Alternatively, they could also be pulled

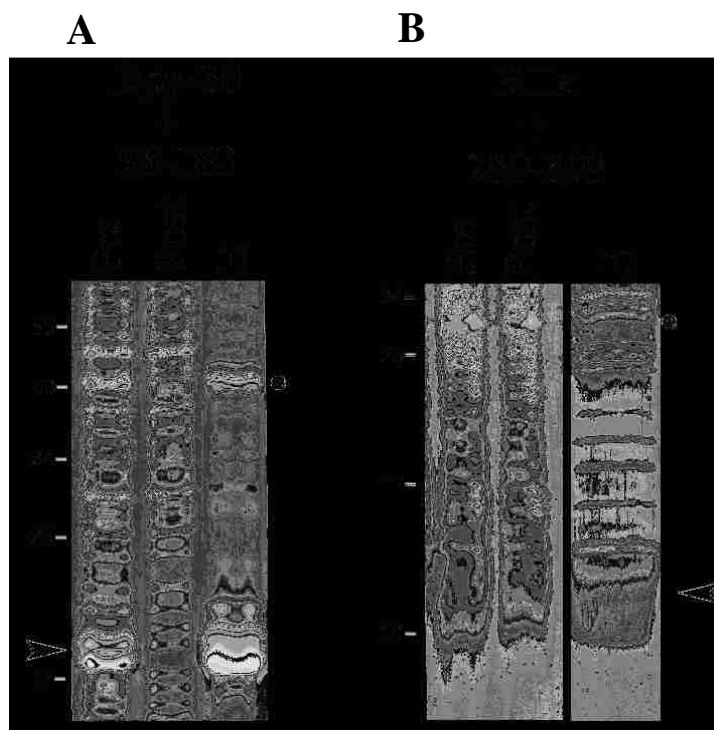


**Figure 4-1. The Dpy-30 domain cross-reacts with the AH<sub>R</sub>.**

(A) His-tagged Dpy-30 protein (arrowhead) or (B) His-tagged RIIa domain from RSP7 (arrowhead) were co-expressed with GST tagged AH<sub>R</sub> or AH<sub>D</sub> respectively (dot). The Ni-NTA pull-down was analyzed by Coomassie stained protein gel. While the AH<sub>R</sub> (dot in A) cross-reacted with the Dpy-30 protein, the AH<sub>D</sub> (dot in B) did not bind to the RIIa domain from RSP7. Pre, the bacterial extract; Post, the flow through from Ni-NTA matrix; and E, the

down by glutathione-agarose that binds GST. The reciprocal co-purification of the GST-tagged RSP3 peptides along with the His-tagged RIIa clan proteins indicate the ability of these two proteins to interact.

To test if the two sets of AHs and the RIIa clan domains cross-react, His-tagged Dpy-30 and GST-tagged AH<sub>R</sub> were co-expressed in bacteria. Although AH<sub>R</sub> binds the RIIa domain *in vivo*, it also co-purified with Dpy-30 (Figure 4-1A). This indicates the similarity and the identical binding principles of these two domains. However, the cross recognition is not universal, since it was not observed in the reverse experiments. The RIIa domain from RSP7 was not pulled down by the GST-tagged AH<sub>D</sub> that binds Dpy-30 domain *in vivo* (Figure 4-1B). The selective cross reactivity is interesting. One possibility is that certain AHs or RIIa clan domains have broad recognition because of their amino acid residues. Alternatively, the cross recognition may be due to the contour of the binding surfaces. The binding cavity in the dimeric RIIa domain tends to be shallower than the Dpy-30 domain and RI's RIIa domain.

This experimental strategy allows us to test the interaction between various combinations of anchoring proteins and docking domains.

#### 4.2.1.2 Native Gel Electrophoresis

The disadvantage of the pull-down assay is that the two proteins to be tested must have different tags. This limitation could be circumvented by native gel electrophoresis that fractionates protein complexes and is tag-independent. However, the two proteins to be tested need to be purified.

To test the principle, Dpy-30 protein was mixed with the two AHs in RSP3: AH<sub>R</sub> at a.a.# 161-178, that interacts with the RIIa domain in vivo; and AH<sub>D</sub> at a.a.# 280-308, that binds to the Dpy-30 domain in vivo. Both AHs were tagged with GST. Also tested was a peptide within the Dpy-30-binding sequence in Ash2, the physiological partner of Dpy-30 protein in the Set-1 methyl transferase complex (South et al., 2010). The peptide was predicted based on its secondary structure and three units of  $\Phi\Phi\text{XX}$  that is typical of the RIIa-clan- binding AHs. Ash2 peptide was tagged with GFP and a His tag at the N terminus. The advantage of GFP is its monomeric nature while GST is inherently dimeric. Secondly, GFP fluoresces and this fluorescence can be used as a reporter for a one-step quantitative assay. However, GFP is not conducive for affinity purification hence a second tag, 8 His in this case, was added for affinity purification.

His-tagged Dpy-30 and His-tagged GFP-Ash2-AH<sub>D</sub> proteins were purified using Ni-NTA. The GST-RSP3-AH<sub>D</sub> polypeptides were purified using glutathione-agarose. Equal amounts of each tagged AH and purified Dpy-30 were mixed together. Following 1-hour incubation, the samples were fractionated on a native gel and visualized by Coomassie stain (Figure 4-2). As protein complexes remain intact in native gels, an interaction between Dpy-30 and tagged AH would result in a shift in the band size as compared to the control samples that contained only one protein.

The results showed that all mixtures contained new bands distinct from the bands of the individual molecules (Figure 4-2). This showed that Dpy-30 forms a complex with AH<sub>D</sub> at RSP3<sub>280-308</sub> as expected and with the predicted AH<sub>D</sub> in Ash2. This is the third line of evidence that the Dpy-30-binding sequences contain triple or quadruple units of  $\Phi\Phi\text{XX}$  a.a., just like the RIIa-binding sequences. In addition, Dpy-30 also binds to AH<sub>R</sub>



that binds the RIIa domain, as shown in the pull-down assay (Figure 4-1A). Thus this method and the pull-down assay are suitable to test the interaction between anchoring motifs and docking domains.

Notably, Dpy-30 band shifts in opposite directions when complexed with GST-tagged or GFP-tagged AH<sub>D</sub>. When Dpy-30 is allowed to interact with the AH tagged to GST that is a dimer, the Dpy-30 oligomers become smaller, slightly bigger than GST tagged-AHs. In contrast, Dpy-30 actually shifted upwards when it forms complex with Ash2-AH<sub>D</sub> that is tagged to the monomeric GFP.

The opposite shifting directions could be due to the differences in tags or AH<sub>D</sub>. Although Dpy-30 is assumed to function as a dimer, purified Dpy-30 domain forms tetramers and higher-ordered oligomers (Dong et al., 2005; Wang et al., 2009). Dimeric GST-tagged AHs may dissociate Dpy-30 oligomers into dimers. The dimeric tag could potentially influence the kinetics of the molecular interaction. To test this, the native gel assay could be conducted to compare two fusion proteins with the same AH<sub>D</sub> but tagged to GFP or GST.

In summary, native gel electrophoresis is a rather straight forward assay for testing the interaction between purified Dpy-30 and candidate target proteins. The resolution of monomers and complex depends on the band shift. However, the shift in this case is sufficient and the method is easy and economical. However, the migration patterns could be influenced by tags and hence it is important to use the same tag when comparing the kinetics of different AHs for Dpy-30.

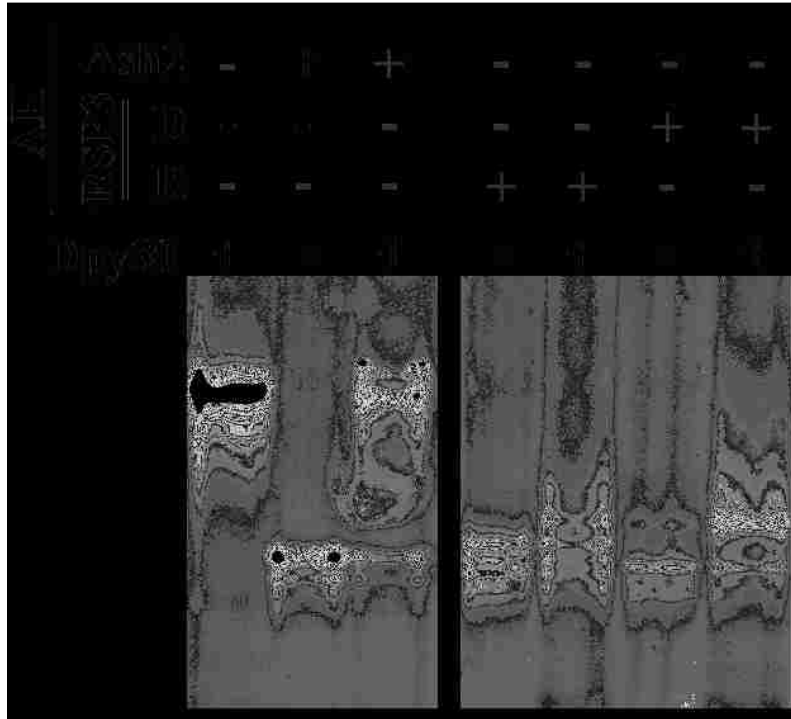


**Figure 4-2. Native gel electrophoresis for identifying Dpy-30-binding peptides.**

GFP-tagged Ash2 and GST-tagged RSP3 peptides purified from bacteria were mixed with purified Dpy-30 protein (dot represents the tetramer) and fractionated on a native gel. AH, amphipathic helix; D, Dpy-30 binding AH in RSP3; R, RIIa-binding AH in RSP3. Polypeptides were revealed by Coomassie stain.

#### 4.2.1.3 Overlay

Compared to the previous two assays, overlay is extraordinarily simple and versatile. It is analogous to a far western assay. Both use a protein ligand as a probe to detect its binding partners on the blot. The ligand can be labeled, for example with radioisotope, biotin or enzymes to aid in the detection. Or the ligand, as in far western assays, could be visualized indirectly through antibodies. These methods have been used successfully to study the interaction between RII and AKAPs (Lohmann et al., 1984).

In particular,  $^{32}\text{P}$ -labeled RII was often used as a ligand to identify AKAPs in different biological systems. The protein samples are separated on SDS-PAGE gels and transferred to a nitrocellulose membrane. Subsequently the membrane is probed with  $^{32}\text{P}$ -labeled RII and the AKAP bands are revealed by autoradiography or a phosphorimager. The ligands can recognize other non-AKAP bands as well. In order to identify AKAPs that interact with RII through the AH and RIIa domain, the control experiment is carried out in the presence of Ht-31, a synthetic peptide derived from the AH of AKAP-Lbc. This peptide has a high affinity for RII and acts as a competitive inhibitor. In theory, a protein that binds RII in an AKAP specific manner will not bind to RII in the presence of Ht-31.

We have tested an overlay, in fact a far western assay, using Dpy-30 as the ligand. In theory, this assay would aid the identification of Dpy-30 binding proteins in various protein samples (Figure 4-3). Axonemes from WT and spokeless *pf14* strains were fractionated in an SDS PAGE gel and transferred onto a nitrocellulose membrane (Figure 4-4A). The membrane was probed with 1  $\mu\text{g}/\text{ml}$  purified Dpy-30 protein. The blot was then probed with  $\alpha$ -Dpy-30 antibody followed by the secondary antibody. The assay

revealed a band which was present in WT axonemes but absent in *pf14* (Figure 4-4A). This suggested that it is a radial spoke specific band. The size of the band suggested that it is RSP3. To test this, the overlay was re-probed with anti-RSP3 antibody (Figure 4-4A). Indeed anti-RSP3 decorated the band picked out by the overlay assay. Interestingly, the antibody also recognized a slightly smaller band corresponding to the hypo-phosphorylated RSP3 (Qin et al., 2004). This suggests that Dpy-30 only binds to the phosphorylated form of RSP3. To differentiate if the bands revealed in the overlay is due to Dpy-30 and not due to the antibodies directly, a control blot was only probed with anti-Dpy-30 and the secondary antibody only. As predicted, the control blot did not reveal RSP3. It remains to be determined whether Dpy-30 binds to RSP3's AH<sub>D</sub> or AH<sub>R</sub> in the overlay assay.

The overlay assay was also used to probe the bacterial extract that contains GST-tagged AH<sub>D</sub> (RSP3<sub>269-316</sub>) and AH<sub>R</sub> (RSP3<sub>96-180</sub>) separated on a SDS-PAGE gel. The Dpy-30 protein was shown to bind both AHs (Figure 4-4B). This further confirmed the cross-reactivity of AH<sub>R</sub> and Dpy-30. However, the antibodies that were raised against proteins purified from the bacterial extract generated undesirable backgrounds in the bacterial samples. This problem could be overcome by using purified protein samples or a different read out that does not depend on antibodies.

Using the well characterized axonemal samples and defined bacterial extract, we showed that Dpy-30 is suitable as a ligand for the overlay assay. Similar to RII overlays, we envision that this Dpy-30 overlay is an amenable tool for testing various protein samples. The next step is to develop a high affinity AH as a blocker, analogous to Ht-31

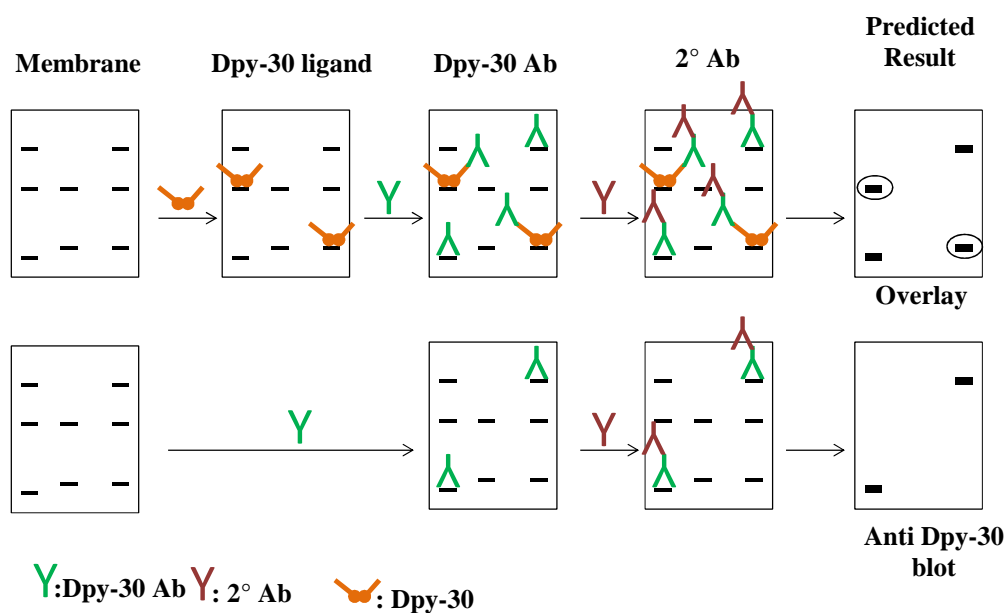


**Figure 4-3. Schematic depicting the Dpy-30 overlay procedure.**

The top panel depicts the overlay strategy and the bottom panel depicts the negative control blot that reveals Dpy-30 specific interactions.

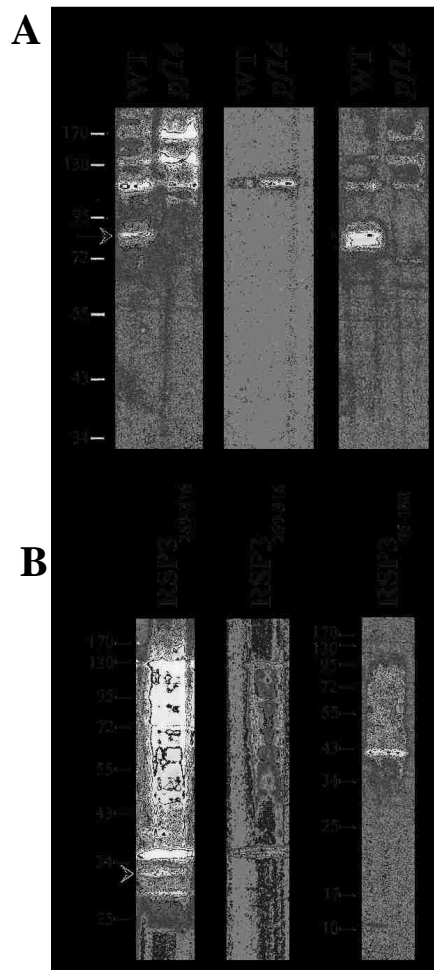


**Figure 4-4. The Dpy-30 overlays.**

(A) Blots of the axonemes from WT and the spoke-less *pf14* were probed for Dpy-30 protein, anti-Dpy-30 and the secondary antibodies (left panel). A band of the size of RSP3 in WT axoneme and absent in *pf14* was decorated (arrow). To test if the band is RSP3, the overlay blot was re-probed with  $\alpha$ -RSP3 antibody (right panel). As expected, RSP3 antibody recognized two bands as RSP3 is a phosphoprotein. Note the upper band that was more phosphorylated (asterisk) was decorated in overlay. This suggests that phosphorylation of RSP3 promotes Dpy-30 binding. The control blot of axonemes was probed with anti-Dpy-30 and the secondary antibody without Dpy-30 (middle panel). (B) The Dpy-30 overlay of the bacterial extract containing GST-AH<sub>D</sub> (RSP3<sub>269-316</sub>) (arrowhead, left panel). The control blot was probed with anti-Dpy-30 and the secondary antibody only (middle panel). The bacterial extract GST-AH<sub>R</sub> (RSP3<sub>96-180</sub>) that binds RIIa domain was decorated by Dpy-30 overlay. Thus Dpy-30 protein cross-reacts with AH<sub>R</sub> in the overlay.

for the RII overlay. Preferably, this AH could block the binding of Dpy-30 to AH<sub>D</sub>, but not AH<sub>R</sub>.

#### **4.2.2 Development of Quantitative Assays**

All three methods developed in this dissertation are suitable for the discovery of new Dpy-30-domain anchoring proteins. Each method has its own advantages and disadvantages. The common result is that Dpy-30 cross-recognizes AH<sub>R</sub>. However, the RIIa domain does not seem to recognize AH<sub>D</sub>. The deeper pocket of dimeric Dpy-30 may associate with AH with less stringency. The common limitation for these three methods mentioned above is that they are excellent for qualitative studies but cannot reveal quantitative data. They show either a positive or negative interaction but cannot differentiate the affinity of the AHs for Dpy-30. It is critical to develop a quantitative assay that could quantify the affinity of the AH-D/D interactions and identify a high affinity AH that would serve as a blocker for overlay and other studies.

The high affinity peptide blockers for Dpy-30 are analogous to Ht-31 for RII. This peptide would act as a competitive inhibitor that disrupts proteins interacting with Dpy-30. We postulate that the AH<sub>D</sub> in RSP3 binds Dpy-30 with a stronger affinity than the AH<sub>D</sub> in Ash2, because the radial spoke complex is an extraordinarily stable complex that can resist upto 0.6 M potassium iodide.

##### 4.2.2.1 GFP as a Reporter for a 96-Well Plate Assay

For high throughput assays of Dpy-30-binding sequences, one way is to immobilize Dpy-30 directly to the wells or indirectly through antibodies (Figure 4-5A). Then the wells can

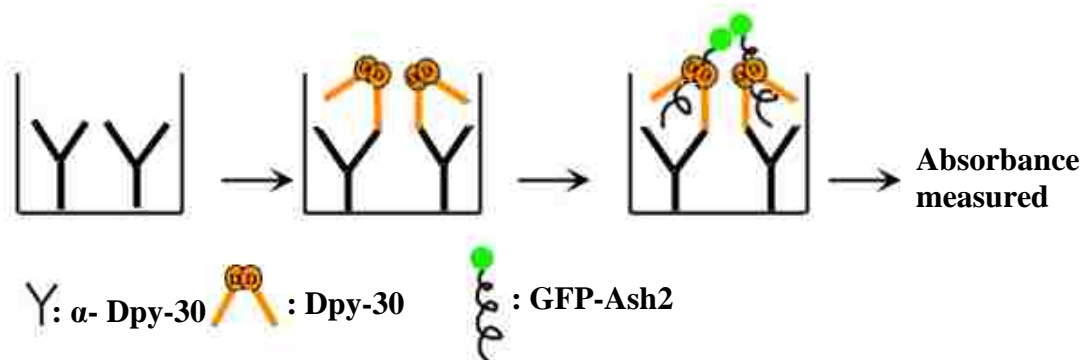
be incubated with AH<sub>D</sub> tagged to a polypeptide that will aid the read out, like GFP. For demonstration, the AH<sub>D</sub> from Ash2 was fused to GFP; this fusion protein can bind to Dpy-30 in the native gel (Figure 4-2).

The purified GFP-AH<sub>D</sub> was first quantified by Bradford protein assay. To test if GFP releases enough fluorescence to be a sensitive reporter, different amounts of GFP-AH<sub>D</sub> was added into each well and the light emitted after excitation was measured with a fluorescence microplate reader. The GFP was excited at 480-nm and the emission was measured at 510 nm (Figure 4-5B). The relative light intensity was plotted against the amount of the total GFP-AH<sub>D</sub> added. Unfortunately, 5-10 µg of GFP-AH<sub>D</sub> is necessary to obtain a reliable signal above the threshold level. Amounts less than that resulted in negative readouts or a high signal to noise ratio. Thus GFP-based assay is at least 1000 fold less sensitive than ELISA that can detect less than 5 ng of molecules (Dixit et al., 2010). Thus although the yield of recombinant GFP-AH<sub>D</sub> is high and the readout is very convenient, the fluorescence emitted per GFP is insufficient for a sensitive assay.

Several parameters need to be established for a quantitative 96 well assay. One is to use different reporter systems, such as anti-GFP and chemiluminescence; or luciferase and luminescence. The former requires two steps of antibody incubations, while the latter allows direct measurement. However, the reagents for the luciferase assay are more expensive and have a shorter life span. In addition different types of 96 well plates need to be tested. Currently, only the high absorbance plate was tested. The preliminary data for ELISA revealed undesirably high signal to noise ratios. It may be necessary to test different types of 96 well plates for each output.



A



B

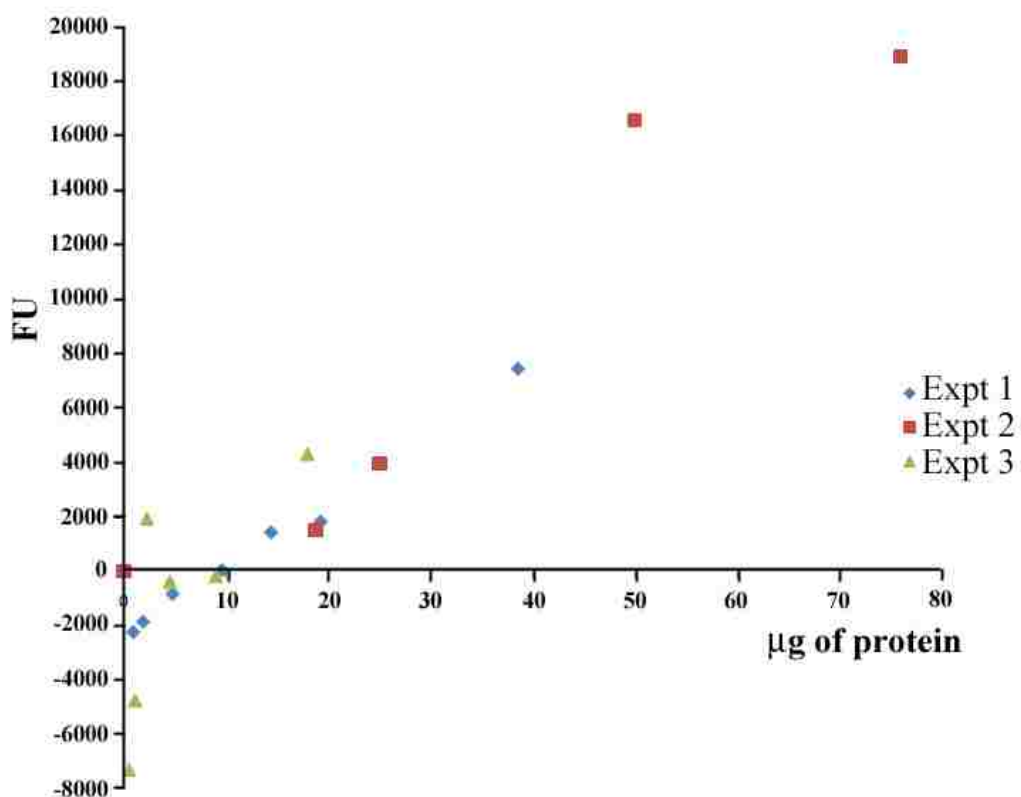


**Figure 4-5. Developing Quantitative assays to test the affinity of Dpy-30 binding peptides.**

(A) Schematic depicting the fluorescence based quantitative assay to measure the affinity of Dpy-30-binding peptides. (B) The light emitted from the bound GFP-tagged-Ash2 AH<sub>D</sub>. FU: Fluorescence Unit.

### 4.2.3 Screening Non-Peptide Blockers for Dpy-30

High affinity blockers, like Ht-31, play a crucial role in RII overlays that identify AKAPs based on the AH<sub>R</sub>-RIIa interaction. However RII also interacts with proteins through undetermined interactions. Thus, in order to identify proteins that bind RII in an AKAP specific manner, high affinity blockers like Ht-31 are employed. Proteins are recognized as AKAPs if their interaction with RII is competitively blocked by Ht-31. Thus, a high affinity AH is instrumental to determine the specificity of the interactions in vitro. Aside from overlays, the high affinity AHs and its membrane-permeable variants have been widely used for functional perturbations in various studies. Recently, small organic compounds were found to block the AKAP-RII interaction in ways similar or distinct from Ht-31 (Klussmann et al., 2006; Christian et al., 2011). Although the specificity of these compounds remain to be assessed, both peptide and non-peptide blockers could be potentially useful for perturbing the Dpy-30 and AH<sub>D</sub> interaction.

#### 4.2.3.1 Screening Chemical Blockers with Native PAGE

The Dpy-30 and AH<sub>D</sub> interaction discovered in this thesis was used to test the feasibility of screening chemical inhibitors. This is a collaborative effort with the lab of Dr. Daniel Sem in the Department of Chemistry at Marquette University. An in-silico analysis using the AutoDock software was first conducted to align the crystal structure of the dimeric Dpy-30 domain with 10,000 compounds in a chemical library.

Ten compounds that could best fit in the binding cavity of the dimeric Dpy-30 domain were identified. The effects of these compounds in perturbing the association between Dpy-30 and an AH<sub>D</sub> was revealed by native gel and pull-down assays (Figure 4-

4 and 4-5). GFP-Ash2-AH<sub>D</sub> was used in this assay, since if the assay is successful, the compound could be used to perturb the interaction of Dpy-30 and Ash2 in histone methyltransferase complex.

An aliquot of 2 μg of Dpy-30 protein was incubated with 25 μM compound for 1 hour at room temperature. Subsequently, GFP-Ash2-AH<sub>D</sub> was added into the mixture. The reaction mixture was then fractionated on a native gel and revealed by Coomassie stain (Figure 4-6). If a compound blocks the interaction between Dpy-30 and GFP-AH<sub>D</sub>, these two molecules will migrate as individual molecules in the native gel rather than a complex. Complex formation was assessed based on the appearance of new bands in the combined sample (Figure 4-6) and the reduced intensity of individual molecules. A sample without chemical compounds served as the negative control. The results showed that the predicted AH<sub>D</sub> from Ash2 binds to Dpy-30 in the presence of all the compounds. Thus none of the candidate compounds identified by the in-silico analysis were able to compete with AH<sub>D</sub> in Dpy-30 binding.

Despite the negative result, this simple assay in theory could be used to identify high affinity compounds or AH peptides. However, this assay has several drawbacks. The number of samples that can be tested in each gel limits the number of compounds that can be screened. Thus this method could be used after candidate compounds are identified but not for a high-throughput assay. A larger chemical library with compounds of more diverse chemical properties than the current one may provide more candidates. Secondly, the Coomassie-stained output is not sensitive and thus a large quantity of compound is required for the assay. In addition, the first generation compounds may not have enough

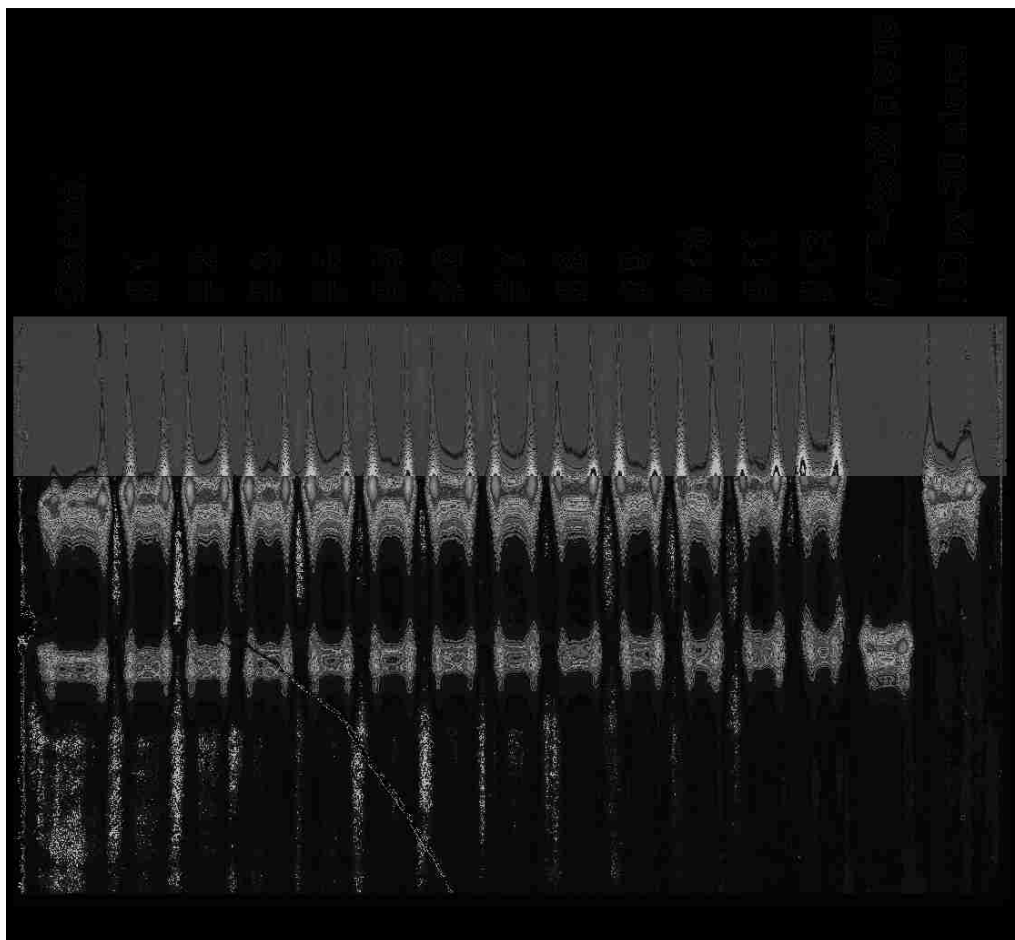


**Figure 4-6. Screening a library of compounds using the native gel assay.**

His-tagged Dpy-30 purified from bacteria was incubated with different compounds. Purified Ash-2 was subsequently added to the mixture and fractionated on a native gel. A mixture that did not contain any compounds served as the negative control. The numbers depict the different compounds. The arrow represents the Dpy-30 tetramer, the arrowhead represents the complex of Ash-2 and Dpy-30.

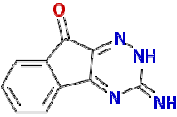
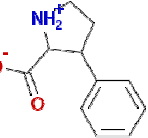
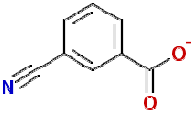
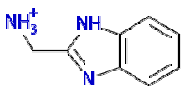
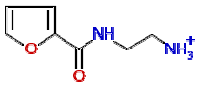
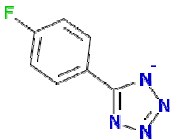
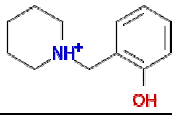
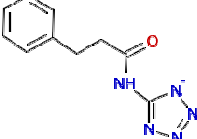
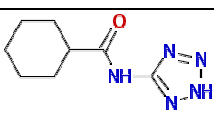
affinity for competition, if the affinity of Ash2-AH<sub>D</sub> for Dpy-30 is high. The dissociation constant,  $K_d$  of Ash2 and Dpy-30 is about 100 nM (Patel et al., 2009).

#### 4.2.3.2 Screening Chemical Blockers with Co-Purification

The compounds were also assessed by co-purification of His-tagged Dpy-30 and GST-AH<sub>R</sub> (RSP3<sub>96-180</sub>) (Figure 4-7). AH<sub>R</sub>, instead of AH<sub>D</sub>, was chosen because AH<sub>R</sub> may have lower affinity for Dpy-30 and the interaction could be more easily blocked by chemical compounds. If a compound could block the interaction, GST-AH<sub>R</sub> will not be co-purified with His-tagged Dpy-30 protein by Ni-NTA.

10 more compounds identified by in-silico analyses were tested with this method. Aliquots of His-tagged Dpy-30 protein pulled down by Ni-NTA was incubated with 50  $\mu$ M candidate compounds for 1 hour at room temperature. Subsequently, GST-AH<sub>R</sub> (RSP3<sub>96-180</sub>) was added into the mixture. After one-hour incubation, the mixture was subjected to Ni-NTA and the flow through was collected. The samples of the input and the flow through were fractionated on an SDS PAGE gel and revealed by Coomassie stain (Figure 4-7). If the compound was able to perturb Dpy-30-AH interaction, the RSP3 peptide in the flow through would be higher than that in the control without any compounds.

The results revealed that the amount of unbound RSP3 peptide did not differ significantly between the experimental and the control sample (Figure 4-7). Although none of the compounds could serve as competitive inhibitors, this method is feasible and rather simple like the native gel assay. However, both methods suffer from the same limitation in sensitivity, qualitative results and the throughput levels. It also requires additional steps in pull-down and the amount of Ni-NTA matrix added to each reaction can vary

Structure	Assigned Name	Chemical Name
	3027 (b)	3-[(dimethylamino)methyl]-1,3-benzoxazol-2(3H)-one
	10173 (d)	3-Phenylproline
	1059 (f)	3-Cyanobenzoate
	1830 (g)	1H-benzimidazol-2-ylmethanaminium
	2027 (h)	2-[(furan-2-ylcarbonyl)amino]ethanaminium
	2908 (c)	5-(4-fluorophenyl)tetrazol-1-ide
	9606 (e)	2-(piperidin-1-ylmethyl)phenol
	4046 (i)	3-phenyl-N-(2H-tetrazol-5-yl)propanamide
	8075 (a)	1-phenyl-1,2-dihydro-5H-tetrazole-5-thione

**Table 4-1. List of Chemical compounds**

The table showcases the structures and chemical names of the organic compounds used in the screening. The number in the assigned name column was designated by Dr. Sem's lab and the letters correspond to those used in Fig 4-7.

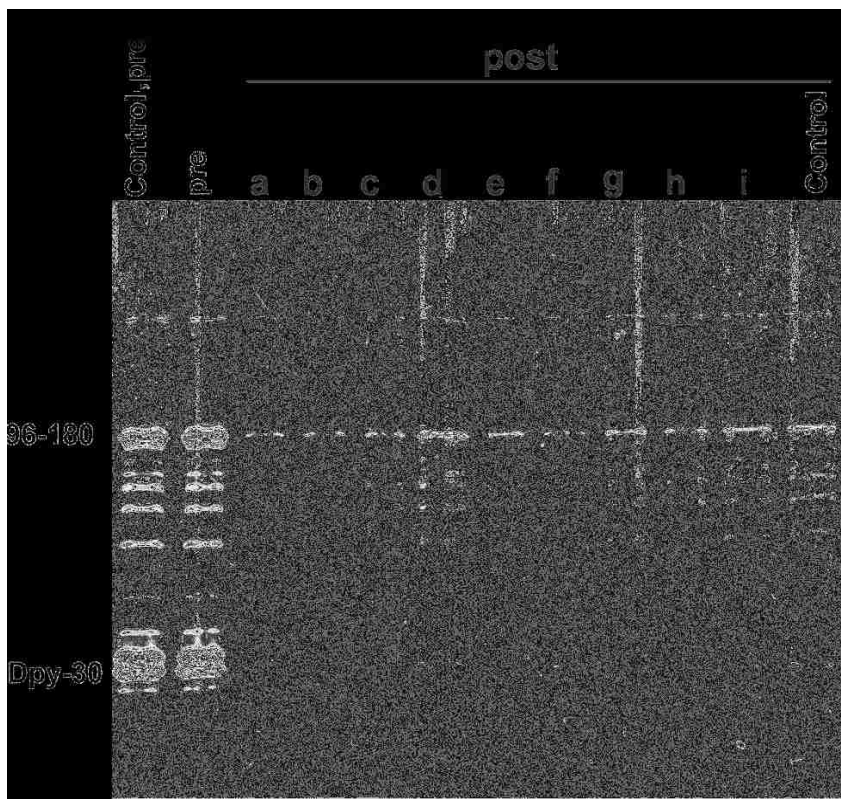


**Figure 4-7. Pull-down assay for screening organic compounds.**

Purified His-tagged Dpy-30 was incubated with different compounds first and the Dpy-30-binding peptide, RSP<sub>396-180</sub>. The mixture (pre) and the flow through (post) from Ni-NTA affinity chromatography were assessed by SDS-PAGE to test if any compound inhibited the interaction of Dpy-30 and RSP<sub>396-180</sub>. The control lanes are samples without any compounds. The letters depict the different compounds that were tried.

easily during experimentation.

### ***4.3 Discussion***

The preliminary studies described in this chapter explored the interactions between the Dpy-30 domain and its binding AHs in the existing anchoring proteins. The reagents and assays developed here demonstrate the direction for future studies. The improved tools will be invaluable for studying the emerging proteins in the RIIa clan and the molecules that anchor these novel proteins.

Taking advantage of the existing reagents, the various assays revealed the cross-reactivity of the Dpy-30 domain and AH<sub>R</sub> that is supposed to bind the RIIa domain. This is not particularly surprising given the similar secondary and tertiary structures of these domains. However, this finding leads to the question of how AH<sub>R</sub> and AH<sub>D</sub> in RSP3 bind to the respective RIIa- and Dpy-30 domain containing RSPs. In addition, how do the numerous anchoring molecules with various AHs in the cell body interact with only the right partners in the cell body? Several possibilities are proposed and will be dealt with in Chapter 5.

The preliminary data revealed the reagents and methods that could be used for the study of Dpy-30 domain and its interactions with various anchoring proteins. Each assay has advantages and drawbacks. Most of them are feasible but need to be optimized. One important contribution of this study is the use of Dpy-30 as a ligand in the overlay. As Dpy-30 exhibits cross-reactivity for AH<sub>R</sub> that binds the RIIa domain, it is possible that the Dpy-30 overlay can replace RII overlay for a broad spectrum screening of anchoring proteins. To further differentiate the RIIa binding proteins, a duplicate blot could be



processed for RII overlays with and without Ht-31 blockers. The bands that are only recognized by Dpy-30 could be the anchoring proteins for Dpy-30 domains. Those recognized by RII and Dpy-30 could be the anchoring proteins with AH<sub>R</sub> or with both AH<sub>R</sub> and AH<sub>D</sub>, like RSP3. It is also desirable to modify the AH<sub>D</sub> into a specific peptide blocker that competitively inhibits binding with Dpy-30 domain while not affecting the binding with RIIa domain.

To develop high affinity AH as blockers, it is preferable to develop quantitative assays to determine the affinity of the existing AH<sub>D</sub> for the Dpy-30 domain. The AH<sub>D</sub> with the highest affinity can be used to devise additional peptides with even higher affinity. If the quantitative assay is sensitive and high throughput, it could be used in the screening of chemical libraries. Other strategies for developing peptide variants could be considered. For example, peptide arrays have been commonly used in the development of high affinity binding peptides. A spectrum of peptides, in which each residue is replaced by every possible a.a., are spot synthesized into a chip-like matrix. The matrix could be probed with ligands, like RII or Dpy-30 in the overlay assay. While some peptides lose the ability to bind the ligand, some others have higher affinities. This unbiased screening strategy led to the discovery of several AHs that bind RII with affinity 5 -10 fold higher than physiological AKAPs (Alto et al., 2003; Burns-Hamuro et al., 2003; Gold et al., 2006). These super AHs can also be further modified to be specific for RII or RI. In addition, this exhaustive technique also can reveal considerable information about the role of each amino acid in the AH. This peptide array is worth considering for developing tools to study the Dpy-30 domain.

## Chapter 5: Discussion

This dissertation set out to discover how an axonemal complex that controls flagellar motility accommodates two pairs of proteins that contain similar RIIa clan domains. The results revealed that the two types of RIIa clan domains, RIIa and Dpy-30, dock to two similar AHs in a dimeric protein, RSP3. These conclusions support a new model that can explain the assembly and function of the RS. They also suggest that the AH and D/D domains constitute a localization mechanism for a spectrum of effector mechanisms much broader than PKA. These findings not only question the existing concepts of these molecular modules but also raise intriguing queries that remain to be investigated. The tools developed in this dissertation could be used to make headway into future studies.

### *5.1 A New RS Model*

Both in vivo and in vitro evidence support a model that the RSP3 dimer extends throughout the spoketalk with two discrete regions for anchoring the two types of D/D domains in four RSPs. A region near Coil 2 anchors the Dpy-30 domain present in RSP2 and RSP23. The helices downstream to the binding region in both RSP2 and RSP3 may form coiled coils with each other and with the head components. As for RSP23, the Dpy-30 domain could tether the associated NDK activity to the RS complex (Patel-King et al., 2004). Finally, the spoke-specific HSP40 (RSP16) is added to this region (Yang et al., 2008). Through these multiple interactions, the head, neck and stalk are linked together as a single unit that can couple the CP and outer doublets at a high frequency.

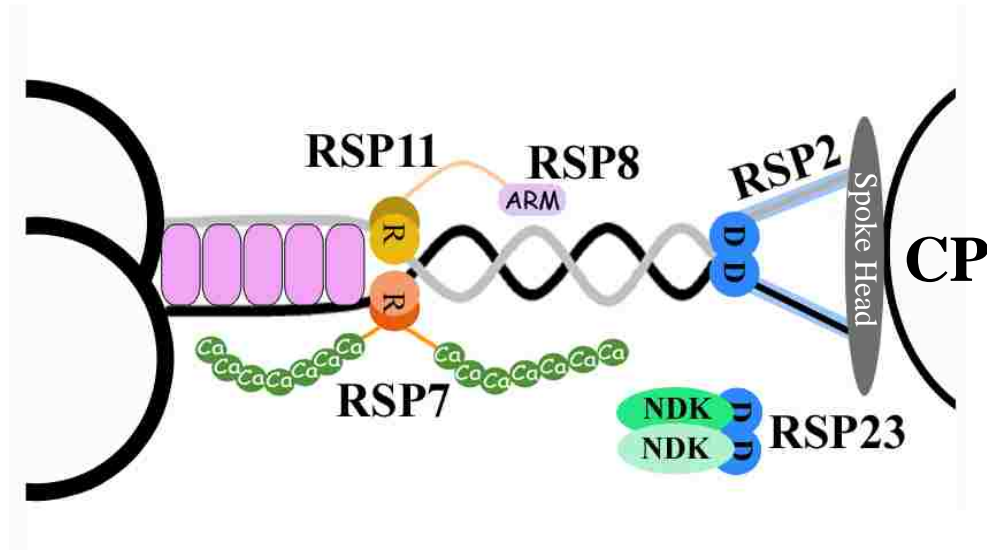


**Figure 5-1. The new RS model.**

Schematic depicting the topology of the radial spoke complex. RSP3 dimer of the conserved region forms the stalk scaffold (black and grey lines). The N terminus of RSP3 docks 5 LC8 molecules (pink ovals) (Gupta et al., unpublished). The AH<sub>R</sub> docks the RIIa-domain containing proteins, RSP7 (orange and red spheres) and RSP11 (yellow and mustard spheres). The binding of these proteins in turn tethers the associated effector mechanisms, the calcium binding motifs (green circles) of RSP7 and the armadillo (ARM) repeat protein (RSP8, light pink oval) which binds to RSP11 and the coil1 region in RSP3 and enhances the rigidity of the spoke stalk. The Dpy-30-domain containing proteins dock onto the downstream AH<sub>D</sub>. Both RSP2 and RSP23 form part of the neck sub-complex and helps to link the spoke head and spoke stalk modules. CP, Central pair apparatus; NDK, Nucleoside Diphosphate Kinase domain; D, Dpy-30 domain; R, RIIa domain; ARM, ARMadillo repeat protein.

The RIIa domain of RSP11 docks onto the AH<sub>R</sub> in RSP3 while the short flanking sequence tethers the armadillo repeat protein, RSP8 to interact with the Coil 1 region in RSP3 directly or indirectly. We speculate that this may enhance the rigidity of the dimeric RSP3 core, since the mutants defective in RSP11 can swim but become paralyzed in the exhausted media (Yang and Yang, 2006). By the same token, RSP7's RIIa domain docks to the same AH<sub>R</sub> in the other RSP3 monomer. Yet contrary to the constitutive function of RSP11, RSP7's EF-hands are in position to allosterically modulate the stalk when calcium increases, in a way analogous to the cAMP-induced allosteric release of the PKA catalytic subunit.

The various functions of these four RSPs are all docked through the D/D domains to the two AHs in RSP3. As RSP3 N-terminus associates with the microtubule outer doublets in the axonemes (Diener et al., 1993) while the C-terminus is involved in the spokehead assembly, the dimeric RSP3 clearly is a bona fide core scaffold of the entire complex. The RSP3 sequence also supports this new RS model. The spoke stalk length has been proposed to be around 38-41 nm by studies of axonemes prepared and visualized by different methods (Nicastro et al., 2005; Yang et al., 2001). Although *Chlamydomonas* RSP3 is 516 a.a. in length; sequence homology and functional studies have shown that the C terminal region is dispensable (Diener et al., 1993). This study further defined that 1-316 a.a region of RSP3 is the smallest essential region.

The N terminus of this essential region contains 5 LC8 binding sites and has been shown to bind LC8, a small ubiquitous molecule that functions as a dimer (Gupta et al., unpublished). Five LC8 molecules span a distance of 20 nm (Stelter et al., 2007). The rest of the conserved region is mainly coiled coil in nature (Fig 3-1 B). Considering the rise

per residue along a straight  $\alpha$ -helix is 0.15nm (Lim et al., 1951), this region between 161 and 316 a.a would span a distance of 23 nm, bringing up the entire spoke stalk length to ~43 nm which is very close to the current estimate. Thus RSP3 can span the spoke stalk distance, supporting this complex that regulates oscillatory beating mechanically and chemically.

### ***5.2 Versatility of the AH-D/D Localization System***

The interactions of AH<sub>R</sub> in RSP3 with RII in vitro (Gaillard et al., 2001) but with non-PKA RSP7 and RSP11 in vivo further confirms the predicted functional equivalence of these domains (Yang and Yang, 2006; Newell et al., 2008). This equivalence is also true for human Dpy-30 protein in histone methyltransferase complex. Dpy-30 binds to Ash2 in the histone methyltransferase complex in vivo (Roguev et al., 2001; Dehe et al., 2006) but recognizes RSP3's AH<sub>D</sub> that binds the Dpy-30 domain in RSP2 and RSP23 in the RS complex.

Contrary to the conserved anchoring and docking domains, the effector mechanisms may not be evolutionarily conserved. The RIIa clan members are drastically diverged. The orthologues of these four members in *Chlamydomonas* RS are not evident in other organisms even though RSP3 orthologues, including the anchoring AHs, are conserved. The orthologous RIIa clan members contain the RIIa clan domains but differ in the nature of the associated flanking sequence. The conserved localization mechanism but divergent effector mechanisms may be an evolutionary scheme to tailor the motility control to suit the special needs of individual cell types in different environments. For instance, calcium and cyclic nucleotides induce motility changes in virtually all motile

cilia and flagella. However each cell type responds differently to these second messengers (Smith and Yang, 2004). Perhaps for different organisms, the second messengers act on the diverged RIIa clan members, including RI or RII, in the RS to induce different motility changes. As motile cilia and flagella are critical for the survival of individual species, these diverged effector mechanisms may have evolved independently and those that give individual species advantages in their respective environment are retained. Thus AHs and D/D domains constitute a versatile system to anchor various effector mechanisms beyond PKA.

### ***5.3 The AH Molecular Scaffolds***

This study shows that, although D/D domains can anchor various effector mechanisms, the molecules with AHs may largely serve as scaffolds of molecular complexes. AKAPs are signal transduction scaffolds that anchor multiple molecular switches and PKA via the AH-D/D interaction (Wong and Scott, 2004). This dissertation shows that RSP3, once known as AKAP, is indeed a signal transduction scaffold as it anchors effector mechanisms like RSP7's EF hands that transduce calcium signals. However, the term signal transduction scaffold falls short of depicting the essence of RSP3 which is to support the entire RS complex structurally. Furthermore, some effector mechanisms anchored to RSP3's AHs are for the assembly or constitutive enhancement of this structural complex. Hence RSP3 is both a structural and signal transduction scaffold.

Recognition that proteins with AHs could serve as structural scaffolds is important to understand the molecular complexes with AH-containing anchoring molecules. The usage of AH-D/D interaction in building up a structural scaffold may not

be unique to RSP3, the RS or flagella. The same could be true for Ash2, a component in the Set 1-like histone methyl transferase complex. Ash2 interacts with Dpy-30 in the core complex in various Set1-like histone methyltransferase complexes (Patel et al., 2009; Cho et al., 2007). Both molecules are important for the enzymatic activity, albeit in different ways (Patel et al., 2010). Ash2 is vital for the enzymatic activity while Dpy-30 is not. Yet Dpy-30 affects the H3K4me3 level across the entire embryonic stem cell genome (Jiang et al., 2011). Aside from Dpy-30, Ash2 also associates with RbBP5, a WD-repeat protein subunit in the core complex (Patel et al., 2009). It is possible that Ash2 serves as a structural scaffold of this complex that transfers methyl groups.

The other examples are BIG1 and BIG2, the paralogous guanine nucleotide exchange factors in the trans-Golgi network. These two large molecules interact with each other. BIG2 also contains three AHs that can interact with RI or RII in vitro (Li et al., 2003), whereas BIG1 contains an AH that anchors Dpy-30 in vivo (Ishizaki et al., 2006; Xia et al., 2010). In addition, each of them also associates with other molecules that mediate critical functions related to membrane trafficking. This heterodimer, like the RSP3 homodimer, may form a hybrid scaffold for structural and signaling purposes.

Thus, it is possible that the molecules that utilize AH for anchoring a variety of the RIIa clan molecules with D/D domains are molecular scaffolds in general. Some are strictly for forming the structural backbone of molecular complexes; some anchor molecular switches for signal transduction and the others have combined features. The term AKAP is appropriate for those molecules that actually anchor PKA yet misleading for those that do not like RSP3. Therefore, we propose to use D/D-domain Anchoring Proteins (DAPs) to designate the molecules that utilize AHs to anchor myriads of

functions tethered through a D/D domain. It would be apt to refer to AKAPs as a sub-family of DAPs that specifically anchor PKA in vivo.

#### ***5.4 The Conservation and Divergence of the AH-D/D System***

We expected that the sequences for anchoring the RIIa and Dpy-30 domains are specific and significantly different for three reasons. These two domains are present in the same complex. Furthermore, the residues and the length of helices in the two domains are diverged enough to be classified into two families. Lastly, the N-termini in these two domains that contact binding peptides are distinct (Wang et al., 2009). Yet the AH<sub>R</sub> for the RIIa domain and the AH<sub>D</sub> for Dpy-30 domain are similar in their sequence pattern and binding principle, and are present in the same molecule, RSP3. And interestingly, the similarity is high enough that AH<sub>R</sub> and Dpy-30 bind in the in-vitro setting.

The cross reactivity indicates that RIIa and Dpy-30 domains are more similar than expected. This notion prompted us look into the RIIa variant—the RIIa domain from the RI subunit of PKA. Interestingly, the N-terminus of Dpy-30 and RI's RIIa domain are both helical (Banky et al., 2003; Wang et al., 2009; Sarma et al., 2010). In contrast to the  $\beta$ -strand in RII's RIIa, the N-terminus of both RI's RIIa and Dpy-30 forms an  $\alpha$ -helix that contributes to a deeper pocket for the AH (Banky et al., 2003; Sarma et al., 2010). Their structural alignment appears equal to, if not greater than, the alignment of Dpy-30 and RII's RIIa domain (Wang et al., 2009). Thus, although the N-terminus of the RIIa clan domains is critical for binding to an AH, it is insufficient to drastically change the interacting peptide sequences. Despite the classification of the RIIa clan into two families, the principle of molecular interactions for the two D/D domains is identical. The



strong resemblance is resonated by the cross-recognition between the Dpy-30 domain and the AH<sub>R</sub>.

### ***5.5 Selective Cross-Reactivity of the AH and D/D Domain***

The similarities between both the AH and D/D domains is reflected in the in vitro recognition of the AH<sub>R</sub> by Dpy-30 as well as RIIa from RSP7 and RSP11. Yet, AH<sub>D</sub> binds to Dpy-30 alone and not the RIIa from RSP7 in either the pull down or the overlay assay (Gaillard et al., 2001).

However, it is premature to generalize that only AH<sub>R</sub> and Dpy-30 have cross reactivity or this cross reactivity is due to unique structural features. It has been demonstrated that some AHs are mono-specific, binding to either RI or RII but not both (Angelo and Rubin, 1998; Hirsch et al., 1992), whereas certain AHs, from dual-specific AKAPs, recognize both RI and RII (Huang et al., 1997; Wang et al., 2009; Li et al., 2003). In this regard, the AH<sub>R</sub> in RSP3 is a dual-specific AH, whereas AH<sub>D</sub> appears mono-specific to Dpy-30. Sequence comparisons of the representative AHs did not reveal any consensus that will distinguish mono-specific or dual-specific AHs. The cross reactivity may be more about the specific amino acids in individual AHs than the D/D domain they bind to. Conversely, given the structural similarity between RI and Dpy-30, it will be interesting to test if AH<sub>D</sub>, in RSP3, Ash2 or other molecules, can recognize the RIIa domain from RI.

The dual-specific AHs in AKAPs bind PKA in both the RI or RII subunits. However, the cross reactivity of AH<sub>R</sub> in vitro with Dpy-30 creates interesting dilemmas in vivo —why does cross recognition not occur in the RS or in the cell body? If this

occurred, the spokehead could potentially form at the middle of the stalk, rather than at the expected distal end. Likewise, Dpy-30 is not expected to dock to AKAPs while PKA is not known to be in the histone methyltransferase complex.

One may assume that there are determinants for the specificity. As most AHs tend to be specific for RI or RII, perhaps the sequences in AH<sub>R</sub> and AH<sub>D</sub> are distinctive enough to localize the respective effector mechanisms precisely. Or the difference in affinity is sufficient to sort out the specificity that is observed *in vivo*. In general, the affinity of the AHs for RI is lower than that for RII (Herberg et al., 2000). Thus RI is often more evenly distributed throughout the cell body while RII is restricted to particular loci (Kinderman et al., 2006). The third possibility is the most interesting-- the specificity of certain AHs and the D/D are not as stringent as the connotations of these domains. In fact the specificity could be facilitated by other molecular cues, like the flanking sequences. It has been demonstrated that in dual-specific AKAPs, a sequence outside of AH<sub>R</sub> contributes to RI recognition (Jarnaess et al., 2008). Similarly, the sequences flanking the AH<sub>D</sub> in RSP3 and the Dpy-30 domain in RSP2 (Gopal et al., unpublished) may be involved in interactions with each other and molecules in the vicinity. If this is true, the AH and D/D domain may be more about docking and less about targeting. While all the eyes are on the AH and D/D domains, the flanking sequences may be equally informative.

### ***5.6 Tools for the DAPs***

The breadth and similarity of the AH and D/D domains presents ample opportunities yet also poses conundrums for research. The AH-RIIa interaction has been exploited for

discovering various AH-containing proteins that were recognized by RII. Two key tools are RII and high-affinity AHs. RII is used as a ligand to identify molecules with AHs (Lohmann et al., 1984). However, molecules could bind to RII ligand via sequences irrelevant to the AH. Thus only the interactions that could be perturbed by the high affinity AHs that originated from AKAPs are considered genuine (Carr et al., 1992). These two key tools led to the discovery of many AKAPs. Similar tools suitable for the Dpy-30 domain could potentially hasten the discoveries in the Dpy-30 field.

This study has demonstrated that Dpy-30 can serve as a ligand in pulldown or in an overlay assay. The axonemal bands revealed by Dpy-30 overlay are similar, if not identical, to that obtained by the RII overlay (Gaillard et al., 2001). This shows that AH<sub>D</sub> in various molecules, not just in Ash2, can bind Dpy-30 in vitro and that Dpy-30 could be used to discover other proteins that have an AH<sub>D</sub>, just like RII was used for the discovery of AKAPs.

From a structural perspective, the ability to utilize Dpy-30 as a ligand is interesting. RII exists as a homodimer, with the binding pocket exposed in solution. However, purified Dpy-30 forms tetramers (Dong et al., 2005). The AH-binding pocket is almost concealed in the tetramer (Wang et al., 2009). The results of the overlay assay and the pulldown suggest that the pocket is still accessible to the AH. Also in the native gel, Dpy-30 shifts in the opposite direction when it complexes with monomeric or dimeric carrier-AHs. It is possible that dimeric AH may further pry open the Dpy-30 tetramers into dimers.

Importantly, AH<sub>D</sub> in RSP3 cannot be recognized by RII (Gaillard et al., 2001) but can be recognized by Dpy-30. Conversely, Dpy-30 recognizes AH<sub>D</sub> as well as AH<sub>R</sub>. The

cross reactivity of Dpy-30 may be exploited in situations where using RII is not suitable. In theory, Dpy-30 overlay can potentially be used as a general screen to reveal all molecules with AH<sub>D</sub> or AH<sub>R</sub>, namely all DAPs. To sort out molecules that contain AH<sub>D</sub> or AH<sub>R</sub>, two additional strategies can be employed. One is to develop a high affinity AH for Dpy-30 domain. This AH, analogous to Ht-31, should be able to abolish the non-specific interactions. It will be of interest to see if it is possible to develop AHs that specifically disrupt the interaction of Dpy-30 with either AH<sub>D</sub> or AH<sub>R</sub>. For this purpose, the existing reagents and methods could be developed into sensitive quantitative 96-well assays either directly or through ELISA. Other high throughput systems, like peptide scan on spot arrays can also aid in the identification of new high affinity AHs (Alto et al., 2003, Burns-Hamuro et al., 2003). Once identified, the assay could be used to measure the affinity of AH variants.

Aside from the overlay assay, the AH<sub>D</sub> with high affinity and high specificity for Dpy-30 could be used in other perturbation assays, both in vitro as well as in vivo. Note high affinity AH<sub>R</sub>, like membrane permeable variants of Ht-31, have been widely used to study the significance of PKA anchoring in cell cultures or organ cultures. The effect is not identical to PKA inhibitors (Vijayaraghavan et al., 1997). This could be due to the inherent differences between the roles of PKA and AKAPs. It is also possible that some of the AH<sub>R</sub> may disturb the interactions of Dpy-30. Likewise, it is foreseeable that a high-affinity AH<sub>D</sub> may modulate H3K4 methylation but in a slightly different way from Dpy-30 knockdown or inhibitors of methyltransferases. Taken together, this dissertation will hasten the expansion of the field of protein anchoring and docking. Modifications of the new tools and assays will take the AH-D/D field to a robust future.

## Bibliography

Afzelius, B.A., A human syndrome caused by immotile cilia. *Science*, 1976. 193(4250): p. 317-9.

Afzelius, B.A., The immotile-cilia syndrome and other ciliary diseases. *Int Rev Exp Pathol*, 1979. 19: p. 1-43.

Afzelius, B.A., Genetical and ultrastructural aspects of the immotile-cilia syndrome. *Am J Hum Genet*, 1981. 33(6): p. 852-64.

Alto, N.M., et al., Bioinformatic design of A-kinase anchoring protein-in silico: a potent and selective peptide antagonist of type II protein kinase A anchoring. *Proc Natl Acad Sci U S A*, 2003. 100(8): p. 4445-50.

Angelo, R. and Rubin .C.S., Molecular characterization of an anchor protein (AKAP<sub>CE</sub>) that binds the RI subunit (R<sub>CE</sub>) of type I protein kinase A from *Caenorhabditis elegans*. *J Biol Chem*, 1998. 273: p. 14633-43.

Baker, K. and P.L. Beales, Making sense of cilia in disease: the human ciliopathies. *Am J Med Genet C Semin Med Genet*, 2009. 151C(4): p. 281-95.

Banky, P., et al., Related protein-protein interaction modules present drastically different surface topographies despite a conserved helical platform. *J Mol Biol*, 2003. 330(5): p. 1117-29.

Belibi, F.A. and C.L. Edelstein, Novel targets for the treatment of autosomal dominant polycystic kidney disease. *Expert Opin Investig Drugs*. 19(3): p. 315-28.

Bessen, M., R.B. Fay, and G.B. Witman, Calcium control of waveform in isolated flagellar axonemes of *Chlamydomonas*. *J Cell Biol*, 1980. 86(2): p. 446-55.

Brokaw, C.J., D.J. Luck, and B. Huang, Analysis of the movement of *Chlamydomonas* flagella:" the function of the radial-spoke system is revealed by comparison of wild-type and mutant flagella. *J Cell Biol*, 1982. 92(3): p. 722-32.

Burns-Hamuro, L.L., et al., Designing isoform-specific peptide disruptors of protein kinase A localization. *Proc Natl Acad Sci U S A*, 2003. 100(7): p. 4072-7.

Carr, D.W., et al., Association of the type II cAMP-dependent protein kinase with a human thyroid RII-anchoring protein. Cloning and characterization of the RII-binding domain. *J Biol Chem*, 1992. 267(19): p. 13376-82.

- Carr, D.W., et al., Interaction of the regulatory subunit (RII) of cAMP-dependent protein kinase with RII-anchoring proteins occurs through an amphipathic helix binding motif. *J Biol Chem*, 1991. 266(22): p. 14188-92.
- Castleman, V.H., et al., Mutations in radial spoke head protein genes RSPH9 and RSPH4A cause primary ciliary dyskinesia with central-microtubular-pair abnormalities. *Am J Hum Genet*, 2009. 84(2): p. 197-209.
- Cho, Y.W., et al., PTIP associates with MLL3- and MLL4-containing histone H3 lysine 4 methyltransferase complex. *J Biol Chem*, 2007. 282(28): p. 20395-406.
- Christsian, F. et al., Small molecule AKAP-protein kinase A (PKA) interaction disruptors that activate PKA interfere with compartmentalized cAMP signaling in cardiac myocytes. *J Biol Chem*, 2011. 286(11): p. 9079-96.
- Curry, A.M. and J.L. Rosenbaum, Flagellar radial spoke: a model molecular genetic system for studying organelle assembly. *Cell Motil Cytoskeleton*, 1993. 24(4): p. 224-32.
- Curry, A.M., B.D. Williams, and J.L. Rosenbaum, Sequence analysis reveals homology between two proteins of the flagellar radial spoke. *Mol Cell Biol*, 1992. 12(9): p. 3967-77.
- Dalagiorgou, G., E.K. Basdra, and A.G. Papavassiliou, Polycystin-1: function as a mechanosensor. *Int J Biochem Cell Biol*. 42(10): p. 1610-3.
- Deane, J.A. and S.D. Ricardo, Polycystic kidney disease and the renal cilium. *Nephrology (Carlton)*, 2007. 12(6): p. 559-64.
- Dehe, P.M., et al., Protein interactions within the Set1 complex and their roles in the regulation of histone 3 lysine 4 methylation. *J Biol Chem*, 2006. 281(46): p. 35404-12.
- Diener, D.R., L.H. Ang, and J.L. Rosenbaum, Assembly of flagellar radial spoke proteins in *Chlamydomonas*: identification of the axoneme binding domain of radial spoke protein 3. *J Cell Biol*, 1993. 123(1): p. 183-90.
- Diener, D.R., et al., Sequential assembly of flagellar radial spokes. *Cytoskeleton (Hoboken)*.
- Dixit, C.K., et al., Development of a High Sensitivity Rapid Sandwich ELISA Procedure and Its Comparison with the Conventional Approach. *Anal. Chem.*, 2010. 82(16): p.7049-52.
- Dong, X., et al., Characterization and crystallization of human DPY-30-like protein, an essential component of dosage compensation complex. *Biochim Biophys Acta*, 2005. 1753(2): p. 257-62.

Dymek, E.E., et al., The CSC is required for complete radial spoke assembly and wild-type ciliary motility. *Mol Biol Cell*. 22(14): p. 2520-31.

Dymek, E.E. and E.F. Smith, A conserved CaM- and radial spoke associated complex mediates regulation of flagellar dynein activity. *J Cell Biol*, 2007. 179(3): p. 515-26.

Gaillard, A.R., et al., Flagellar radial spoke protein 3 is an A-kinase anchoring protein (AKAP). *J Cell Biol*, 2001. 153(2): p. 443-8.

Gaillard, A.R., et al., Disruption of the A-kinase anchoring domain in flagellar radial spoke protein 3 results in unregulated axonemal cAMP-dependent protein kinase activity and abnormal flagellar motility. *Mol Biol Cell*, 2006. 17(6): p. 2626-35.

Gold, M.G., et al., Molecular basis of AKAP specificity for PKA regulatory subunits. *Mol Cell*, 2006. 24(3): p. 383-95.

Goodenough, U.W. and J.E. Heuser, Substructure of inner dynein arms, radial spokes, and the central pair/projection complex of cilia and flagella. *J Cell Biol*, 1985. 100(6): p. 2008-18.

Habermacher, G. and W.S. Sale, Regulation of flagellar dynein by an axonemal type-1 phosphatase in *Chlamydomonas*. *J Cell Sci*, 1996. 109 ( Pt 7): p. 1899-907.

Harris, H.H. (2009) *Chlamydomonas* SourceBook, 2<sup>nd</sup> Ed. Chapter8, Volume1. Elsevier Inc., Oxford, UK.

Heberg, F.W., et al., Analysis of A-kinase anchoring protein (AKAP) interaction with protein kinase A (PKA) regulatory subunits: PKA isoform specificity in AKAP binding. *J Mol. Biol*, 2000. 298(2): p.329-39.

Hildebrandt, F., T. Benzing, and N. Katsanis, Ciliopathies. *N Engl J Med*. 364(16): p. 1533-43.

Hirokawa, N., Y. Tanaka, and Y. Okada, Left-right determination: involvement of molecular motor KIF3, cilia, and nodal flow. *Cold Spring Harb Perspect Biol*, 2009. 1(1): p. a000802.

Hirsch, A.H., et al., Cloning and expression of an intron-less gene for AKAP 75, an anchor protein for the regulatory subunit of cAMP-dependent protein kinase II beta. *J Biol Chem*, 1992. 267(4): p. 2131-4.

Hoops, H.J. and G.B. Witman, Outer doublet heterogeneity reveals structural polarity related to beat direction in *Chlamydomonas* flagella. *J Cell Biol*, 1983. 97(3): p. 902-8.

Howard, D.R., et al., Regulation of *Chlamydomonas* flagellar dynein by an axonemal protein kinase. *J Cell Biol*, 1994. 127(6 Pt 1): p. 1683-92.

- Hsu, D.R. and B.J. Meyer, The dpy-30 gene encodes an essential component of the *Caenorhabditis elegans* dosage compensation machinery. *Genetics*, 1994. 137(4): p. 999-1018.
- Huang, B., et al., Radial spokes of *Chlamydomonas* flagella: genetic analysis of assembly and function. *J Cell Biol*, 1981. 88(1): p. 80-8.
- Huang, L.J., et al., D-AKAP2, a novel protein kinase A anchoring protein with a putative RGS domain. *Proc Natl Acad Sci U S A*, 1997. 94(21): p. 11184-9.
- Huang, B., Z. Ramanis, and D.J. Luck, Suppressor mutations in *Chlamydomonas* reveal a regulatory mechanism for Flagellar function. *Cell*, 1982. 28(1): p. 115-24.
- Ishikawa, H. and W.F. Marshall, Ciliogenesis: building the cell's antenna. *Nat Rev Mol Cell Biol*. 12(4): p. 222-34.
- Ishizaki, R., et al., AMY-1 (associate of Myc-1) localization to the trans-Golgi network through interacting with BIG2, a guanine-nucleotide exchange factor for ADP-ribosylation factors. *Genes Cells*, 2006. 11(8): p. 949-59.
- Jarnaess E., et al., Dual specificity A-kinase anchoring proteins (AKAPs) contain an additional binding region that enhances targeting of protein kinase A type I. *J Biol Chem*, 2008. 283(48): p.33708-18.
- Jiang, H., et al., Role for Dpy-30 in ES cell-fate specification by regulation of H3K4 methylation within bivalent domains. *Cell*. 144(4): p. 513-25.
- Jivan, A., et al., Radial spoke protein 3 is a mammalian protein kinase A-anchoring protein that binds ERK1/2. *J Biol Chem*, 2009. 284(43): p. 29437-45.
- Kamiya, R., Functional diversity of axonemal dyneins as studied in *Chlamydomonas* mutants. *Int Rev Cytol*, 2002. 219: p. 115-55.
- Kamiya, R. and G.B. Witman, Submicromolar levels of calcium control the balance of beating between the two flagella in demembrated models of *Chlamydomonas*. *J Cell Biol*, 1984. 98(1): p. 97-107.
- Kartagener, M. 1933. Zur Pathologie der Bronchiektasien : Bronchiektasien bei Situs viscerum invertus. *Beitr. Klin.Tuberk.* 83:489-S01
- Kaupp, U.B., N.D. Kashikar, and I. Weyand, Mechanisms of sperm chemotaxis. *Annu Rev Physiol*, 2008. 70: p. 93-117.
- Kinderman, F.S., et al., A dynamic mechanism for AKAP binding to RII isoforms of cAMP-dependent protein kinase. *Mol Cell*, 2006. 24(3): p. 397-408.



- Kindle, K.L., High-frequency nuclear transformation of *Chlamydomonas reinhardtii*. Proc Natl Acad Sci U S A, 1990. 87(3): p. 1228-32.
- King, S.J. and S.K. Dutcher, Phosphoregulation of an inner dynein arm complex in *Chlamydomonas reinhardtii* is altered in phototactic mutant strains. J Cell Biol, 1997. 136(1): p. 177-91.
- Klauck, T.M., et al., Coordination of three signaling enzymes by AKAP79, a mammalian scaffold protein. Science, 1996. 271(5255): p. 1589-92.
- Klussmann E, Rosenthal W, Christian F, Rademann J & Meyer S: Nonpeptidic inhibitors of AKAP-PKA interaction. PCT/DE2006/000897
- Kohno, T., et al., Subunit interactions within the *Chlamydomonas* flagellar spokehead. Cytoskeleton (Hoboken). 68(4): p. 237-46.
- Lechtreck, K.F., et al., The *Chlamydomonas reinhardtii* BBSome is an IFT cargo required for export of specific signaling proteins from flagella. J Cell Biol, 2009. 187(7): p. 1117-32.
- Lee, L., Mechanisms of mammalian ciliary motility: Insights from primary ciliary dyskinesia genetics. Gene. 473(2): p. 57-66.
- Li, J.B., et al., Comparative genomics identifies a flagellar and basal body proteome that includes the BBS5 human disease gene. Cell, 2004. 117(4): p. 541-52.
- Lindemann, C.B. and K.A. Lesich, Flagellar and ciliary beating: the proven and the possible. J Cell Sci. 123(Pt 4): p. 519-28.
- Liu, W., et al., Mechanoregulation of intracellular Ca<sup>2+</sup> concentration is attenuated in collecting duct of monocilium-impaired orpk mice. Am J Physiol Renal Physiol, 2005. 289(5): p. F978-88.
- Logue, J.S. and J.D. Scott, Organizing signal transduction through A-kinase anchoring proteins (AKAPs). Febs J. 277(21): p. 4370-5.
- Lohmann, S.M., et al., High-affinity binding of the regulatory subunit (RII) of cAMP-dependent protein kinase to microtubule-associated and other cellular proteins. Proc Natl Acad Sci U S A, 1984. 81(21): p. 6723-7.
- Luck, D., et al., Flagellar mutants of *Chlamydomonas*: studies of radial spoke-defective strains by dikaryon and revertant analysis. Proc Natl Acad Sci U S A, 1977. 74(8): p. 3456-60.
- Lyons, R.A., E. Saridogan, and O. Djahanbakhch, The reproductive significance of

- human Fallopian tube cilia. *Hum Reprod Update*, 2006. 12(4): p. 363-72.
- Mastrorarde, D.N., et al., Arrangement of inner dynein arms in wild-type and mutant flagella of *Chlamydomonas*. *J Cell Biol*, 1992. 118(5): p. 1145-62.
- Nauli, S.M., et al., Polycystins 1 and 2 mediate mechanosensation in the primary cilium of kidney cells. *Nat Genet*, 2003. 33(2): p. 129-37.
- Newlon, M.G., et al., A novel mechanism of PKA anchoring revealed by solution structures of anchoring complexes. *Embo J*, 2001. 20(7): p. 1651-62.
- Newlon, M.G., et al., The molecular basis for protein kinase A anchoring revealed by solution NMR. *Nat Struct Biol*, 1999. 6(3): p. 222-7.
- Nicastro, D., J.R. McIntosh, and W. Baumeister, 3D structure of eukaryotic flagella in a quiescent state revealed by cryo-electron tomography. *Proc Natl Acad Sci U S A*, 2005. 102(44): p. 15889-94.
- Nicastro, D., et al., The molecular architecture of axonemes revealed by cryoelectron tomography. *Science*, 2006. 313(5789): p. 944-8.
- Nonaka, S., et al., Determination of left-right patterning of the mouse embryo by artificial nodal flow. *Nature*, 2002. 418(6893): p. 96-9.
- Nonaka, S., et al., Randomization of left-right asymmetry due to loss of nodal cilia generating leftward flow of extraembryonic fluid in mice lacking KIF3B motor protein. *Cell*, 1998. 95(6): p. 829-37.
- Okada, Y., et al., Abnormal nodal flow precedes situs inversus in *iv* and *inv* mice. *Mol Cell*, 1999. 4(4): p. 459-68.
- Omoto, C.K., et al., Ability of paralyzed flagella mutants of *Chlamydomonas* to move. *Cell Motil Cytoskeleton*, 1996. 33(2): p. 88-94.
- Omoto, C.K., et al., Rotation of the central pair microtubules in the eukaryotic flagella. *Mol Biol Cell*, 1999. 10(1): p. 1-4.
- Patel, A., et al., On the mechanism of multiple lysine methylation by the human mixed lineage leukemia protein-1 (MLL1) core complex. *J Biol Chem*, 2009. 284(36): p. 24242-56.
- Patel, A., et al., A novel non-SET domain multi-subunit methyltransferase required for sequential nucleosomal histone H3 methylation by the mixed lineage leukemia protein-1 (MLL1) core complex. *J Biol Chem*. 286(5): p. 3359-69.
- Patel-King, R.S., et al., Flagellar radial spokes contain a Ca<sup>2+</sup>-stimulated nucleoside diphosphate kinase. *Mol Biol Cell*, 2004. 15(8): p. 3891-902.

- Pauling, L., et al., The Structure of Proteins: Two Hydrogen-Bonded Helical Configurations of the Polypeptide Chain. *Proc Natl Acad Sci*, 1951. 37(4): p. 205-11.
- Pazour, G.J., et al., *Chlamydomonas* IFT88 and its mouse homologue, polycystic kidney disease gene *tg737*, are required for assembly of cilia and flagella. *J Cell Biol*, 2000. 151(3): p. 709-18.
- Pedersen, H. and H. Rebbe, Absence of arms in the axoneme of immobile human spermatozoa. *Biol Reprod*, 1975. 12(5): p. 541-4.
- Pidoux, G. and K. Tasken, Specificity and spatial dynamics of protein kinase A signaling organized by A-kinase-anchoring proteins. *J Mol Endocrinol*. 44(5): p. 271-84.
- Piperno, G., B. Huang, and D.J. Luck, Two-dimensional analysis of flagellar proteins from wild-type and paralyzed mutants of *Chlamydomonas reinhardtii*. *Proc Natl Acad Sci U S A*, 1977. 74(4): p. 1600-4.
- Piperno, G., et al., Radial spokes of *Chlamydomonas* flagella: polypeptide composition and phosphorylation of stalk components. *J Cell Biol*, 1981. 88(1): p. 73-9.
- Piperno, G., et al., Mutations in the "dynein regulatory complex" alter the ATP-insensitive binding sites for inner arm dyneins in *Chlamydomonas* axonemes. *J Cell Biol*, 1994. 125(5): p. 1109-17.
- Piperno, G., K. Mead, and W. Shestak, The inner dynein arms I2 interact with a "dynein regulatory complex" in *Chlamydomonas* flagella. *J Cell Biol*, 1992. 118(6): p. 1455-63.
- Porter, M.E., et al., Mutations in the SUP-PF-1 locus of *Chlamydomonas reinhardtii* identify a regulatory domain in the beta-dynein heavy chain. *J Cell Biol*, 1994. 126(6): p. 1495-507.
- Praetorius, H.A., et al., Bending the primary cilium opens Ca<sup>2+</sup>-sensitive intermediate-conductance K<sup>+</sup> channels in MDCK cells. *J Membr Biol*, 2003. 191(3): p. 193-200.
- Qin, H., et al., Intraflagellar transport (IFT) cargo: IFT transports flagellar precursors to the tip and turnover products to the cell body. *J Cell Biol*, 2004. 164(2): p. 255-66.
- Roguev, A., et al., The *Saccharomyces cerevisiae* Set1 complex includes an Ash2 homologue and methylates histone 3 lysine 4. *Embo J*, 2001. 20(24): p. 7137-48.
- Rohatgi, R., L. Milenkovic, and M.P. Scott, Patched1 regulates hedgehog signaling at the primary cilium. *Science*, 2007. 317(5836): p. 372-6.
- Sarma, G.N., et al., Structure of D-AKAP2:PKA RI complex: insights into AKAP specificity and selectivity. *Structure*. 18(2): p. 155-66.

- Satir, P., Structural basis of ciliary movement. *Environ Health Perspect*, 1980. 35: p. 77-82.
- Schrevel, J. and C. Besse, [A functional flagella with a 6 + 0 pattern]. *J Cell Biol*, 1975. 66(3): p. 492-507.
- Scott, J.D., et al., Type II regulatory subunit dimerization determines the sub-cellular localization of the cAMP-dependent protein kinase. *J Bio Chem*, 1990. 265: p.21561-21566.
- Scott, J.D. and T. Pawson, Cell signaling in space and time: where proteins come together and when they're apart. *Science*, 2009. 326(5957): p. 1220-4.
- Silflow, C.D. and P.A. Lefebvre, Assembly and motility of eukaryotic cilia and flagella. Lessons from *Chlamydomonas reinhardtii*. *Plant Physiol*, 2001. 127(4): p. 1500-7.
- Singla, V. and J.F. Reiter, The primary cilium as the cell's antenna: signaling at a sensory organelle. *Science*, 2006. 313(5787): p. 629-33.
- Smith, E.F., Regulation of flagellar dynein by calcium and a role for an axonemal calmodulin and calmodulin-dependent kinase. *Mol Biol Cell*, 2002. 13(9): p. 3303-13.
- Smith, E.F. and P. Yang, The radial spokes and central apparatus: mechano-chemical transducers that regulate flagellar motility. *Cell Motil Cytoskeleton*, 2004. 57(1): p. 8-17.
- Snell, W.J., J. Pan, and Q. Wang, Cilia and flagella revealed: from flagellar assembly in *Chlamydomonas* to human obesity disorders. *Cell*, 2004. 117(6): p. 693-7.
- South, P.F., et al., A conserved interaction between the SDI domain of Bre2 and the Dpy-30 domain of Sdc1 is required for histone methylation and gene expression. *J Biol Chem*. 285(1): p. 595-607.
- Stelter, .P., et al., Molecular basis for the functional interaction of dynein light chain with the nuclear-pore complex. *Nat. Cell. Biol.*, 2007. 9: p. 788-796.
- Summers, K.E. and I.R. Gibbons, Adenosine triphosphate-induced sliding of tubules in trypsin-treated flagella of sea-urchin sperm. *Proc Natl Acad Sci U S A*, 1971. 68(12): p. 3092-6.
- Tamm, S.L. and S. Tamm, Ciliary reversal without rotation of axonemal structures in ctenophore comb plates. *J Cell Biol*, 1981. 89(3): p. 495-509.
- Tash, J.S., Protein phosphorylation: the second messenger signal transducer of flagellar motility. *Cell Motil Cytoskeleton*, 1989. 14(3): p. 332-9.
- Theurkauf, W.E. and R.B. Vallee, Molecular characterization of the cAMP-dependent

protein kinase bound to microtubule-associated protein 2. *J Biol Chem*, 1982. 257(6): p. 3284-90.

Vallee, R.B., M.J. DiBartolomeis, and W.E. Theurkauf, A protein kinase bound to the projection portion of MAP 2 (microtubule-associated protein 2). *J Cell Biol*, 1981. 90(3): p. 568-76.

Vijayaraghavan, S. et al., Protein kinase A-anchoring inhibitor peptides arrest mammalian sperm motility. *J Biol Chem*, 1997. 272(8): p4747-52.

Wang, X., et al., Crystal structure of the C-terminal domain of human DPY-30-like protein: A component of the histone methyltransferase complex. *J Mol Biol*, 2009. 390(3): p. 530-7.

Warner, F.D. and Satir, P. The structural basis of ciliary bend formation. Radial spoke positional changes accompanying microtubule sliding. *J Cell Bio*, 1974. 63(1):p35-63.

Welch, E.J., B.W. Jones, and J.D. Scott, Networking with AKAPs: context-dependent regulation of anchored enzymes. *Mol Interv*. 10(2): p. 86-97.

Williams, B.D., et al., Molecular cloning and sequence analysis of the *Chlamydomonas* gene coding for radial spoke protein 3: flagellar mutation *pf-14* is an ochre allele. *J Cell Biol*, 1989. 109(1): p. 235-45.

Wirschell, M., et al., Building a radial spoke: flagellar radial spoke protein 3 (RSP3) is a dimer. *Cell Motil Cytoskeleton*, 2008. 65(3): p. 238-48.

Witman, G.B., J. Plummer, and G. Sander, *Chlamydomonas* flagellar mutants lacking radial spokes and central tubules. Structure, composition, and function of specific axonemal components. *J Cell Biol*, 1978. 76(3): p. 729-47.

Wong, W. and J.D. Scott, AKAP signalling complexes: focal points in space and time. *Nat Rev Mol Cell Biol*, 2004. 5(12): p. 959-70.

Xia, B., et al., Modulation of cell adhesion and migration by the histone methyltransferase subunit mDpy-30 and its interacting proteins. *PLoS One*. 5(7): p. e11771.

Xu, Z., et al., A role of histone H3 lysine 4 methyltransferase components in endosomal trafficking. *J Cell Biol*, 2009. 186(3): p. 343-53.

Yang, C., M.M. Compton, and P. Yang, Dimeric novel HSP40 is incorporated into the radial spoke complex during the assembly process in flagella. *Mol Biol Cell*, 2005. 16(2): p. 637-48.

Yang, C., H.A. Owen, and P. Yang, Dimeric heat shock protein 40 binds radial spokes

for generating coupled power strokes and recovery strokes of 9 + 2 flagella. *J Cell Biol*, 2008. 180(2): p. 403-15.

Yang, C. and P. Yang, The flagellar motility of *Chlamydomonas pf25* mutant lacking an AKAP-binding protein is overtly sensitive to medium conditions. *Mol Biol Cell*, 2006. 17(1): p. 227-38.

Yang, P., et al., Localization of calmodulin and dynein light chain LC8 in flagellar radial spokes. *J Cell Biol*, 2001. 153(6): p. 1315-26.

Yang, P., et al., Radial spoke proteins of *Chlamydomonas* flagella. *J Cell Sci*, 2006. 119(Pt 6): p. 1165-74.

Yang, P. and W.S. Sale, Casein kinase I is anchored on axonemal doublet microtubules and regulates flagellar dynein phosphorylation and activity. *J Biol Chem*, 2000. 275(25): p. 18905-12.

Yang, P., C. Yang, and W.S. Sale, Flagellar radial spoke protein 2 is a calmodulin binding protein required for motility in *Chlamydomonas reinhardtii*. *Eukaryot Cell*, 2004. 3(1): p. 72-81.

Zariwala, M.A., M.R. Knowles, and H. Omran, Genetic defects in ciliary structure and function. *Annu Rev Physiol*, 2007. 69: p. 423-50.